ACCURATE AND RELIABLE PREDICTION OF ENERGETIC AND SPECTROSCOPIC PROPERTIES VIA ELECTRONIC STRUCTURE METHODS

Marie L. Laury, B.A.

Dissertation Prepared for the Degree of

DOCTOR OF PHILOSOPHY

UNIVERSITY OF NORTH TEXAS

August 2013

APPROVED:

Angela K. Wilson, Major Professor
Thomas R. Cundari, Committee Member
Paul Marshall, Committee Member
Mohammad Omary, Committee Member
William E. Acree, Jr., Chair of the Department of Chemistry
Mark Wardell, Dean of the Toulouse Graduate School

Laury, Marie L. Accurate and Reliable Prediction of Energetic and Spectroscopic Properties via Electronic Structure Methods. Doctor of Philosophy (Chemistry – Physical Chemistry), August 2013, 178 pp., 28 tables, 13 illustrations, 247 numbered references.

Computational chemistry has led to the greater understanding of the molecular world, from the interaction of molecules, to the composition of molecular species and materials. Of the families of computational chemistry approaches available, the main families of electronic structure methods that are capable of accurate and/or reliable predictions of energetic, structural, and spectroscopic properties are ab initio methods and density functional theory (DFT). The focus of this dissertation is to improve the accuracy of predictions and computational efficiency (with respect to memory, disk space, and computer processing time) of some computational chemistry methods, which, in turn, can extend the size of molecule that can be addressed, and, for other methods, DFT, in particular, gain greater insight into which DFT methods are more reliable than others. Much, though not all, of the focus of this dissertation is upon transition metal species – species for which much less method development has been targeted or insight about method performance has been well established.

The ab initio approach that has been targeted in this work is the correlation consistent composite approach (ccCA), which has proven to be a robust, *ab initio* computational method for main group and first row transition metal-containing molecules yielding, on average, accurate thermodynamic properties, i.e., within 1 kcal/mol of experiment for main group species and within 3 kcal/mol of experiment for first row transition metal molecules. In order to make ccCA applicable to systems containing any element from the periodic table, development of the method for second

row transition metals and heavier elements, including lower p-block (5*p* and 6*p*) elements was pursued. The resulting method, the relativistic pseudopotential variant of ccCA (rp-ccCA), and its application are detailed for second row transition metals and lower p-block elements.

Because of the computational cost of ab initio methods, DFT is a popular choice for the study of transition metals. Despite this, the most reliable density functionals for the prediction of energetic properties (e.g. enthalpy of formation, ionization potential, electron affinity, dissociation energy) of transition metal species, have not been clearly identified. The examination of DFT performance for first and second row transition metal thermochemistry (i.e., enthalpies of formation) was conducted and density functionals for the study of these species were identified.

And, finally, to address the accuracy of spectroscopic and energetic properties, improvements for a series of density functionals have been established. In both DFT and ab initio methods, the harmonic approximation is typically employed. This neglect of anharmonic effects, such as those related to vibrational properties (e.g. zero-point vibrational energies, thermal contributions to enthalpy and entropy) of molecules, generally results in computational predictions that are not in agreement with experiment. To correct for the neglect of anharmonicity, scale factors can be applied to these vibrational properties, resulting in better alignment with experimental observations. Scale factors for DFT in conjunction with both the correlation and polarization consistent basis sets have been developed in this work.

ACKNOWLEDGEMENTS

My graduate career at the University of North Texas has been shaped by many people in both my academic and family life. I am grateful to my research advisor, Regents Professor Dr. Angela K. Wilson for her encouraging comments regarding class work, teaching, and research, which contributed to my achievements in the classroom and to the work presented in this dissertation. Thank you to Wilson group members past and present, especially Dr. Nathan J. DeYonker, Dr. Wanyi Jiang and Matthew Carlson for their work with me on projects and Dr. Kameron Jorgensen for many rich conversations about chemistry and her help in managing the many stresses of graduate school. Also, a thank you to Dr. Hector E. Gonzalez for his inquisitive personality that helped me to appreciate the vast amount of information learned during my graduate work. I have a great appreciation for the administrators, Dr. Dave Hrovat and Dr. Scott Yockel, of the UNT computing resources. My committee members, both internal and external, have contributed to the knowledge I have gained in graduate school and have influenced the way I tackle research problems. I would like to thank my parents, Gerry and Cheryl Majkut, and my younger siblings (Angela and Joe) for their support throughout all of the successes and struggles of graduate school. The words of wisdom offered by my parents throughout the years have helped me to develop a greater appreciation for my studies. Finally, I am eternally grateful to the love of my life, my husband Marc Laury. Thank you for listening to my crazy rants about quantum chemistry and for your never ending patience with me that has helped me to just keep swimming through the challenges (and to our dog Simon who always knew that if I gave him a belly rub then I would feel better).

TABLE OF CONTENTS

Page

LIST OF TABLES

LIST OF FIGURES

CHAPTER 1

INTRODUCTION

The research presented in this dissertation aims to address a central issue of electronic structure methods: How can the accuracy and reliability of current computational methods be improved? The presented research entails the development of computational methodologies to provide accurate prediction of energetic and spectroscopic properties of molecules and the calibration of current methods to assess reliability.

Computational chemistry has wide application to the study of atoms and molecules and chemical environments, and provides information to guide, aid, and provoke experiments. While computational chemistry can be used in the elucidation of many different properties, structural, energetic, and spectroscopic properties are among those most frequently computed. Atomic and molecular energies are used to determine a range of properties, including dissociation energies, electron affinities, and enthalpies of formation, which can afford an understanding of reaction mechanisms and molecular stability. The determination of accurate energetic (i.e., enthalpies of formation) and spectroscopic (vibrational frequencies) properties for any element on the periodic table is key for applications including the prediction and design of experimental work; furthermore, the theoretically determined properties may be used in the parameterization or design of novel computational methods.

To utilize computational chemistry for the determination of atomic or molecular properties of a system, the accuracy and reliability of the methods should be well established. Accuracy is generally defined in terms of deviation from high quality

experimental data, e.g. a generally accepted definition of chemical accuracy for main group systems is the determination of properties within one kcal mol^{-1} from experimental values. This level of accuracy is necessary as demonstrated by examples such as in the examination of barrier heights for a synthesis reaction, where a few tenths of a kcal mol^{-1} may change the desired product ratio, and in kinetics, where one kcal mol^{-1} deviation from experiment is derived from theoretical rate constants being within an order of magnitude of experimental rate constants. Reliability is gauged over a large number of test systems, such as the enthalpies of formation of transition metal molecules, and whether or not a method can achieve a similar level of performance, e.g. accuracy level, over all the molecules studied. For example, how can there be confidence in the selection of a method if for one metal-ligand combination the enthalpy of formation is in agreement with experiment but for the same metal with a different ligand, the enthalpy of formation deviates by 100 kcal mol^{-1} from experiment?

Advancements in the methods employed for computational chemistry have increased exponentially over the past two decades, permitting the development of more accurate and reliable methodologies. With advances in computational methodologies, the utilization of computational chemistry has become widespread throughout many fields, inclusive of chemistry, physics, biology, and materials science. The increased utility and progress of computational methods has been spurred forward by technological improvements as well, allowing for calculations to be executed more rapidly, with greater precision, and in greater bulk. Ideally a computational method would achieve a uniform high accuracy for molecules composed of elements from any area of the periodic table. Unfortunately, different parts of the periodic table present

different methodology requirements and a single computational procedure for every system is not possible without including unnecessary calculations for some molecules. Examples include: transition metals differing from most main group elements in the need for a description of relativistic effects and the fact that the electronic separation between the ground state and the first excited state is not uniform or of the same magnitude for all elements and molecules. A reliable theoretical method would aid in the study of novel complexes, for example, by studying the energetics of various metal-ligand combinations and determining which would be more favorable as a catalyst. The design of an accurate computational methodology for second row transition metals, the calibration of current methods for first and second row transition metals, and a systematic way to correct for approximations in the methodologies are detailed in this dissertation.

Computational chemistry methodologies can be classified into a number of categories, including electronic structure methods (defined via quantum mechanics), molecular mechanics (defined by classical mechanics), and molecular dynamics (introduction of a time dependence). Selection of a method is based on the size of the system of interest, property of interest, and the desired accuracy level. While the importance and utility of molecular mechanics and dynamics is noted, electronic structure methods, and their accuracy and reliability, are further detailed.

Electronic structure methods include ab initio methods and density functional theory (DFT) and are based on quantum mechanics. One of the main differences between the two methods is the choice to describe the system of interest with respect to electron coordinates (ab initio methods) or with respect to the electron density (DFT).

Ab initio methods can determine properties in closest agreement with experiment, where the molecule size that can be addressed is dictated by the desired accuracy level and computational requirements. In systems having a larger number of electrons, e.g. those with second row transition metals, the selection of a method can be limited due to computational requirements, and, thus, reduced computational cost alternatives are needed. Recent developments in DFT have yielded density functionals which have improved accuracy for some properties of interest, but DFT is based on fitting to experimental data and the errors are generally larger than those observed for ab initio methods. If a molecule is studied that is dissimilar to the parameterization set, the quality of DFT results may be questionable. Generally, density functionals are parameterized against test sets containing main group elements and molecules, prompting the question of the reliability of the functionals for transition metal systems.

In the design of any new computational methodology, whether ab initio or DFT, the calibration of the method is crucial and is the key to confidence in the performance of the method in future research. While theory, principles, and laws may be the foundation of a new method and guide the proof of the method, robust experimental data is essential for testing any new method. Comparison to experimental data allows for the validation of the method's accuracy and reliability. The accuracy desired varies with respect to method, property, and system of interest. The demonstrated accuracy (i.e., within a defined error margin from experimental values) and reliability of a method is crucial for the extension of the method to experimentally untested compounds. The accurate prediction of thermodynamic properties, specifically the enthalpy of formation,

is of exceptional importance, since this property is considered the most stringent test of a computational method.

Chapter 3 defines a composite method, a quantum mechanical approach, for the determination of thermodynamic properties, within experimental uncertainties, of second row transition metal-containing molecules. Generally, composite methods are considered cost-effective (in terms of memory, disk space, and computer processing time) in comparison to the method needed to meet the composite method's intended level of accuracy. As compared to development for main group species or lighter metals, the development of ab initio methods for calculation of accurate thermochemical properties of 4*d* transition metal-containing molecules has lagged behind. In this chapter a variant of ccCA for second row transition metals has been proposed, the relativistic pseudopotential ccCA (rp-ccCA). The method has been calibrated against 4*p* molecules before application to second row transition metals. Further utilization of rp-ccCA for the determination of thermodynamic properties of the lower p-block elements (In-I and Tl-At) is detailed in Chapter 4.

In Chapters 5 and 6, scale factors for vibrational frequencies and zero-point vibrational energies calculated with density functional theory (DFT) in conjunction with correlation consistent (Chapter 5) and polarization consistent (Chapter 6) basis sets is presented. For the description of thermochemical properties such as entropies and enthalpies, spectroscopic properties are required. These properties can be computed, but, due to the implementation of the harmonic approximation, i.e., the neglect of anharmonic effects, the calculated results deviate from the experimentally-known values. It has been shown there is a systematic deviation between computed and

experimental vibrational frequencies,[1-3] which are integral in the determination of spectroscopic properties. The systematic deviation allows for the development of multiplicative scale factors for application to the calculated frequencies to provide comparison with the experimentally observed frequencies. Because theoretical results are dependent upon the method selection, scale factors that are unique to each methodology are needed and have been defined.

Chapter 7 outlines the performance of DFT for first and second row transition metal thermochemistry. The study employs a wide range of density functionals, varying in their approximations and parameterizations, to determine the enthalpy of formation of over 200 first row transition metal-containing molecules and 30 second row transition metal-containing molecules. The reliability of various density functionals for theoretically-determined enthalpies of formation is studied. The transition metal molecules studied vary in their metal center, coordination, and experimental uncertainties, among other properties.

CHAPTER 2

COMPUTATIONAL QUANTUM CHEMISTRY

2.1 Schrödinger Equation

The field of quantum mechanics (QM) lies where the areas of chemistry, physics, and mathematics overlap. The central equation of quantum mechanics in the non-relativistic limit, within the context of electronic structure and stationary state wave functions, is the time-independent Schrödinger equation:[4]

$$\hat{H}\Psi = E\Psi \tag{2.1}$$

Where $\hat{H}$ is the Hamiltonian operator for the nuclei and electrons in a molecule:

$$\hat{H} = -\sum_{i=1}^{N}\frac{1}{2}\nabla_i^2 - \sum_{A=1}^{M}\frac{1}{2M_A}\nabla_A^2 - \sum_{i=1}^{N}\sum_{A=1}^{M}\frac{Z_A}{r_{iA}} + \sum_{i=1}^{N}\sum_{j>i}^{N}\frac{1}{r_{ij}} + \sum_{A=1}^{M}\sum_{B>A}^{M}\frac{Z_A Z_B}{R_{AB}} \tag{2.2}$$

In Equation 2, i and j are the electrons, A and B are the nuclei, N is the total number of electrons, M is the total number of nuclei, M_A is the mass ratio of the nucleus A to an electron, Z_A is the atomic number of nucleus A, r_{iA} is the distance between an electron and a nucleus, r_{ij} is the distance between two electrons, R_{AB} is the distance between two nuclei, and ∇ is the Laplacian of the electrons and nuclei. The terms describe the kinetic energy of the electrons, the kinetic energy of the nuclei, the attraction between the nuclei and electrons, the repulsion between the electrons, and the repulsion between the nuclei, respectively. The energy, E, determined by Equation 2.1 allows for the determination of chemical properties including molecular geometries, electronic ground states, spectroscopic properties, vibrational frequencies, zero-point energies, ionization potentials, electrons affinities, atomization energies, and enthalpies of formation.

Though the Schrödinger equation appears to be a facile eigenvalue equation, difficulties arise when working towards a solution for a system with more than one electron. Approximations must be introduced to arrive at a solution for the electronic energy. By implementing the Born-Oppenheimer approximation,[5] the nucleus is assumed to be stationary due to the large mass ratio between the nucleus and the electrons; therefore, the electrons are assumed to be moving in a field of fixed nuclei. Under the Born-Oppenheimer approximation the electronic and nuclear terms become separable and the Hamiltonian, $\hat{H}$, of the Schrödinger equation is simplified into an electronic form:

$$\widehat{H}_{elec} = -\sum_{i=1}^{N} \frac{1}{2}\nabla_i^2 - \sum_{i=1}^{N}\sum_{A=1}^{M} \frac{Z_A}{r_{iA}} + \sum_{i=1}^{N}\sum_{j>i}^{N} \frac{1}{r_{ij}} \quad (2.3)$$

And the electronic Schrödinger equation is

$$\widehat{\mathrm{H}}_{\mathrm{elec}}\Psi_{\mathrm{elec}} = E_{elec}\Psi_{\mathrm{elec}} \quad (2.4)$$

The electronic Hamiltonian is composed of the kinetic energy of the electrons, the attractions between the electrons and the nucleus, and the repulsion between the electrons. The additional terms of Equation 2.2, specifically for the nuclear kinetic energy and the repulsion between the nuclei, become zero and a constant, respectively, under the Born-Oppenheimer approximation. While it may be obvious that the electronic wavefunction of Equation 2.4 is dependent on the electronic coordinates, the electronic wavefunction is also dependent on the nuclear coordinates; a change in the nuclear coordinates will change the electron coordinates and, in turn, the electronic wavefunction. The electronic energy in combination with the nuclear-nuclear repulsion yields the total energy solution (Equation 2.5) to the non-relativistic time-independent Schrödinger equation (Equation 2.1).

$$E_{tot} = E_{elec} + \sum_{A=1}^{M} \sum_{B>A}^{M} \frac{Z_A Z_B}{R_{AB}} \quad (2.5)$$

The Schrödinger equation presented in Equations 2.1 and 2.3 do not include relativistic effects; relativistic effects will be discussed in Section 2.7. In order to solve the Schrödinger equation, method (Hamiltonian) and basis set (wavefunction) combinations must be employed. Methods relevant to this dissertation will be presented in Sections 2.2 and 2.3, while basis sets will be detailed in Section 2.4.

2.2 Ab initio Computational Methods

Ab initio (in Latin "from the beginning") methods may be employed to obtain solutions to the Schrödinger equation without reference to experimental data. These methods utilize the electron spatial coordinates (r,θ,φ) and spin (α for spin up, β for spin down) as variables of the wavefunction, defining x={r,θ,φ,w}. The wavefunction, Ψ, for an N electron system is a function of electrons described by spin and space coordinate, $x_1, x_2, \ldots, x_N$, for each electron:

$$\Psi(x_1, x_2, \ldots, x_N) \quad (2.6)$$

The Pauli Exclusion Principle states no two electrons are able to occupy the same quantum state simultaneously.[6] To meet the requirement of the Pauli Exclusion Principle, the wavefunction (Ψ) must be antisymmetric with respect to the interchange of space and spin of any two electrons since they are fermions:

$$\Psi(x_1, x_2, \ldots, x_N) = -\Psi(x_2, x_1, \ldots, x_N) \quad (2.7)$$

To approximate the solution to the Schrödinger equation for a many electron system (Ψ), the product of one-electron wavefunctions or orbitals (Φ_i, i=1,2…N), referred to as the Hartree product, is employed.

$$\Psi = \prod_{i=1}^{N} \Phi_{\mathrm{i}} \tag{2.8}$$

The Hartree product does not fulfill the antisymmetry principle; therefore, the total wavefunction must be written as a Slater determinant, which antisymmetrizes the wavefunction.[7] For a two electron system the Slater determinant is:

$$\Psi(x_1, x_2) = \frac{1}{\sqrt{2}}\left[\Phi_{\mathrm{i}}(\mathrm{x}_1)\Phi_{\mathrm{j}}(\mathrm{x}_2) - \Phi_{\mathrm{i}}(\mathrm{x}_2)\Phi_{\mathrm{j}}(\mathrm{x}_1)\right] \tag{2.9}$$

Alternatively, the Slater determinant for the two electron system written in matrix form is:

$$\Psi(x_1, x_2) = \frac{1}{\sqrt{2}}\begin{bmatrix} \Phi_{\mathrm{i}}(\mathrm{x}_1) & \Phi_{\mathrm{j}}(\mathrm{x}_1) \\ \Phi_{\mathrm{i}}(\mathrm{x}_2) & \Phi_{\mathrm{j}}(\mathrm{x}_2) \end{bmatrix} \tag{2.10}$$

For the case of an N electron system, the Slater determinant is

$$\Psi(x_1, x_2) = \frac{1}{\sqrt{N!}}\begin{bmatrix} \Phi_{\mathrm{i}}(\mathrm{x}_1) & \cdots & \Phi_{\mathrm{n}}(\mathrm{x}_1) \\ \vdots & \ddots & \vdots \\ \Phi_{\mathrm{i}}(\mathrm{x}_{\mathrm{N}}) & \cdots & \Phi_{\mathrm{n}}(\mathrm{x}_{\mathrm{N}}) \end{bmatrix} \tag{2.11}$$

The factor in front of the matrix is the normalization factor of the determinant.

The simplest ab initio method is the Hartree-Fock approximation[8] which utilizes the variational principle in order to obtain optimized one-electron wavefunctions (or orbitals in the context of a minimal basis). The variational principle states that if a normalized wavefunction (Ψ) satisfies boundary conditions, such as the wavefunction goes to zero at infinity, then the Hamiltonian expectation value is an upper bound to the exact ground state energy:

$$\langle \Psi | \hat{H} | \Psi \rangle \geq E_0 \tag{2.12}$$

Therefore, the energy of an approximate wavefunction, e.g. as determined by Hartree-Fock, will always be higher than the exact ground state energy. By varying the one-electron wavefunctions, the minimal E_o may be determined and the result is the Hartree-Fock equation:

$$f(i)\Phi(x_i) = e_\Phi(x_i) \quad (2.13)$$

where $f(i)$ is the one-electron Fock operator. The solutions of the Hartree-Fock equation are a set of orthonormal one-electron wavefunctions, or orbitals, with corresponding energies. A Slater determinant composed of the solutions to the Hartree-Fock equation is the lowest energy obtainable for the ground state via the variational principle and an uncorrelated single determinant method.

The Hartree-Fock approximation accounts for approximately 99% of the total electronic energy.[9] The remaining 1% of energy is chemically important; for example, in the dissociation of carbon monoxide, where Hartree-Fock incorrectly predicts the dissociation of the molecule into ions.[10] The Hartree-Fock approximation accounts for the exchange correlation between electrons of parallel spin. The difference between the Hartree-Fock energy and the total electronic energy is defined as the correlation energy,

$$E_{corr} = E_{tot} - E_{HF} \quad (2.14)$$

Since the Hartree-Fock energy is variationally determined to be above the ground state energy, the correlation energy, E_{corr}, is negative ($E_{corr} < 0$).

To account for the correlation energy beyond the Hartree-Fock approximation, often referred to as addressing the N-electron problem, correlated methods may be employed. In this dissertation, two correlated methods, coupled cluster theory and Møller-Plesset second order perturbation theory, are utilized.

Coupled cluster theory is best understood by first introducing configuration interaction (CI). CI uses the ground state wavefunction (Ψ_0) determined by Hartree-Fock (HF) to solve the non-relativistic time-independent electronic Schrödinger equation

exactly (assuming the solution is obtained with a complete basis set).[11] The wavefunction for the CI method is

$$\Psi = c_0\Psi_0 + c_1\Psi_1 + \cdots + c_k\Psi_k = \sum_k c_k\Psi_k \quad (2.15)$$

The first term of the CI wavefunction is the Hartree-Fock ground state wavefunction multiplied by a constant. The second term describes all of the determinants (or configuration state functions) of singly excited electrons, the third term describes the doubly excited electrons, and so on. A singly excited determinant represents the excitation of one electron from the Hartree-Fock ground state into a virtual orbital. Similarly, a doubly excited determinant is the excitation of two electrons. A single, a double, and a triple excitation are depicted in Figure 2.1.

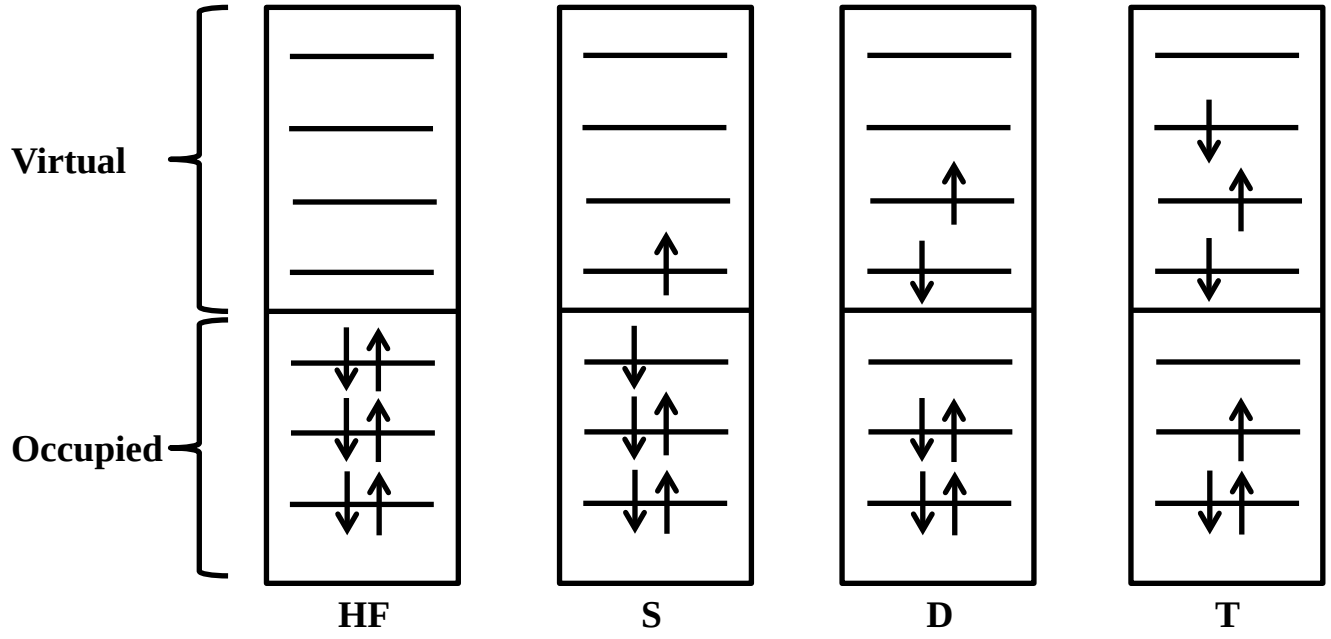

Figure 2.1. The Hartree-Fock wavefunction and examples of a single (S), double (D), and triple (T) excitations.

Each of these excitations represents a different configuration and the resulting sum is the CI method. If all possible excitations and configurations are included within the CI wavefunction, then the method is referred to as Full CI. Generally, only single

and double excitations are considered for the CI method. This method is referred to as the CISD (configuration interaction with single and double excitations) method. For a two electron system, the determinants within the CISD are depicted in Figure 2.2, where the “g” and “u” denote the symmetry of the orbital as gerade and ungerade, respectively, and i, j, k, … represent occupied orbitals and a, b, c, … represent virtual orbitals.

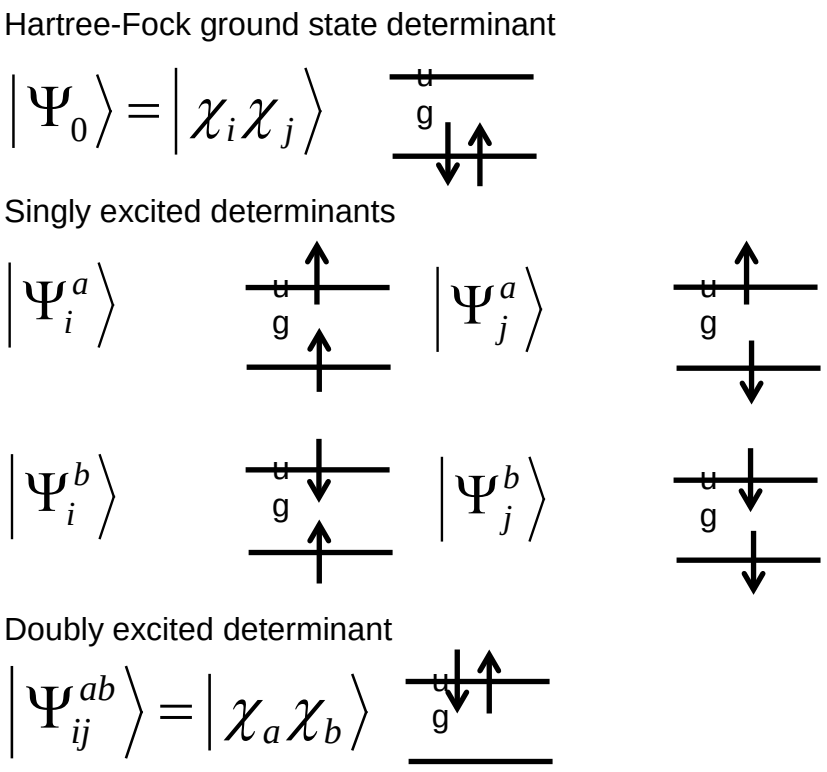

Figure 2.2. Configuration interaction with single and double excitations (CISD) with respect to determinants.

When the CI method is truncated, the method maintains size consistency (the energy of A-B infinitely separated is equal to the energy of A plus the energy of B), but is no longer size extensive (correct linear scaling with respect to the number of electrons). In order to overcome the size extensivity problem of truncated CI, the wavefunction may be written as an exponential, such as in coupled cluster theory.[12]

The coupled cluster wavefunction is written as:

$$\Psi_{\mathrm{CC}} = \mathrm{e}^{\hat{\mathrm{T}}}\Phi_0 \tag{2.16}$$

$$e^{\hat{T}} = 1 + \hat{T} + \frac{1}{2!}\hat{T}^2 + \cdots = \sum_{k=0}^{\infty}\frac{1}{k!}\left(\hat{T}^k\right) \tag{2.17}$$

where $\hat{T}$ is the cluster operator

$$\hat{T} = \hat{T}_1 + \hat{T}_2 + \cdots + \hat{T}_N \tag{2.18}$$

The cluster operator acts on the Hartree-Fock reference wavefunction (Ψ_0) and generates excited Slater determinants. The subscript of $\hat{T}$ ($\hat{T}_\mathrm{i}$) represents the i$^{\mathrm{th}}$ excited Slated determinant. For example,

$$\hat{T}_1\Psi_0 = \sum_{\mathrm{i}}^{\mathrm{occ}}\sum_{\mathrm{a}}^{\mathrm{virt}}\mathrm{t}_{\mathrm{i}}^{\mathrm{a}}\,\Psi_{\mathrm{i}}^{\mathrm{a}} \tag{2.19}$$

$$\hat{T}_2\Psi_0 = \sum_{\mathrm{i}<j}^{\mathrm{occ}}\sum_{\mathrm{a}<b}^{\mathrm{virt}}\mathrm{t}_{\mathrm{ij}}^{\mathrm{ab}}\,\Psi_{\mathrm{ij}}^{\mathrm{ab}} \tag{2.20}$$

where t are the expansion coefficients or amplitudes and Ψ_i^a represents a single excitation of an electron in an occupied orbital, i, into a virtual orbital a. Therefore, the exponential of the coupled cluster wavefunction can be expanded as

$$e^{\hat{T}} = 1 + \hat{T}_1 + \left(\hat{T}_2 + \frac{1}{2}\hat{T}_1{}^2\right) + \cdots \tag{2.21}$$

The first term describes the Hartree-Fock reference, the second term describes the singly excited states, the third term describes the doubly excited states; the exponential operator is expanded through all possible excitations. The Schrödinger equation under coupled cluster is

$$\hat{H}e^{\hat{T}}\Psi_0 = \mathrm{E}e^{\hat{T}}\Psi_0 \tag{2.22}$$

If all cluster operators, $\hat{T}_1$ through $\hat{T}_\mathrm{N}$, are included, then the coupled cluster method is equal to CI. Similar to CI, limiting the number of excitations with coupled cluster yields a truncated version of the method. If the cluster operator is limited to

$\hat{T}=\hat{T}_2$, the method is coupled cluster doubles (CCD). The inclusion of only single excitations does not improve over Hartree-Fock; therefore, couple cluster singles (CCS) does not exist. The inclusion of single and double excitations, $\hat{T}=\hat{T}_1+\hat{T}_2$, is coupled cluster singles and doubles (CCSD).[13] As opposed to CI, the truncated forms of coupled cluster are size extensive due to the inclusion of cross-terms in the cluster operator expansion. A commonly employed coupled cluster method is coupled cluster with single, double, and perturbative triple excitations [CCSD(T)]. [14]

While CI and coupled cluster theories rely on excitations to recover the correlation energy beyond the Hartree-Fock approximation, correlation energy is also recoverable by introducing a perturbation to the ground state system. In many-body perturbation theory (MBPT),[15] the Hamiltonian is composed of the ground state Hamiltonian ($\widehat{H}_0$) and the Hamiltonian as a result of perturbation ($\widehat{H'}$). The MBPT Hamiltonian is

$$\widehat{H} = \widehat{H}_0 + \lambda\widehat{H'} \tag{2.23}$$

where λ represents the perturbation parameter. When λ=0, the Hamiltonian simplifies to $\widehat{H} = \widehat{H}_0$. If the unperturbed Hamiltonian is defined as a sum over Fock operators, as introduced in Hartree-Fock theory, then the method is Møller-Plesset (MP) perturbation theory.[16] Based on the definition of the perturbation operator in MP perturbation theory, the first order energy is zero and thus first order MP theory (MP1) yields the Hartree-Fock energy; therefore, second order MP perturbation theory (MP2) is employed in order to recover correlation energy beyond the Hartree-Fock approximation. The second-order correction to the reference energy includes all perturbations between the reference and excited states; therefore, the correction consists of the sum over all doubly excited determinants, $|\Psi_{ij}^{ab}\rangle$, as depicted in Figures 2.1 and 2.2.

Similar to coupled cluster theory, MP2 is size extensive. Perturbation theory does not determine the energy via a variational procedure, such as coupled cluster and configuration interaction; therefore, the energy obtained by MP2 may be lower in energy than the exact energy and the series of MPn (n=order) does not converge monotonically toward the exact energy as you increase the order of the perturbation.

2.3 DFT

As detailed, ab initio methods approximate the solution to the Schrödinger equation by utilizing the coordinates of electrons to derive the wavefunction. Alternatively, density functional theory employs the electron density. The electron density is defined as the square of the wavefunction integrated over N-1 electron coordinates:

$$\rho(r) = N \sum_{i=1}^{N_{elec}} \int |\Psi(r_1, r_2, \dots, r_N)|^2 \, dr_2 dr_3 \dots dr_N \quad (2.24)$$

The electron density is, in itself, a function. In order to determine the electronic energy a function of the electron density is necessary, i.e., a function of a function, commonly known as a functional.

The initial implementation of the electron density to determine the electronic structure was defined in Thomas-Fermi theory.[17] The original theory lacked the ability to determine molecular binding. The next step in the development of using the one-electron density was Slater's Xα method,[18] combining Thomas-Fermi theory and the Hartree orbital method. The next advancement in the utilization of the electron density was founded by two theorems from Hohenberg and Kohn.[19] The first theorem states:

The electron density determines the external potential (to within an additive constant).

This theorem is commonly understood as: the electron density uniquely determines the Hamiltonian operator. Since the Hamiltonian is dictated by the external potential and the total number of electrons, N, the density is determined by integration; therefore, with the density, the Hamiltonian can be determined uniquely and the wavefunctions computed. In general, the first theorem states the energy is a functional of the density.

The second theorem of Hohenberg and Kohn states:

For any positive definite trial density, ρ_t, such that the integral of $\rho_t(r)dr=N$, then $E[\rho_t]\geq E_o$

This theorem is proven with the variational principle. Based on the two theorems of Hohenberg and Kohn, the fundamental equation of density functional theory is

$$|E[\rho] - \int \rho(r)dr - N| = 0 \tag{2.25}$$

and it can be concluded that there exists a universal functional E[ρ] such that when the functional is inserted into the above equation and the functional is minimized, the exact ground state density and energy are obtained.

From the Schrödinger equation, the energy functional can be defined by the sum of three energetic terms

$$E[\rho] = T[\rho] + V_{ext}[\rho] + V_{ee}[\rho] \tag{2.26}$$

where T is the kinetic energy, V_{ext} is the interaction with the external potential and V_{ee} is the electron-electron interaction. The external potential interaction is defined as

$$V_{ext}[\rho] = \int V_{ext}(r)dr \tag{2.27}$$

In order to solve for the kinetic energy and electron-electron repulsion functionals, Kohn and Sham selected a single determinant wavefunction constructed of N “orbitals” to describe a system of N non-interacting electrons.[20] The non-interacting system allows for the exact definition of the kinetic energy functional

$$T_S[\rho] = -\frac{1}{2}\sum_i^N \langle \rho_i | \nabla^2 | \rho_i \rangle \quad (2.28)$$

and the ground state density is

$$\rho(r) = \sum_i^N |\rho_i|^2 \quad (2.29)$$

Through the definition of the density via a set of orbitals, an antisymmetric wavefunction can be constructed. The electron-electron interaction is then composed of the Coulomb interaction

$$V_{eec} = \frac{1}{2}\int \frac{\rho(r_1)\rho(r_2)}{(|r_1 - r_2|)} dr_1 dr_2 \quad (2.30)$$

and the remaining exchange-correlation energy, defined as E_{XC}. The resulting total energy of Equation 2.26 can be rewritten as

$$E[\rho] = T_S[\rho] + V_{ext}[\rho] + V_{eec}[\rho] + E_{XC}[\rho] \quad (2.31)$$

The exchange-correlation functional recovers the energy omitted by assuming a non-interacting system and the additional energy beyond the Coulomb interaction

$$E_{XC}[\rho] = (T[\rho] - T_S[\rho]) + (V_{ee}[\rho] - V_{eec}[\rho]) \quad (2.32)$$

The implementation of the non-interacting system yields the Kohn-Sham set of non-linear equations to describe the non-interacting electrons in an effective local potential. Hohenberg and Kohn proved there is a unique functional relating the ground state energy to the electron density. Kohn-Sham density functional theory, therefore, is not exact since the unique functional is not known. The E_{XC} functional in Kohn-Sham DFT can be refined by determining properties in a variety of systems and developing the approximations employed within the functional.

Since the introduction of Kohn-Sham density functional theory (DFT), the theory has been developed to better address chemical properties, such as binding energies and long-range interactions, and to approach accuracy levels obtained by ab initio

methods. To describe the various approximations of DFT, Perdew coined the term "Jacob's Ladder".[21] The ladder is composed of five rungs and as the ladder is climbed the sophistication of the theory is increased. The ground of the ladder is the Hartree world, where only the Hartree energy is determined. The first rung is the Local (Spin) Density Approximation (LSDA), the second rung is the Generalized Gradient Approximation (GGA), the third rung is Meta-GGA (MGGA), the fourth rung is hybrid functionals (HGGA), and the fifth rung is generally composed of double hybrid functionals (DHGGA).

In the LDA approximation, the density is treated locally as a uniform electron gas and the exchange energy is defined as

$$E_X^{LDA}[\rho] = -Cx \int \rho^{\frac{4}{3}}(r)dr \quad (2.33)$$

If the alpha and beta spin densities are not equal, then the LSDA is employed.[22] On average, the LSDA underestimates exchange energy by 10% and the correlation energy is overestimated by a factor of two;[23] in turn, bond strengths are overestimated. Since the energy of the LSDA is a functional of only the electron density, inclusion of additional functions in the functional was considered in order to address the shortcomings of LSDA

GGA functionals incorporate the gradient (derivatives) of the electron density (∇_ρ) in the form of the functional, in addition to the electron density.[24,25] GGA functionals generally have the form

$$E_{XC} \approx \int \rho(r) E_{XC}(\rho, \nabla\rho)dr \quad (2.34)$$

Functionals following this form include BLYP (Becke 88 exchange[26] and Lee-Yang-Parr correlation[27]) and BP86 (Becke 88 exchange and Perdew 86 correlation[28]). The

functionals differ by how they include the gradient of the density. GGA functionals improve on the overestimation of binding energies by LSDA.

The third rung of the DFT Jacob's Ladder is the MGGA functionals.[29] The meta-functionals include a dependence on the local kinetic energy density, in addition to the gradient of the density and the density. The inclusion of the local kinetic energy density results in a functional form

$$E_{XC} \approx \int \rho(r) E_{XC}(\rho, |\nabla\rho|, \nabla\rho^2) dr \quad (2.35)$$

Hybrid functionals[30] compose the fourth rung of Jacob's Ladder. The non-interacting system of DFT and the fully interacting many-body system are exactly connected via the adiabatic approach.[31] The adiabatic approach gradually increases the electron-electron interaction from non-interacting (λ=0) to fully interacting (λ=1). When λ=0, the system can be described by Hartree-Fock. The GGA functional can then be optimized to describe the fully interacting system. The exchange-correlation energy of a hybrid functional can be written as

$$E_{XC} \approx aE_{HF} + bE_{XC}^{GGA} \quad (2.36)$$

As implemented by Becke, the HGGA exchange-correlation energy is determined by

$$E_{XC} = E_{XC}^{LDA} + a(E_X^{HF} - E_X^{LDA}) + b\Delta E_X^{GGA} + c\Delta E_C^{GGA} \quad (2.37)$$

The coefficients a, b, c are optimized with respect to reference data and the GGA and LDA selected is defined in the development. Popular HGGA's include B3LYP, B3PW91, and PBE1PBE. These functionals include 20%, 20%, and 25% Hartree-Fock exchange (i.e., the value of a=0.20, 0.20, and 0.25), respectively. With the inclusion of non-local Hartree-Fock exchange, the locality of LSDA and GGA is nearly cancelled; therefore, HGGA functionals produce binding energies closer to experimental energies.

Double hybrid functionals have been deemed fifth rung functionals due to their inclusion of an additional variable, as well as their generally observed improved accuracy.[32-35] DHGGA exchange-correlation energy includes correlation energy from second-order perturbation theory in addition to Hartree-Fock exchange energy. The DHGGA exchange-correlation energy is

$$E_{XC} = (1 - a_X)E_X^{DFT} + a_X E_X^{HF} + (1 - a_c)E_C^{DFT} + a_c E_C^{PT2} \quad (2.38)$$

Generally, the percentage of Hartree-Fock exchange in DHGGA functionals is greater than in HGGA functionals; for example, Grimme's B2-PLYP functionals has coefficients a_x=0.53 and a_c=0.27.[32]

Additional approximations have been implemented in DFT, including a correction for dispersion[36] or long-range effects and introducing a parameter to separate the exchange energy at long ranges.[37] DFT in its general definition does not account for van der Waals interactions.[38] To address the long-range interactions, Grimme introduced a dispersion correction for modern DFT. The dispersion correction is defined as

$$E_{disp} = -s_6 \sum_{i=1}^{N_{at}-1} \sum_{j=i+1}^{N_{at}} \frac{C_{ij}^6}{R_{ij}^6} f_{dmp}(R_{ji}) \quad (2.39)$$

where N_{at} is the number of atoms, s_6 is a scaling factor depending on the functional used, R_{ij} is the interatomic distance, C_{ij} is the dispersion coefficient for atom pair ij and the damping function f_{dmp} is defined as

$$f_{dmp}(R_{ij}) = \frac{1}{1 + e^{-d\left(\frac{R_{ij}}{R_f} - 1\right)}} \quad (2.40)$$

where R_f is the sum of the atomic van der Waals radii. The dispersion corrected DFT exchange-correlation energy is then

$$E_{XC}^{DFT-D} = E_{XC}^{DFT} + E_{disp} \quad (2.41)$$

Long-range corrected functionals address the rapid decay of the non-Coulomb part of exchange functionals. There are different ways to define the exchange-correlation energy of long-range corrected functionals. Within this dissertation, the long-range corrected functionals developed by Head-Gordon and co-workers are employed.[39,40] These functionals have the form

$$E_{XC}^{DFT} = E_X^{LR-HF} + E_X^{SR-DFT} + E_C^{DFT} \quad (2.42)$$

To establish the range cutoff, an error function is employed and the range parameter, ω, is within the error function.

$$\frac{1}{r_{12}} = \frac{\mathrm{erf}(\omega r_{12})}{\mathrm{r}_{12}} + \frac{\mathrm{erfc}(\omega r_{12})}{\mathrm{r}_{12}} \quad (2.43)$$

where $r_{12} = |r_{12}| = |r_1 - r_2|$. A smaller value of ω is associated with the SR operator being used for a longer range.

A variant of the long-range corrected functionals has also been defined, which includes a fraction of SR HF exchange in conjunction with the SR DFT exchange. These functionals have the form

$$E_{XC}^{DFT} = E_X^{LR-HF} + c_X E_X^{SR-HF} + E_X^{SR-DFT} + E_C^{DFT} \quad (2.44)$$

and the value of c_X is determined via fitting to experimental data. The range-separated functionals have demonstrated a better performance than hybrid functionals for properties including dissociation energies and charge-transfer problems.[39,40]

2.4 Basis Sets

To solve the Schrödinger equation, the wavefunction must be constructed to represent the system of interest. Mathematically, the wavefunction is composed of

basis functions combined in a linear combination in order to describe molecular orbitals. The wavefunction, as described in polar coordinates, can be separated into a product of two functions, radial (R) and angular (Y)

$$\Psi_{n,m,l}(r,\theta,\varphi) = R_{n,l}(r)Y_{l,m}(\theta,\varphi) \quad (2.45)$$

The angular or spherical harmonic function is defined by the angular and magnetic quantum numbers (*l,m*). The angular function determines the shape of the orbital space, i.e., *s, p, d, f*. The radial function is variable with respect to r, the distance of the electron from the nucleus. $R_{n,l}(r)$ describes the electron position and is expanded as

$$R_{n,l}(r) = r^{x(n,l)}e^{-y(r)} \quad (2.46)$$

To describe the radial component of the wavefunction, there are two types of basis function: Slater-type orbitals (STOs)[41] and Gaussian-type orbitals (GTOs)[42]. STOs have the form

$$R_{n,l}(r) = r^{n-1}e^{-\zeta r} \quad (2.47)$$

and GTOs are of the form

$$R_{n,l}(r) = r^{2n-1-l}e^{-\zeta r^2} \quad (2.48)$$

The more notable differences between the two basis function types are in the regions: 1) as r approaches zero and 2) as r approaches infinity. In comparing the slopes of the basis functions at r=0, the STOs have a non-zero slope (often referred to as a cusp) and the GTOs have a slope equal to zero. The 1*s* STO and GTO functions are depicted in Figure 2.3.

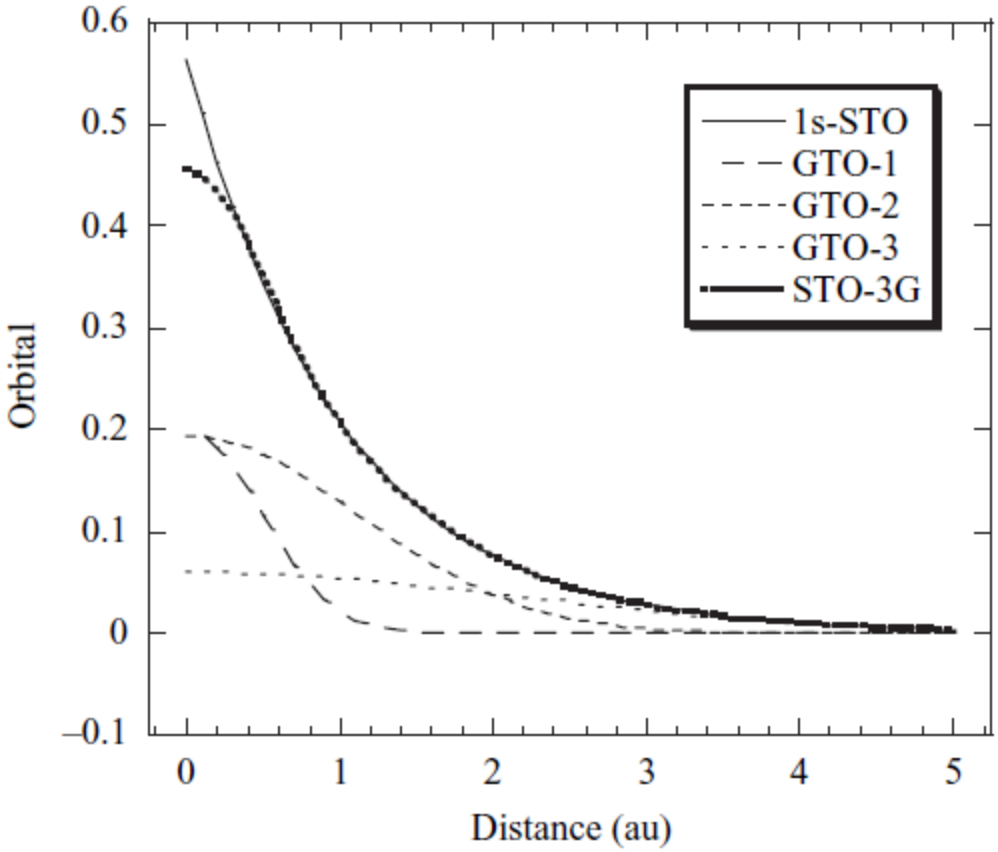

Figure 2.3. The use of GTOs to model a 1s STO. A linear combination of three GTOs is depicted (STO-3G).[23]

When r is large, the exponential of the GTOs decays more rapidly than the exponential of the STOs. To qualitatively describe molecular orbitals, STOs are preferred over GTOs since STOs are able to model the molecular orbitals with less basis functions than would be needed with GTOs, STOs reproduce the cusp at the nucleus, a description necessary for properties such as nuclear magnetic resonance (NMR) and electron spin resonance (ESR), and STOs properly describe the tail of the function which is necessary to accurately model long-range effects, such as van der Waals interactions. A downfall of STOs is the two-, three-, and four-centered integrals cannot be evaluated analytically. The construction of the GTOs allows, for example, the reduction of a four-center integral into a two-center integral for the 1*s* function, in

addition to higher angular momentum functions. While GTOs provide a simplified way to solve complex integrals, in comparison to STOs, the description of molecular orbitals by GTOs differs from an exact solution of the hydrogen atom, from which the concept of an orbital is derived. To remedy shortcomings of GTOs, linear combinations of GTOs can be made to form a new GTO that more accurately reproduces an STO. By making linear combinations of GTOs, referred to as primitives, a new Gaussian function, a contracted Gaussian function, is composed (see Figure 2.3 for STO-3G). The contracted functions can be used to form molecular orbitals and save computational effort by fixing the coefficients of the functions in the linear combination to coefficients optimized for the atomic orbitals.

The Gaussian basis functions are modified based on the exponent and coefficient. The exponents of GTOs and STOs are directly proportional to the value of ζ (zeta), which controls the width of the function. If a basis function has a large exponent (i.e., large ζ value), the function is considered tight. If a basis function has a small exponent, the function is diffuse. Diffuse functions are important for the description of long-range interactions.

The most commonly employed construction schemes for Gaussian-type basis sets are the Pople-type basis sets and Dunning correlation consistent basis sets. Correlation consistent basis sets are utilized within this dissertation and will be described. The polarization consistent basis sets are an offshoot of the Dunning basis sets, but have been adapted for DFT.

Correlation consistent basis sets were developed by Dunning and co-workers.[43-47] The sets are constructed in order to systematically recover correlation energy from

the valence electrons through the systematic addition of basis functions according to their contribution to the correlation energy; for example, correlation consistent basis sets will have the form 3*s*2*p*1*d*, 4*s*3*p*2*d*1*f*, 5*s*4*p*3*d*2*f*1*g*, etc. The correlation consistent basis sets are built from a minimal set of basis functions, e.g. 2*s*1*p* for lithium. The basis sets are referred to as the correlation consistent polarized valence *n*-zeta basis sets (cc-pV*n*Z), where *n* is the zeta level of the basis set. To construct a double zeta, *n*=2 (D), basis set, additional polarized functions (one of each symmetry) of *s*, *p*, and *d* character are added to the minimal basis set. For the example of lithium, the cc-pVDZ basis set would be composed of 3*s*2*p*1*d* basis functions. With the systematic recovery of the correlation energy, the energies of the correlation consistent basis set converge asymptotically to the complete basis set (CBS) limit as the zeta level increases. Since it is not possible to have an infinitely large basis set, the systematic nature of the correlation consistent basis sets allows for an extrapolation of the correlation energy to the CBS limit. At the CBS limit, the error associated with the selection of basis set is removed and the remaining error in the (nonrelativistic) calculation is inherent to the selected method, e.g. CI, CCSD(T), MP2.[48] Diffuse functions added to the correlation consistent basis sets are referred to as augmenting functions and the resulting basis sets are aug-cc-pV*n*Z.[43] The inclusion of augmenting functions in the correlation consistent basis sets is used to aid in describing van der Waals interactions, hydrogen bonding, and anionic species. While the cc-pVnZ sets recover correlation energy between valence electrons, there is additional correlation energy between the core and valence electrons and between the core electrons. For the recovery of core-valence and core-core correlation energies, the correlation consistent basis sets can be

augmented with functions to account for the difference between all-electron and valence electron calculations (denoted cc-pCV*n*Z).[49] Further work revealed that the core-valence correlation energy converges more slowly than the core-core correlation energy; therefore, the weighted core-valence basis sets (cc-pwCV*n*Z) were developed to enhance convergence of the core-valence correlation energy.[45] The balanced construction of the correlation consistent basis sets, coupled with the fact that properties determined with the basis sets can be extrapolated to the CBS limit, can enable accurate determination of molecular properties, including electron affinities, ionization potentials, and total energies when paired with a correlation method, such as CCSD(T).

Since the basis functions of the correlation consistent basis sets were optimized with ab initio methods, the monotonic convergence of the correlation energy as seen for ab initio methods is not guaranteed for density functional theory (DFT). To address this deficiency, Jensen and co-workers constructed the polarization consistent basis sets to converge in a smooth and efficient manner for density functional calculations.[50,51] As polarization effects occur within a molecule, as opposed to an atom, molecular calculations were used in the development of the polarization consistent basis sets. The resulting basis sets are noted as pc-*n* (*n*=0–4), where n is the polarization level beyond the isolated atom. For example, pc-0 for a first row element consists of an *s* and a *p* function. The pc-1 basis set adds a *d*-function, while the pc-2 basis set adds an *f*-function. The *s* and *p* functions were optimized for the atom, while the exponents of the additional ‘‘polarization’’ functions were optimized for a variety of bonding environments within molecules.

2.5 Scaling and Accuracy

As eluded to in the discussions of ab initio methods, DFT, and basis sets, not all method and basis set combinations are appropriate for the determination of molecular properties. Considerations must be made regarding the computational cost, i.e., memory, disk space, and CPU time requirements, and the desired accuracy level. Associated with the computational cost is the scaling of a method. When referring to computational cost or computational scaling, the definition herein is with respect to N number of basis functions. For ab initio methods, Hartree-Fock scales formally as N^4, MP2 scales as N^5, and CCSD(T) scales as N^7. While Full CI, with a complete basis set, would yield the exact solution to the electronic Schrödinger equation, the method scales as $N^{N!}$. Since there are a variety of approximations within DFT, the theory typically scales as N^3 or N^4. As computational resources are a limiting factor for a calculation, the scaling of the method can be an important consideration.

In addition to the scaling of the method, the desired accuracy level of the calculation should be considered in the selection of a computational method. Generally, post-Hartree-Fock methods have higher accuracy levels, i.e., in better agreement with experimental data for calibration, than DFT, though the accuracy comes with a higher scaling. For computational work involving main group atoms, the definition of "chemical accuracy" is generally accepted as theoretically determined energetic properties (e.g. dissociation energies, enthalpies of formation) within one kcal mol^{-1} of reliable experimental data. This definition of chemical accuracy was derived from the Arrhenius equation[52]

$$k = Ae^{\frac{-E_a}{RT}} \tag{2.49}$$

where k is the rate constant, A is the frequency factor, E_a is the activation energy, R is the gas constant, and T is the temperature of a reaction. Experimental and theoretical rate constants should agree within an order of magnitude

$$0.1 < \frac{k_{cal}}{k_{expt}} < 10 \quad (2.50)$$

Therefore, at 298K (room temperature) the theoretical solution should be within one kcal mol^{-1} of the experimental energy, i.e., obtain chemical accuracy. This definition of chemical accuracy is considered for main group elements. Chemical accuracy for heavier systems, such as transition metals, will be discussed in Chapters 3 and 4. In addition to chemical accuracy, another metric used by some composite methods is spectroscopic accuracy defined 1 kilojoule mol^{-1}.

2.6 Model Chemistries

To reduce the computational costs associated with increasing molecule size and basis set, model chemistries, or composite approaches, have been introduced within ab initio methodologies. The result of a CCSD(T) calculation with a large basis set has been referred to as the "gold standard" for computational methods.[47] Due to the scaling of CCSD(T), N^7 where N is the number of basis functions, a CCSD(T) calculation with a large basis set has a high computational cost. Through the combination of a high level of theory and small basis set (with respect to number of basis functions) calculations and low levels of theory paired with large basis sets, composite methods attempt to reproduce results obtained when a high level of theory is combined with a large basis set (i.e., the gold standard). Thus, composite methods can obtain a high accuracy property, e.g. within chemical accuracy, at a lower computational cost than the gold

standard. Examples of composite methods include the Gaussian-n methods (G*n*),[53-55] the Weizmann-n methods (W*n*),[56,57] the High accuracy Extrapolated Ab initio Thermochemistry method (HEAT),[58] the Complete Basis Set (CBS-*n*) theories,[59] the focal point method,[60] the Multi-Coefficient Correlation Method (MCCM),[61] the Feller-Peterson-Dixon (FPD) approach,[62] and the correlation consistent Composite Approach (ccCA).[63-72]

While there are a variety of composite methods, each method differs by the components (methods and basis sets employed) of the methodology, the accuracy goal (chemical versus spectroscopic accuracy, i.e., on average within one kJ/mol of experiment), and the variants (designed for specific elements). In this dissertation only two composite methods are discussed: the G*n* methods, since this is the earliest and most widely used family of composite methods,[53] and ccCA, since a new variant of the method is the focus of Chapters 3 and 4. To note, the W*n* methods have proven to be one of the most accurate composite methods aming for chemical accuracy for main group species,[56,57] but a further discussion of the W*n* methods is not included.

The G*n* methods utilize Pople basis sets (e.g. 6-311G**, 6-311+G**) in conjunction with DFT and ab initio methods; for example, the G3 method includes MP2 and QCISD single-point calculations.[55] The G*n* methods include a correction, which contains more than one empirical parameter, known as the high-level correction (HLC). The original HLC in G1 attempted to account for basis set deficiencies and was fitted to the experimental data of the test set. In further developments of the G*n* methods (*n*=2, 3, 4), the number of parameters within the HLC increased to compensate for effects such as additional basis set deficiencies and unpaired electrons. The major drawback

of the G*n* methods is the HLC, which introduces a bias into the method since it depends on parameter(s) derived to fit computed data to a selected set of experimental results. It has been shown the magnitude of the HLC can be over 100 kcal mol^{-1}.[65]

The correlation consistent Composite Approach (ccCA) was developed by Wilson and co-workers and represents an ab initio composite method designed to approximate the energy obtained by a CCSD(T,FC1)-DK/aug-cc-pCV∞Z-DK calculation at the CBS limit. The ccCA method was designed with the goal of developing a theoretical model chemistry which is cost-effective as compared with methods such as W1 and HEAT, provides a chemically accurate (within 1 kcal mol^{-1} of experiment, on average) description of physical effects, is free of empirical parameters, and is applicable to a wide-range of systems. The convergence behavior of the correlation consistent basis sets is used to obtain a reference energy via extrapolation and then a series of additive single-point energy calculations are used to obtain the corrections to the reference energy; the resulting ccCA method approaches the CCSD(T,FC1)-DK/aug-cc-pCV∞Z-DK energy at a reduced computational cost. The ccCA method has been applied to a wide range of molecules, demonstrating the robustness of ccCA. The ccCA methodology is MP2-based and involves no empirical parameters.

The initial step in ccCA is a geometry optimization obtained with the B3LYP level of theory and cc-pVTZ basis set. The geometry is then utilized in a series of single energy point calculations. MP2 level calculations are computed with aug-cc-pVnZ basis sets with n=D(2), T(3), Q(4). The energies from these calculations are extrapolated to the CBS limit for the HF energy and the MP2 correlation energy, similar to the separate extrapolations employed by Halkier and co-workers,[73] since the correlation energy

converges at a different rate than the HF energy. For the HF/CBS energy, an extrapolation scheme first proposed by Feller is utilized.[74] The extrapolation proposed by Feller follows the form of:

$$E(n) = E_{CBS} + Bexp(-Cn) \quad (2.51)$$

Further studies were carried out by Halkier and co-workers and an ideal C value of 1.63 was determined for HF/CBS extrapolations with triple and quadruple-zeta basis sets.[75] Multiple extrapolation schemes can be utilized for the MP2 energy, but the following extrapolations were selected for ccCA. The mixed Gaussian/exponential equation was developed by Peterson and co-workers and is represented as:[76]

$$E(n) = E_{CBS} + Bexp\big(-(n-1)\big) + Cexp(-(n-1)^2) \quad (2.52)$$

With respect to ccCA, the Peterson extrapolation is referred to as ccCA-P. An alternative extrapolation, inversely related to the angular momentum, was developed by Schwartz and co-workers. Two versions are utilized: l_{max}^3 and l_{max}^4, where l_{max} is the highest order angular momentum with respect to the basis functions. For main group elements, l_{max} is equal to n. For transition metal species, l_{max} is equal to n+1. The Schwartz extrapolation is described as:[77]

$$E(l_{max}) = E_{CBS} + \frac{B}{(l_{max}+\frac{1}{2})^x} \quad (2.53)$$

The ccCA variant with x=3 is designated ccCA-S3 and to the fourth power (x=4) is ccCA-S4. A final extrapolation option is ccCA-PS3, which is the average of the ccCA-P and ccCA-S3 extrapolations. Through the Feller extrapolation the HF/CBS ($E_{HF/CBS}$) energy is obtained and with the Peterson or Schwartz extrapolations the MP2/CBS ($E_{MP2/CBS}$) energy is obtained. Additional effects considered are scalar relativistic effects, core-valence effects, higher-order correlation energy beyond the MP2 level of

theory, and anharmonicity with respect to the zero-point energy. ccCA includes these effects as additive corrections.

The Douglas-Kroll term, ΔE(DK), accounts for the scalar relativistic effects and is obtained with a spin-free, one electron Douglass-Kroll- Hess (DKH) second-order Hamiltonian and the triple-zeta correlation consistent basis set:

$$\Delta E(DK) = E(MP2/cc-pVTZ-DK) - E(MP2/cc-PVTZ) \quad (2.54)$$

The core-valence electron correlation term, ΔE(CV), is determined via a frozen core MP2 calculation:

$$\Delta E(CV) = E(MP2,FC1)/aug-cc-pCVTZ) - E(MP2/aug-cc-pVTZ) \quad (2.55)$$

The FC1 keyword denotes the additional electrons to be correlated in the calculation. For example, for elements Li to Ne, all electrons are correlated; for Na to Ar, all electrons except 1*s* are correlated; and for K to Kr, all electrons excluding 1*s*2*s*2*p* are correlated. In other words, all electrons are correlated except those of the inner noble gas core.

To account for higher order electron correlation effects, i.e., beyond the MP2 level, a single point energy calculation is carried out with CCSD(T). The correlation correction, deemed ΔE(CC), is calculated as:

$$\Delta E(CC) = E(CCSD(T)/cc-pVTZ) - E(MP2/cc-pVTZ) \quad (2.56)$$

To finalize the ccCA energy, the scaled harmonic zero point energy must be added. In order to account for anharmonicity, a scale factor of 0.9890 was applied in calculating the zero point energy. The zero-point energy is determined with B3LYP/cc-pVTZ. The scaled zero point energy is denoted ΔE(ZPE). The spin orbit coupling for

the atoms is included in the term $\Delta E(SO)_a$. With the additive corrections defined above and the extrapolated HF and MP2 energies, the ccCA energy is defined as:

$$E_{ccCA} = E_{HF/CBS} + E_{MP2/CBS} + \Delta E(CV) + + \Delta E(CC) + \Delta E(DK) + \Delta E(ZPE) + \Delta E(SO)_a \quad (2.57)$$

Additional variants of ccCA have been developed, including a variant for first row transition metals (ccCA-TM), an implementation of the resolution-of-the-identity (RI-ccCA), a layered approach using our own N-layered integrated molecular orbital and molecular mechanics (ONIOM-ccCA), a method for molecules with near-degeneracies or multireference character (MR-ccCA), and the relativistic pseudopotential variant (rp-ccCA). rp-ccCA is the subject of Chapters 3 and 4. Each variant of ccCA has proven to be accurate, overall, and computationally efficient (as compared with a high-level calculation for the system studied, e.g. CCSD(T,FC1)-DK/aug-cc-pCV∞Z-DK).

ccCA is often applied to study the thermochemistry, e.g. enthalpy of formation, of a molecule via atomization energy, defined as:

$$\Delta H_{f,m}(298K) = \sum_{atoms} n\Delta H_{f,A}(0K) - (\sum_{atoms} nE_A - E_M - E_{ZPE}) + \big(H_M(298K) - H_M(0K)\big) - \sum_{atoms} n(H_A(298K) - H_A(0K)) \quad (2.58)$$

In Equation 2.58, the first term describes the enthalpy contribution from the atoms at 0 K, the second term describes the atomization energy of the molecule, the third term describes the thermal contribution to the enthalpy from the molecule, and the fourth term describes the thermal contribution to the enthalpy from the atoms.

2.7 Relativistic effects

Relativistic effects were briefly mentioned in Section 2.6 and a more detailed discussion is warranted. The requirement that the speed of light be constant in all

coordinate systems is the root of the theory of relativity. Additionally, physical laws should be equal in these systems; consequently; the description of a particle with the inclusion of relativity requires three space coordinates (e.g. x, y, z), as well as a time coordinate such that space-time is represented by a Lorentz invariant 4-vector, w, where w=(x,y,z,t). A particle moves at a fraction of the speed of light; therefore, the mass of a moving particle is greater than when the mass of the particle at rest.

$$m = m_0 \left[\sqrt{1 - \frac{v^2}{c^2}} \right]^{-1} \tag{2.59}$$

where m_o is the mass of the particle at rest, v is the speed of the particle, and c is the speed of light.

The inclusion of relativistic effects will change the chemistry of the particle in several ways. If the Bohr radius is considered

$$a = \frac{\varepsilon_0 h^2}{\pi m e^2 Z} \tag{2.60}$$

where ε_o is the permittivity of free space (1/4π), h is Planck's constant, m is the mass of the particle, e is the charge of the particle, and Z is the atomic number, the relativistic increase in the mass of the particle will inversely affect the Bohr radius.[78] As the atomic number increases the contraction of the Bohr radius will be greater, signifying the relativistic effects will increase with the atomic number; therefore, relativistic effects will be greater for heavier elements, such as transition metals. The relativistic effects result in the contraction of the core orbitals. In a many-electron system, the contraction of the core orbitals results in an increased screening of the nuclear charge for the valence orbitals. In general, *s* and *p* orbitals will contract, and the *d* and *f* orbitals will expand. In a molecular system, the contraction of the *s* and *p* orbitals will shorten the chemical

bond. The contraction and expansion of orbitals due to relativity are referred to as direct and indirect effects, respectively; furthermore, these are considered scalar relativistic effects.

Further examination of relativity yields the spin-orbit interaction,[79] resulting from the interaction of the spin and orbital angular momentum of an electron. A moving electron generates an electric field, which will interact with the intrinsic magnetic moment, i.e., spin, of the electron. Evidence of the spin-orbit interaction is seen in the splitting of *p* and *d* orbitals into sublevels with different energies. As an example, subshells with orbital angular momentum, ℓ=1 split into ℓ-1/2 and ℓ+1/2 with the ℓ-1/2 subgroup being lower in energy. If ℓ=2, then the splitting is ℓ-1/2, ℓ+1/2, ℓ-3/2 and ℓ+3/2. The spin-orbit splitting corresponds to the quantum number *j*, the total angular momentum.

The Schrödinger equation introduced in Equation 2.1 was in the non-relativistic limit. In order to account for relativistic effects, corrections to the non-relativistic energy must be determined, including mass-velocity, Darwin, and spin-orbit. The mass-velocity term and Darwin terms are considered scalar relativistic effects. The mass-velocity term corrects the kinetic energy due to the relativistic change in mass. Conceptually, the Darwin term is high frequency oscillations of the electron around its average position and can generally be thought of as a retarded potential due to the finite speed of light. The spin-orbit term is related to the electric field generated by the moving electron.

There are a variety of methods to include relativity within a calculation. An exact treatment of relativistic effects requires the Dirac equation,[80,81] a Lorentz invariant formulation of the Schrödinger equation that requires use of a 4-component

wavefunction. Alternatively, an approximate decoupling of the large and small components can be used (e.g. Douglas-Kroll) to obtain scalar relativistic corrections to non-relativistic solutions of the Schrödinger equation.[82,83] Within this dissertation, scalar relativistic effects are accounted for via an effective core potential, while the spin-orbit interaction is determined via an *a posteriori* calculation.

Heavy elements, such as transition metals, have a large number of core electrons, which are generally considered chemically unimportant. A large number of basis functions are necessary to describe the core orbitals in order to properly describe the electron-electron repulsion with the valence orbitals. In addition to the large number of core electrons, the effect of relativity cannot be ignored for heavier elements. In 1935 Hellmann proposed the replacement of the chemically inert core electrons with a function, referred to as a pseudopotential or effective core potential (ECP).[84] ECPs are designed to model the core electrons, leaving the valence electrons to be treated explicitly with a corresponding basis set. Since scalar relativistic effects directly impact the core electrons but only indirectly impact the valence electrons, the scalar relativistic effects can be modeled within the potential; therefore, the ECPs in conjunction with a non-relativistic method can yield energies that neglect only spin-orbit coupling. By reducing the number of electrons in a calculation and accounting for relativistic effects with a non-relativistic method, ECPs afford the opportunity to use a high level of theory, i.e., greater scaling, to obtain more accurate results than would be possible with a system composed of a large number of explicitly treated electrons.

Considerations in the generation of an ECP include core size, fitting scheme of the core (energy consistent vs. shape consistent), and the level of calculations

employed for the fit. ECPs are constructed as either large core or small core. When a large-core potential is implemented, the valence electrons treated are the outermost valence electrons. A small-core potential includes the outermost valence and the first sub-valence shell of electrons. The additional electrons included in the valence of small-core potentials improve the accuracy, transferability, and uniformity of correlation energies and overall energetic results with generally a negligible loss of relativistic effects.[85] Selection of the reference data, to which the potential is fit, determines whether the potential is energy consistent or shape consistent. Energy consistent potentials are fitted to atomic energy spectra, while shape consistent potentials are fitted with respect to orbital shapes. The ECPs can have the form

$$U_{ECP}(r) = -\frac{Q}{r} + \sum_{l,j} V_{lj}(r)\, P_{lj} \qquad (2.61)$$

where Q is the core charge (and -$\frac{Q}{r}$ represents the monopole potential of the spherically symmetric bare core), P_{lj} is the projector onto functions with quantum numbers l and j, and V_{lj} is defined as

$$V_{lj} = \sum_k B_{lj,k} e^{-\beta_{lj,k} r^2} \qquad (2.62)$$

where B and β are adjustable parameters to fit the potential to the reference data. V_{lj} is designed to describe the short-range radial potentials for Coulomb and exchange potentials of the core with Pauli-repulsion and relativistic effects, while the $-\frac{Q}{r}$ describes the long-range part of the radial potentials. The Gaussian functions within the potential are optimized to fit the reference data. For the optimization, methods including relativistic Dirac-Hartree-Fock[86] or numerical Hartree-Fock may be employed.[87] The selection of the method for optimization is dictated by the intended use of the potentials.

If the potentials are designed to recover relativistic effects while being used with a non-relativistic Hamiltonian, Dirac-Hartree-Fock calculations or other approximate relativistic methods may be used in the fit.

The obvious question regarding the potentials is the effect, with respect to accuracy, of replacing an all-electron basis set with pseudopotentials. Dolg, Stoll, and co-workers have evaluated the accuracy of energy consistent ab initio pseudopotentials in comparison to all-electron results.[88] Upon calculation of atomic excitation and ionization energies for first row transition elements, a difference of less than 0.1 eV (2.3 kcal mol^{-1}) was observed. Advantages of the studied pseudopotentials include the computational savings and the facile inclusion of relativistic effects via re-optimization of the exponents and coefficients in the basis set with respect to valence energies. The description of total valence correlation energies was assessed and the pseudopotentials gathered on average 2% more correlation energy than the all-electron values. Based on the comparisons of pseudopotential and all-electron basis sets, pseudopotentials are considered a reliable means for studying heavy elements.

Though spin-orbit coupling may be parameterized within an ECP, there are additional methods to account for spin-orbit coupling in the energy of a system. The spin-orbit Hamiltonian is defined as[89]

$$\hat{H}_{SO} = \left(\frac{1}{2m_e ec^2}\right)\left(\frac{1}{r}\right)\left(\frac{\partial V}{\partial r}\right)\hat{L}\cdot\hat{S} = \xi\hat{L}\cdot\hat{S} \qquad (2.63)$$

where V is the Coulombic potential of the electrons, $\hat{L}$ is the operator for the orbital angular momentum, and $\hat{S}$ is the operator for the spin angular momentum. The eigenfunctions (Ψ) and eigenvalues (E) of the Schrödinger equation can be determined with the spin-orbit coupling neglected, and then the spin-orbit coupling is accounted for

by perturbation theory. Multireference Configuration Interaction (MRCI) can be used to determine the spin-orbit coupling contribution to the total energy by considering the energy splitting of the ground state of the system.[90] As opposed to using one electron configuration to determine the energy, multiple configurations are employed. Further discussion of multireference methods is outside of the scope of this dissertation. The utilization of MRCI to determine spin-orbit coupling is addressed in context in Chapter 4.

CHAPTER 3

A PSEUDOPOTENTIAL-BASED COMPOSITE METHOD: THE RELATIVISTIC PSEUDOPOTENTIAL CORRELATION CONSISTENT COMPOSITE APPROACH (RP-CCCA) FOR MOLECULES CONTAINING 4D TRANSITION METALS (Y-CD)[1]

3.1 Introduction

Second row (4*d*) transition metals have wide applicability from their use in catalysis in areas such as ruthenium catalyzed reduction of alkenes[91] to their use in medicine in areas such as soluble molybdenum-centered complexes to treat diabetes.[92] From diatomics to clusters to organometallics, second row transition metals (Y – Cd) are exploited for their unique properties such as conductivity and magnetic properties and promising industrial technologies including hydrogen fuel storage and olefin metathesis catalysis.[93] As compared to development for main group species or lighter metals, the development of theoretical methods for accurate calculation of the thermochemical properties of 4*d* transition metal-containing molecules has lagged behind. As the number of electrons increases for a species, there are an additional number of basis functions necessary to describe accurately the polarization of the atom and, in turn, molecules containing heavy (i.e., 4*d*) atoms. The large basis sets limit the computational feasibility for calculations including heavier elements, such as the 4*d* transition metals. Further computational hurdles may be encountered when high levels of theory are implemented, e.g. coupled cluster singles, doubles, and perturbative

[1] Work reported in this chapter has been published in M.L. Laury, N.J. DeYonker, W. Jiang, and A.K. Wilson, "A Pseudopotential-based Composite Method: The Relativistic Pseudopotential Correlation Consistent Composite Approach (rp-ccCA) for Molecules Containing 4*d* Transition Metals (Y-Cd)," *J. Chem. Phys*. **135**, 214103 (2011).

triples (CCSD(T)), due to the scaling of the methods (N^7 for CCSD(T), where N is the number of basis functions). With the development of pseudopotentials and composite methods, quantitative computational studies for second row transition metal molecules are feasible.

The correlation consistent Composite Approach (ccCA)[64,66-71,94-96] is based on Møller-Plesset second-order perturbation (MP2) theory[97] and utilizes the systematic convergence of the correlation consistent basis sets to approach the complete basis set (CBS) limit.[9,43-45,49,98] Additive corrections for higher-order correlation by CCSD(T), core–valence electron interaction and relativistic effects by MP2 are included in the ccCA scheme. The robustness and effectiveness of ccCA has been demonstrated by successful application to a wide-range of molecules.[7] For molecules containing only main group elements, ccCA can yield a mean absolute deviation (MAD) of less than 1.0 kcal mol^{-1} (within chemical accuracy) from experimental values.[68,69] The properties of interest included enthalpies of formation, dissociation energies, ionization potentials, electron affinities, and proton affinities. For first row transition metal thermochemistry, a modified version of ccCA, referred to as ccCA-TM, achieved transition metal accuracy, i.e., an MAD of 3.0 kcal mol^{-1} as compared to experimental and recommended values for enthalpies of formation and dissociation energies.[70] ccCA has proven to be a reliable method for a wide variety of molecules and bonding types, and the extension to heavier elements, such as second row transition metals, is the focus of this work.

An all-electron treatment of molecules containing transition metal atoms becomes computationally expensive due to an increase in basis set size and the number of correlated valence and core electrons.[99,100] Since all electrons are included in

the SCF procedure to generate reference wave functions for correlated methods, HF convergence can become the bottleneck for molecules containing elements from the 4*p* block and beyond. Furthermore, for these heavier elements the inner electron radial velocities can be near the speed of light and relativistic effects become more significant.[99,100] A viable means for studying molecules containing atoms from first row transition metals and beyond is the utilization of effective core potentials (ECP), or pseudopotentials, with corresponding valence basis sets.[101] ECPs facilitate calculations by reducing the number of low-lying occupied orbitals, e.g. core orbitals, while simultaneously incorporating relativistic effects. Small core pseudopotentials include the (n-1)s^2(n-1)p^6(n)s^n(n-1)d^m electrons explicitly; in contrast, large-core pseudopotentials include only the outermost *s* and *d* electrons, i.e., (n)s^n(n-1)d^m, in the valence region explicitly.[102] The additional electrons considered in small-core potentials improve the accuracy, transferability, and uniformity of correlation energies and overall energetic results.[85] Treatment of relativistic effects can be included within the potential.[103]

Computational methodologies, such as density functional theory (DFT), have been used in conjunction with effective core potentials in order to determine geometries, ground states, vibrational frequencies, electron affinities, ionization potentials, and dissociation energies. However, thermodynamic studies have been limited to specific types of molecules, including metal halides, carbides, oxides, nitrides, and borides, and are generally diatomic species. For example, Cheng *et al*. studied the bond distances, vibrational frequencies, dipole moments, dissociation energies, electron affinities, and ionization potentials for second row transition metal halides with the hybrid functional

B3LYP and the Stuttgart/Dresden relativistic effective core potential for the metals and Gaussian basis sets for the halides.[104] Qualitative trends for the row of 4d metals were reported. Additionally, B3LYP and the Los Alamos potentials (LanL2DZ) have been utilized by Kharat *et al*. to determine spin states, bond lengths, vibrational frequencies, binding energies, and ionization potentials for diatomic metal carbides, oxides, nitrides, and borides.[105] Though DFT provides efficient and viable methods for studying transition metal-containing molecules, many of the functionals (e.g. hybrid B3LYP) include multiple parameters. There exist DFT methods designed for transition metals, e.g. M06, but, in spite of their construction, DFT may fall short for the accurate prediction of thermodynamic properties, such as enthalpies of formation.[71,106] A comprehensive study by Tekarli et al. examined the performance of 44 DFT methods with correlation consistent basis sets for the determination of the enthalpy of formation of 3*d* transition metal molecules.[71,106] For the range of functionals, the mean absolute deviations (MADs) ranged from seven to over sixty kcal mol^{-1}, well outside any definition of accuracy. Cundari et al. determined the enthalpies of formation for a set of first, second, and third row transition metals using B3LYP with the Los Alamos (LANL) effective core potentials and the Stevens effective core potentials (CEP-31G).[107] The implementation of the LANL potentials resulted in an average absolute error of 50 kcal mol^{-1}, while the CEP-31G protocol produced an average absolute error of 75 kcal mol^{-1}. The errors were reduced when the carbonyl-containing molecules were excluded, but the B3LYP/LANL and B3LYP/CEP-31G methods, on average, significantly overestimated the enthalpy of formations for the molecule set.[107]

Wavefunction-based electron correlation methods, e.g. MP2 and CCSD(T), are void of empirical parameters and, specifically CCSD(T), is a high level of theory used for comparison to experimental results. These electron structure methods are necessary for the accurate prediction of transition metal thermochemistry. CCSD(T) and MP2 calculations with Stuttgart/Dresden and LanL2DZ effective core potentials have been compared by Wu et al. to a range of density functionals for the determination of the electron affinities and ionization potentials of 4*d* atoms.[108] The selected hybrid and pure density functionals were outperformed by the wavefunction-based methods as the basis set size increased. Furthermore, Dixon et al. determined the geometries, electron affinities, fluoride affinities, and enthalpies of formation for six 4*d* hexaflourides (Mo, Tc, Ru, Rh, Pd, Ag) with a variety of DFT methods and utilized CCSD(T) calculations with correlation consistent basis sets with corresponding effective core potentials as benchmarks.[109] The only experimental value for comparison was the enthalpy of formation of MoF_6, for which the CCSD(T) level calculation was within 2 kcal mol^{-1}. Fluoride affinities, electron affinities, and bond dissociation energies calculated via DFT had deviations from the CCSD(T) results ranging from 5 kcal mol^{-1} to 28 kcal mol^{-1}. While the hybrid functionals yielded the best performance, the average deviations were still 5-6 kcal mol^{-1}.[109] Another study by Dixon et al. determined thermochemical properties, including total atomization energies and enthalpies of formation, for transition metal oxide clusters via CCSD(T) and DFT methods. The DFT results were found to degrade with increasing cluster size and performance was strongly dependent on the electronic state of the transition metal atom.[110,111]

To complement the wavefunction-based electron correlation methods, the correlation consistent basis sets can be utilized with the ab initio method to obtain accurate, parameter-free results.[9,43-45,49,98] Energies determined with the correlation consistent basis sets exhibit systematic convergence to the complete basis set (CBS) limit,[98,112] and these energies may be obtained with the correlation consistent basis sets extrapolated to the CBS limit. With the extrapolated energies, thermochemical and spectroscopic properties can be determined free of basis set truncation error.[56,113] At the CBS limit the only remaining error is intrinsically related to the choice of method.[48]

Energy-consistent relativistic pseudopotentials and accompanying correlation consistent basis sets for 4*d* transition metals (Y-Cd) have been developed by Peterson and co-workers.[114] The pseudopotentials and corresponding valence and core–valence correlation consistent basis sets contain an [Ar]3d^{10} effective core and converge to the CBS limit as the ζ-level increases. The pseudopotentials were determined through calculations with a Dirac–Coulomb Hamiltonian at the multi-configuration Dirac–Hartree–Fock (MCDHF) level.[114] The Breit interaction was included perturbatively. Through this construction scheme the pseudopotentials implicitly describe relativistic effects, e.g. scalar, magnetic interactions and retardation effects. By parametrizing relativistic effects in the pseudopotentials, a non-relativistic Hamiltonian can be used. Neutral, low-charge (0, +1, +2) and high-charge configurations were included in the reference data for the fitting of the *spd* part of the pseudopotential. Within the potential lies the mathematical description of the core charge, the Coulomb and exchange terms for the core, the Pauli-repulsion, and relativistic effects. The pseudopotentials reproduce atomic valence spectra, i.e., orbital energies and electron configurations,

when combined with a non-relativistic Hamiltonian. The maximum deviation of the pseudopotentials relative to the all-electron valence energies ranged from 0.03 eV for the yttrium atom to 0.39 eV for the palladium atom.[114] The increase in deviation across the row is as expected, since the gap between the core and valence levels decreases. For the low lying states of each atom, the absolute differences in valence energies were usually within 0.01 eV.[114] With the generation of relativistic pseudopotential and correlation consistent basis sets, the quantitative study of second row (4*d*) transition metals at the CBS limit becomes computationally amenable.

In this work, a variant of ccCA that utilizes relativistic pseudopotentials and correlation consistent basis sets, referred to as the relativistic pseudopotential ccCA (rp-ccCA), has been constructed. By utilizing the correlation consistent pseudopotentials within the ccCA methodology, larger transition metal molecules can be examined, as compared to previous CCSD(T)-based studies. Additionally, ccCA has been shown, in general, to properly describe molecules with reasonable amounts of nondynamical correlation.[68,69] Here, the accuracy, as compared to experimental data, and computational cost of rp-ccCA are examined for a greater range of molecules, whether single-reference or multireference. The accuracy and computational cost in terms of CPU times of rp-ccCA is compared to all-electron ccCA for a set of molecules containing 4*p* elements referred to as G3/05-4*p*. Upon establishment of the pseudopotential accuracy, the enthalpies of formation for 4*d* transition metal containing molecules, ranging from diatomics to carbonyl-containing systems, are evaluated with rp-ccCA and compared to experimental data. The transition metal molecule set is designated TM-4*d*.

3.2 Computational Methodology

The rp-ccCA energy calculations based on restricted open shell Hartree-Fock (ROHF) reference wavefunction were performed with MOLPRO 2009.1,[115] while the unrestricted Hartree-Fock (UHF) computations were carried out with the Gaussian 03 software package.[116] To note, for the calculations denoted ROHF, a spin-restricted HF reference is used for the coupled cluster wavefunction and, due to the coupled cluster ansatz, spin contamination is introduced in the CCSD(T) calculation.[117]

The rp-ccCA methodology follows a form similar to ccCA-TM.[68] The steps where the two schematics differ are noted. Additionally, the ccCA, ccCA-TM, and rp-ccCA schematics are listed in Table 3.1. For rp-ccCA, pseudopotentials are implemented for elements gallium through krypton[118,119] and the second row transition metals (Y-Cd), in place of the Douglas–Kroll basis sets used in ccCA-TM.[114] The optimized geometry is obtained at the B3LYP/cc-pVTZ-PP level of theory. At stationary points, harmonic vibrational frequencies are computed and scaled by 0.989 to account for anharmonicity.[68] Thermal energy corrections are computed at 298.15K and 1 atm. Upon determination of the optimized geometry, single point energy calculations are carried out at higher levels of theory in order to determine the rp-ccCA energy. To determine the reference energy of the molecule, single point energies are calculated at the MP2 level of theory with the aug-cc-pVnZ-PP (n=D, T, Q) basis sets. Unlike all-electron ccCA variants, no DKH Hamiltonian is employed in any portion of the rp-ccCA calculations since the pseudopotentials are not compatible with the DKH Hamiltonian and are constructed to account for relativistic effects from the heavy atom. Separate

extrapolations are carried out for the Hartree-Fock (HF) and MP2 energies. Feller and The Feller extrapolation is used for the determination of the HF/CBS energy:[74,120]

$$E(n) = E_{HF/CBS} + Be^{-Cn} \quad (3.1)$$

where C has previously been determined to be 1.63 by Halkier *et al*.[75] The utilization of C=1.63 for extrapolations of transition metal energies has been proven to perform well.[96] The extrapolation of the MP2 energy follows the form of a mixed exponential/Gaussian functional developed by Peterson, Woon, and Dunning,[76] stated as

$$E(n) = E_{MP2/CBS} + Be^{-(n-1)} + Ce^{-(n-1)^2} \quad (3.2)$$

where the double, triple, and quadruple-zeta level basis sets are utilized. Previous ccCA studies include additional extrapolation schemes, such as the Schwartz inverse cubic (denoted ccCA-S3). The selection of the Peterson extrapolation for the rp-ccCA development is based on previous transition metal studies with ccCA (i.e., ccCA-TM).[70] To determine the total energy of the molecule, additive corrections are applied to the HF/CBS and MP2/CBS energies.

To account for correlation effects beyond the second-order perturbation, single-point energy calculations at the CCSD(T) level of theory in conjunction with the cc-pVTZ-PP basis set are employed. The correlation correction was computed by

$$E_{CC} = [CCSD(T)/cc-pVTZ-PP] - E[MP2/cc-pVTZ-PP] \quad (3.3)$$

To adjust for core–valence correlation effects, an “FC1” calculation was utilized with CCSD(T) and the aug-cc-pCVDZ-PP basis set:

$$E_{CV} = E[CCSD(T,FC1)/aug-cc-pCVDZ-PP] - E[CCSD(T)/aug-cc-pCVDZ-PP] \quad (3.4)$$

The “FC1” Gaussian keyword denotes adding the next inner noble gas shell to the correlated molecular orbitals. For the second row transition metals, “FC1” indicates 4*s*4*p*4*d*5*s* orbitals are correlated and the 3*d* orbitals are within the pseudopotential.

For molecules, the complete rp-ccCA energy follows the form:

$$E_{rp-ccCA} = E_{HF/CBS} + E_{MP2/CBS} + E_{CC} + E_{CV} + E(ZPE) \quad (3.5)$$

while atomic rp-ccCA energies include experimental thermal corrections and spin–orbit corrections when needed.

Correlation consistent pseudopotential basis sets are available for the 4*p* elements,[118,119] which allows for comparison to all-electron calculations previously carried out with ccCA. For comparison between rp-ccCA and ccCA, dissociation energies (and ΔH_f’s when available) for the G3/05 set were determined by rp-ccCA and all-electron ccCA.[70] Additionally, ccCA-TM results were calculated for further comparison. The selected molecules in the G3/05-4*p* set are: Br_2, AsH, AsH_2, AsH_3, SeH, SeH_2, BrH, GeO, BrO, BrCl, BrF, GaCl, KrF_2, $BrCH_3$, NaBr, Br_2CO, BrC_2H_3, BrC_3H_7, $BrCCl_3$, $BrCF_3$, $Br_2C_3H_6$, $Br_2C_5H_8$, BrC_2H_5, and BrC_6H_5. Enthalpies of formation under standard conditions were computed with rp-ccCA for 30 4*d* TM-containing molecules, which compose the TM-4*d* set: YO, ZrO, ZrO_2, ZrBr, ZrCl, $ZrCl_2$, $ZrCl_4$, $ZrBr_4$, NbO, NbO_2, MoF, MoF_2, MoO_2Cl_2, MoO_2, MoF_6, MoO_3, $MoOCl_4$, $Mo(CO)_5$, $Mo(CO)_6$, RuO_4, RhC, RhO, $RhCl_2$, AgH, Cd_2, CdH, CdCl, $CdCl_2$, CdBr, and $CdBr_2$. These molecules were selected based on their size (less than 15 atoms) and presence of an experimental gas phase enthalpy of formation in the literature.

Table 3.1. Comparison of ccCA, ccCA-TM, and rp-ccCA methodology.

	ccCA	ccCA-TM	rp-ccCA
Geometry Optimization	B3LYP/cc-pVTZ	B3LYP/cc-pVTZ	B3LYP/cc-pVTZ-PP
Harmonic Frequencies	B3LYP/cc-pVTZ scaled by 0.989	B3LYP/cc-pVTZ scaled by 0.989	B3LYP/cc-pVTZ-PP scaled by 0.989
HF CBS	HF/aug-cc-pVTZ	HF/aug-cc-pVTZ-DK	HF/aug-cc-pVTZ-PP
	HF/aug-cc-pVQZ	HF/aug-cc-pVQZ-DK	HF/aug-cc-pVQZ-PP
HF CBS fit	$E(n)=E_{HF}-E_{CBS}+Bexp(-1.63n)$	$E(n)=E_{HF}-E_{CBS}+Bexp(-1.63n)$	$E(n)=E_{HF}-E_{CBS}+Bexp(-1.63n)$
MP2 CBS	MP2/aug-cc-pVDZ	MP2/aug-cc-pVDZ-DK	MP2/aug-cc-pVDZ-PP
	MP2/aug-cc-pVTZ	MP2/aug-cc-pVTZ-DK	MP2/aug-cc-pVTZ-PP
	MP2/aug-cc-pVQZ	MP2/aug-cc-pVQZ-DK	MP2/aug-cc-pVQZ-PP
MP2 CBS fit	$E(x)=E_{CBS}+Bexp[-(x-1)]+Cexp[-(x-1)^2]$	$E(x)=E_{CBS}+Bexp[-(x-1)]+Cexp[-(x-1)^2]$	$E(x)=E_{CBS}+Bexp[-(x-1)]+Cexp[-(x-1)^2]$
ΔCC	CCSD(T)/cc-pVTZ	CCSD(T)/cc-pVTZ-DK	CCSD(T)/cc-pVTZ-PP
	-MP2/cc-pVTZ	-MP2/cc-pVTZ-DK	-MP2/cc-pVTZ-PP
ΔCV	MP2(FC1)/aug-cc-pCVTZ	CCSD(T,FC1)/aug-cc-pCVDZ-DK	CCSD(T,FC1)/aug-cc-pCVDZ-PP
	-MP2/aug-cc-pVTZ	-CCSD(T)/aug-cc-pCVDZ-DK	-CCSD(T)/aug-cc-pCVDZ-PP
ΔDK	MP2/cc-pVTZ-DK	Included in each energy calculation	Included in potential
	-MP2/cc-pVTZ		
ΔSO	Experimental atomic values	Experimental atomic values	Experimental main group atomic values
		FOCI Stuttgart ECP for molecules	

3.3 Results and Discussion

3.3.1 G3/05-4*p* Set

3.3.1.1 Overall Statistics

Before evaluating rp-ccCA for a molecule set of second row transition metal species, the performance must be compared to energetic properties obtained by all-electron versions of ccCA, i.e., main group ccCA and ccCA-TM, for an established training set. As a result, the G3/05-4*p* set containing 25 molecules (Table 3.2) with 4*p* elements (Ga – Kr) is used. The molecular properties for assessment were the dissociation energy (D_0) for the smaller molecules (oxides, hydrides, halides, and methyl-substituted) and the enthalpy of formation (ΔH_f) for the larger bromine-containing molecules. The electronic ground states, experimental D_0 and ΔH_f values, and deviations from experimental data for rp-ccCA, ccCA-TM, and ccCA are listed in Table 3.2. The MAD for rp-ccCA in comparison to experiment is 0.89 kcal mol^{-1}, which is almost the same as the ccCA-TM MAD of 0.85 kcal mol^{-1}, and only slightly inferior to the ccCA MAD of 0.76 kcal mol^{-1}. However, all three methodologies are within the targeted main group chemical accuracy, with an MAD less than or equal to 1.0 kcal mol^{-1}. The mean signed deviations (MSDs), 0.42 kcal mol^{-1} for ccCA, 0.00 kcal mol^{-1} for ccCA-TM, and 0.07 kcal mol^{-1} for rp-ccCA, indicate almost no overall bias for rp-ccCA and no bias for ccCA-TM. Previously, ccCA and ccCA-TM have been proven to be reliable methodologies, and with the results presented here, the replacement of all-electron basis sets with pseudopotentials does not adversely affect the accuracy of ccCA.

Table 3.2. The ccCA, ccCA-TM and rp-ccCA signed deviations from experiment and statistical analysis for molecules containing 4*p* elements. Units are in kcal mol^{-1}.

Property	Species	Exptl. Ground State[121]	ccCA Signed Deviation[a]	ccCA-TM Signed Deviation[a]	rp-ccCA Signed Deviation[a]	Expt.
D_o	GaCl	$^1\Sigma^+$	0.4	0.8	0.6	109.9
	GeO	$^1\Sigma^+$	-2.0	-2.2	-2.1	155.2
	AsH	$^3\Sigma^-$	1.5	1.0	0.8	64.6
	AsH_2	$^2B_1$	-0.5	-0.5	-0.8	131.1
	AsH_3	$^1A_1$	0.6	0.1	0.1	206.0
	SeH	$^2\Pi$	-0.2	-0.6	-0.7	74.3
	SeH_2	$^1A_1$	-0.2	-0.8	-1.1	153.2
	Br_2	$^1\Sigma_g^+$	-0.6	-1.1	-1.1	45.4
	BrH	$^1\Sigma^+$	-0.9	-1.1	-1.1	86.5
	BrO	$^2\Pi$	0.9	1.2	1.0	55.3
	BrF	$^1\Sigma^+$	0.1	0.7	0.5	58.9
	NaBr	$^1\Sigma^+$	-0.1	-0.9	0.0	86.2
	BrCl	$^1\Sigma^+$	0.1	0.4	0.3	51.5
	$BrCH_3$	$^1A_1$	-0.4	-0.3	-0.8	358.2
	KrF_2	$^1\Sigma_g^+$	0.3	0.1	-1.6	21.9
ΔH_f(298K)	BrC_2H_3		1.5	0.3	1.0	18.9
	$BrCF_3$		0.5	-1.0	-0.2	-155.0
	$BrCCl_3$		0.9	0.6	1.2	-10.0
	BrC_3H_7		0.6	1.1	0.3	-23.8
	Br_2CO		1.4	0.7	1.2	-27.1
	BrC_2H_5		1.3	0.7	1.3	-14.8
	BrC_6H_5		-0.2	-1.4	0.4	25.2
	$Br_2C_3H_6$		2.2	2.0	2.2	-17.1
	$Br_2C_5H_8$		2.9	0.1	0.3	-13.1
MSD			0.42	0.00	0.07	
MAD			0.76	0.85	0.89	
RMSD			1.12	0.97	1.03	
Standard Deviation			0.92	0.99	1.05	

[a] Signed deviation determined by experimental value minus theoretical value.

3.3.1.2 CPU Time Savings

The computational CPU times by rp-ccCA are compared to all-electron calculations by ccCA-TM (Table 3.3). Comparisons between rp-ccCA and ccCA are less meaningful as different methods (CCSD(T) versus MP2) have been used for the core–valence correction step. The all-electron basis sets and the pseudopotentials have the same number of valence electrons for the corresponding correlated calculation step (see Table 3.1 for details), i.e., MP2 or CCSD(T); therefore, the CPU time savings is rooted in the HF calculation due to a reduction in the number of explicit electrons and orbitals and in correlation methods due to an effective reduction in external orbital space. It is understood that computations using ECPs will have reduced computational cost in comparison to all-electron basis sets due to reduced requirements in the SCF procedure and the initial computation of integrals, albeit there is a slight tradeoff in the accuracy of energies when utilizing pseudopotentials.[118] A quantitative comparison of the CPU time is given as follows. The pseduopotential percent CPU time savings ranges from 7% for $Br_2C_3H_6$ to 67% for BrO, with an overall average CPU time savings of 32.5%. Since both rp-ccCA and ccCA-TM are composite approaches, the examination of the rp-ccCA computational time savings for each step is warranted. The largest average CPU time savings (40%) was observed for the utilization of the pseudopotential basis set in place of the Douglas–Kroll basis set for the MP2/aug-cc-pVTZ step. Here and in the following text, the appendices of DK for the Douglas-Kroll basis set and PP for the pseudo-potential basis set are omitted for clarity. Overall, rp-ccCA not only obtains results in agreement with experimental, ccCA, and ccCA-TM values, but gives a 32.5% CPU time savings over ccCA-TM and a similar HF

convergence for molecules where correlation consistent pseudopotentials and accompanying basis sets are available.

Table 3.3. Percent of CPU time savings of rp-ccCA relative to ccCA-TM for each step within the composite method for the 4*p* molecule set.

Composite method Components [a]	Percent CPU time savings
MP2/aug-cc-pVDZ	23.0
MP2/aug-cc-pVTZ	40.2
MP2/aug-cc-pVQZ	35.4
CCSD(T,FC1)/aug-cc-pCVDZ	15.0
CCSD(T)/aug-cc-pCVDZ	20.3
CCSD(T)/cc-pVTZ	24.3
Overall	32.5

[a] The appendices of DK for the Douglas-Kroll basis set and PP for the pseudo-potential basis set (e.g. aug-cc-pVDZ-DK) are omitted for clarity.

3.3.2 TM-4d Set

3.3.2.1 Overall Statistics

The 30 4*d* molecules and their electronic ground states are included in Table 3.4. For the complete TM-4*d* set, the MAD of ROHF-rp-ccCA is 2.89 kcal mol^{-1}, compared to 3.29 kcal mol^{-1} for UHF-rp-ccCA. Transition metal chemical accuracy[70] was previously defined as a MAD of less than 3 kcal mol^{-1}, and ROHF-rp-ccCA is within the threshold of this definition. To note, the average experimental uncertainty for the 4*d* molecule set is 3.43 kcal mol^{-1}. Experimental data for molecules containing only main group elements has been reported with smaller uncertainties, e.g. overall less than 2 kcal mol^{-1},[109] while transition metal species tend to be associated with larger experimental uncertainties. Since the rp-ccCA MADs are within the average experimental uncertainty for the set, the validity of the rp-ccCA method is statistically supported.

Table 3.4. Signed deviations of UHF-and ROHF-rp-ccCA enthalpies of formation (ΔH_f) at 298.15 K as compared with experiment. Units are in kcal mol^{-1}.

Molecule	Ground State	UHF rp-ccCA deviation	ROHF rp-ccCA deviation	Expt.
YO	$^2\sum^+$ [122]	-9.8	-9.5	-11.0 ± 2.5 [123]
ZrO	$^1\sum^+$ [122]	-0.9	-0.8	21.8 [123]
ZrO_2	$^1A_1$ [124]	-2.4	-2.2	-68.4 ± 11.0 [125]
ZrCl	$^2\Delta$ [104]	3.0	2.6	67.6 ± 5.7 [123]
$ZrCl_2$	$^3\Delta$ [126]	3.2	2.4	-34.9 ± 3.6 [123]
$ZrCl_4$	$^1A_1$ [127]	4.1	3.6	-208.0 ± 0.6 [123]
ZrBr	$^2\Delta$ [127]	-3.8	-3.5	71.9 ± 0.5 [125]
$ZrBr_4$	$^1A_1$ [127]	-2.5	-2.4	-166.0 ± 2.0 [123]
NbO	$^4\sum^-$ [122]	-3.7	-3.4	47.5 ± 5.0 [128]
NbO_2	$^2A_1$ [124]	-4.5	-4.1	-47.8 ± 5.0 [125]
MoO_2	$^3B_1$ [124]	0.3	0.1	-2.0 ± 3.0 [125]
MoO_3	$^1A_1$ [124]	0.2	0.2	-86.7 ± 5.0 [123]
$MoOCl_4$	$^1A_{1g}$ [129]	0.7	0.6	-135.9 ± 1.4 [123]
MoO_2Cl_2	$^1A_{1g}$ [130]	0.1	0.1	-151.6 ± 3.5 [125]
MoF	$^6\sum^+$ [105]	1.6	0.7	67.6 ± 3.0 [125]
MoF_2	$^5B_2$ [126]	2.1	1.4	-38.9 ± 4.0 [125]
MoF_6	$^1A_{1g}$ [131]	7.0	5.9	-372.3 ± 2.2 [123]
$Mo(CO)_5$	$^1A_1$ [132]	3.5	2.4	-157.5 ± 5.0 [123]
$Mo(CO)_6$	$^1A_1$ [133]	7.4	6.3	-219.0 ± 1.1 [123]
RuO_4	$^1A_1$ [124]	-1.2	-0.9	-46.0 ± 1.0 [133]
RhC	$^2\sum^+$ [105]	-1.9	-1.8	164.1 ± 2.3 [123]
RhO	$^4\sum^-$ [122]	-1.1	-0.8	97.9 ± 10.0 [123]
$RhCl_2$	$^4\sum^-$ [126]	-7.5	-6.4	30.0 ± 3.0 [123]
AgH	$^1\sum^+$ [134]	-1.7	-1.0	66.3 [123]
Cd_2	$^1\sum^+$ [128]	-0.5	-0.5	51.4 [123]
CdH	$^2\sum^+$ [134]	-8.8	-8.7	62.3 [123]
CdCl	$^2\sum^+$ [104]	-5.9	-5.7	6.6 [123]
$CdCl_2$	$^1\sum^+$ [126]	-3.7	-3.7	-46.5 ± 1.1 [123]
CdBr	$^2\sum^+$ [104]	-3.0	-2.7	15.9 [123]
$CdBr_2$	$^1\sum^+$	-2.7	-2.2	-33.5 ± 1.1 [123]
Open Shell MSD		-3.11	-2.63	
Open Shell MAD		4.01	3.59	4.00 [a]
Open Shell RMSD		4.85	4.52	
Open Shell Std. Dev.		4.09	3.68	

Closed Shell MSD	-1.03	0.36	
Closed Shell MAD	2.41	2.05	2.90 [a]
Closed Shell RMSD	3.38	2.89	
Closed Shell Std. Dev	3.68	2.87	
Overall MSD	-2.63	-1.13	
Overall MAD	3.29	2.89	3.43 [a]
Overall RMSD	4.18	3.79	
Overall Std. Dev.	4.33	3.62	

[a] The average value of reported experimental uncertainties.

The TM-4*d* set is composed of 15 closed shell and 15 open shell molecules, warranting the investigation of the performance of rp-ccCA for closed shell versus open shell molecules, which are often more challenging for theoretical methods. The MADs of UHF- and ROHF-rp-ccCA (3.93 and 3.59 kcal mol^{-1}, respectively) are both within the average experimental uncertainty of 4.00 kcal mol^{-1} for open shell molecules. For closed shell molecules, the average experimental uncertainty is 2.90 kcal mol^{-1}, smaller than that of the open shell set, and UHF- and ROHF-rp-ccCA results (MADs of 2.41 and 2.05 kcal mol^{-1}, respectively) are within the average experimental uncertainty and more accurate than open shell molecules. While the molecular energies are the same for both UHF- and ROHF-rp-ccCA for closed shell molecules, the larger MAD of UHF-rp-ccCA originates from the difference in the atomic energies for open shell constitute atoms. Even though the size of the TM-4*d* set does not allow sub-categorization based on the range of experimental uncertainty, the two subsets of open and closed shell molecules do indicate a positive correlation between the accuracy of rp-ccCA and the experimental uncertainty.

Statistical analysis beyond the MAD includes the mean signed deviations (MSDs), root mean square (RMS) and standard deviation (σ) of rp-ccCA (Table 3.4).

Again, the results have been grouped into closed shell, open shell, and the complete set. On average, both UHF- and ROHF-rp-ccCA overestimate the enthalpy of formation for the 4*d* molecules. Overall, the ROHF-rp-ccCA results in an improvement of the MAD by 0.40 kcal mol^{-1} over UHF-based rp-ccCA. The scatter plot of Figure 3.1 depicts the ROHF-rp-ccCA enthalpy of formation relative to the experimental value. With an R^2 value of 0.9993 and a slope of 1.017, ROHF-rp-ccCA determines gas phase enthalpies of formation with minimal systematic error. The intercept value is positive (1.7433), indicating that ROHF-rp-ccCA overestimates the enthalpies of formation for the TM-4*d* set.

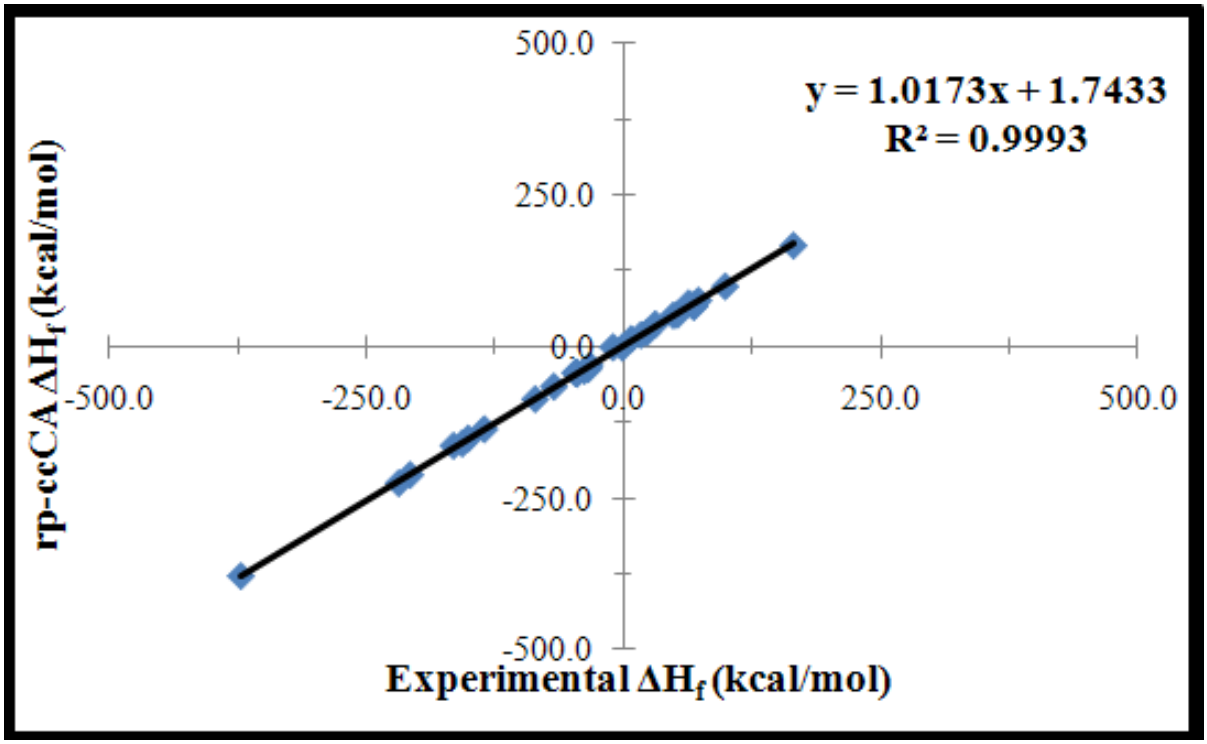

Figure 3.1. rp-ccCA computed enthalpies of formation versus experimental enthalpies of formation for the TM-4*d* set. Units are in kcal mol^{-1}.

3.3.2.2 Spin Contamination and T1/D1 diagnostics

As previously mentioned, prior ccCA developments, namely ccCA-TM,[70] made note of the pronounced spin contamination for the first row transition metals studied. The MADs for the UHF- and ROHF-ccCA-TM were different by more than one kcal mol^{-1}, with the ROHF-based method yielding the lower MAD. Compared to the difference of more than one kcal mol^{-1} for ccCA-TM for 3*d* transition metals, the discrepancy between the UHF- and ROHF-based MADs for rp-ccCA is smaller (0.40 kcal mol^{-1}), but the discrepancy is still of great significance. The smaller discrepancy between UHF and ROHF-based rp-ccCA as compared to the ccCA-TM results may be ascribed to the greater energy splitting between the 5*s* and 4*d* atomic orbitals, and thus less mixing of these two types of orbitals, as compared to the 4*s* and 3*d* atomic orbitals of the first row transition metals.[114] Though the rp-ccCA results may point to negligible spin contamination in the second row transition metal molecule set, the possibility of spin contamination, as well as multireference character, were investigated. The expectation value of S^2-S_z^2-S_z and the T_1/D_1 diagnostics, for spin contamination and multireference character analysis respectively, are reported in Table 3.5. The expectation values and diagnostics were determined by CCSD(T) with the aug-cc-pVDZ-PP basis set. For open shell molecules, the implementation of a UHF-based method may significantly reduce the accuracy of an *ab initio* calculation. UHF theory uses different orbitals for alpha and beta electrons. While this often leads to lower atomic/molecular energies, it may result in an artificial mixing of states with higher spin multiplicity because the UHF wavefunction is not an eigenfunction of the S^2 operator, the square of the total electronic spin angular momentum.[135] The ROHF calculations are based on a single

configuration; therefore, the ROHF wavefunction is an eigenfunction of the S^2 operator. The single configuration of ROHF is composed of doubly and singly occupied molecular orbitals, where the different spins are not separately optimized.[136] Even though spin contamination may be introduced in subsequent correlation calculations such as UCCSD(T), the amount of spin contamination is usually much less significant than UMP2 and UCCSD(T) based on UHF wavefunction. Examination of the $<S^2\text{-}S_z^2\text{-}S_z>$ expectation values for the open shell 4*d* molecules reveals values on the order of thousandths and, therefore, spin contamination is not a factor in the deviation of ROHF-rp-ccCA.

Table 3.5. The T_1 and D_1 diagnostic values, T_1/D_1 ratio, and $S^2\text{-}S_z^2\text{-}S_z$ expectation value (for open shell molecules) for the 4*d* set of molecules.

Molecule	T_1	D_1	T_1/D_1	$<S^2\text{-}S_z^2\text{-}S_z>$
YO	0.0352	0.0794	0.4432	0.0003
ZrO	0.0288	0.0757	0.3812	
ZrO_2	0.0290	0.0861	0.3368	
ZrCl	0.0198	0.0485	0.4087	0.0060
$ZrCl_2$	0.0179	0.0421	0.4243	0.0024
$ZrCl_4$	0.0126	0.0536	0.2345	
ZrBr	0.0226	0.0457	0.4956	0.0064
$ZrBr_4$	0.0123	0.0593	0.2070	
NbO	0.0394	0.0756	0.5206	0.0033
NbO_2	0.0408	0.0861	0.4743	0.0063
MoO2	0.0485	0.1186	0.4088	0.0022
MoO_3	0.0297	0.1263	0.2355	
$MoOCl_4$	0.0192	0.1281	0.1502	
MoO_2Cl_2	0.0204	0.0968	0.2106	
MoF	0.0301	0.0624	0.4818	0.0029
MoF_2	0.0266	0.0832	0.3198	0.0026
MoF_6	0.0246	0.1061	0.2322	
$Mo(CO)_5$	0.0194	0.0651	0.2980	
$Mo(CO)_6$	0.0184	0.0493	0.3722	
RuO_4	0.0281	0.1039	0.2700	
RhC	0.0298	0.0499	0.5978	0.0004
RhO	0.0720	0.1828	0.3937	0.0042

Molecule	T_1	D_1	T_1/D_1	$<S^2-S_z^2-S_z>$
AgH	0.0241	0.1031	0.2338	
Cd_2	0.0123	0.0530	0.2318	
CdH	0.0267	0.0671	0.3978	0.0012
CdCl	0.0224	0.0654	0.3432	0.0006
$CdCl_2$	0.0100	0.0623	0.1602	
CdBr	0.0253	0.0741	0.3414	0.0008
$CdBr_2$	0.0094	0.0623	0.1506	

T_1 and D_1 diagnostics are utilized in order to examine the multireference character of the 4*d* molecules. While the diagnostics are a qualitative guide, cutoff values for the diagnostics have been suggested, e.g. for main group species, when a T_1 diagnostic value is greater than 0.02 and a D_1 value is greater than 0.05, single-reference electron correlation methods may not be reliable.[137] Both diagnostic values from CCSD/aug-cc-pVDZ-PP calculations are reported since T_1 values reflect the overall quality of the single-reference wavefunction, while D_1 values may pinpoint local problem areas for the molecule.[138] The ratio T_1/D_1 describes the homogeneity of the system, where a T_1/D_1 value of $\frac{1}{\sqrt{2}}$ indicates a homogeneous system.[138]

For this molecule set, the T_1, D_1 and T_1/D_1 values are reported in Table 3.5. There are eleven molecules with a T_1 diagnostic value less than 0.02 (ZrCl, $ZrCl_2$, $ZrCl_4$, $ZrBr_4$, $MoOCl_4$, MoO_2Cl_2, $Mo(CO)_5$, $Mo(CO)_6$, Cd_2, $CdCl_2$, $CdBr_2$). The MAD for the subset is 2.85 kcal mol^{-1} for UHF-rp-ccCA and 2.44 kcal mol^{-1} for ROHF-rp-ccCA. Within the subset, only two of the molecules have large D_1 values, 0.1281 for $MoOCl_4$ and 0.0968 for MoO_2Cl_2, but both have very small rp-ccCA deviations (0.6 kcal mol^{-1} and 0.1 kcal mol^{-1} respectively). Consequently, for the molecules within the single-reference T_1 requirement, rp-ccCA performs well, which is expected since rp-ccCA is

composed of single-reference electron correlation steps. There is one significant outlier, $Mo(CO)_6$, within the single-reference character molecules. The UHF-rp-ccCA deviation is 7.4 kcal mol^{-1} and the ROHF-rp-ccCA deviation is 6.3 kcal mol^{-1}. The closed shell, single-reference $Mo(CO)_6$ should be accurately described by rp-ccCA and the resulting deviations suggest the experimental value for the enthalpy of formation may need to be re-evaluated (*vida infra)*. An example of a molecule on the border of the cutoff for the diagnostic values, ZrO_2 (T_1=0.0290, D_1=0.0861), has been included in a CCSD(T) study by Li et al.[111] The diagnostic values suggest that ZrO_2 should still be accurately described by a single-reference method, e.g. CCSD(T). The rp-ccCA ΔH_f for ZrO_2 is -66.2 kcal mol^{-1}, in good agreement with the experimental value of -68.4±11.0 kcal mol^{-1} from the NIST-JANF tables[123] and the previously calculated CCSD(T) value of -67.4 kcal mol^{-1}. The underestimation of the calculated values in comparison to experimental values was also observed in our laboratory for the 3*d* transition metal molecule TiO_2, where the comparison included the CCSD(T)-based value and ccCA-TM.[72] The agreement between rp-ccCA and the high level of theory, CCSD(T), further validates the composite method results, specifically for molecules with single-reference character.

There are six molecules (MoO_2, MoO_3, $MoOCl_4$, MoF_6, RhO, $RhCl_2$) with D_1 > 0.1, significantly greater than the 0.05 cutoff. For this subset of six molecules, UHF-rp-ccCA yields an MAD of 2.80 kcal mol^{-1}, while ROHF-rp-ccCA has an MAD of 2.33 kcal mol^{-1}. The experimental ΔH_f for MoO_3 as reported in the Yungman compendium[125] (-86.7±5.0 kcal mol^{-1}) is different from the value (-82.8±5.0 kcal mol^{-1}) from the NIST-JANAF tables.[123] The rp-ccCA prediction of -86.5 kcal mol^{-1} is closer to the former data

by a deviation of 0.2 kcal mol^{-1}. Apparently, the performance of rp-ccCA does not deteriorate with the presence of multireference character in the molecular system. Among the molecules, RhO has the largest diagnostic values, a T_1 value of 0.0720 and a D_1 value of 0.1828. Even though both diagnostics indicate RhO may not be reliably described by a single-reference method, the signed deviations of UHF- and ROHF-based rp-ccCA for RhO are only -1.1 and -0.8 kcal mol^{-1} respectively, as compared to the experimental uncertainty of 10 kcal mol^{-1}.

In the study by Li et al.,[111] total atomization energy (TAE) at 0 K and ΔH_f at 298K were determined for ZrO_2 and MoO_3 by CCSD(T) energies extrapolated to CBS limit with the correlation consistent basis sets and ECPs. The rp-ccCA TAE for ZrO_2 is 324.1 kcal mol^{-1}, compared to 328.5 kcal mol^{-1} obtained by CCSD(T).[111] Similarly for MoO_3, rp-ccCA obtained a TAE of 417.6 kcal mol^{-1}, while Li et al. reported 412.3 kcal mol^{-1}. The large D_1 diagnostic value (0.1263) for MoO_3 suggests the open-shell coupled cluster wavefunction may not be appropriate. The observed discrepancy between rp-ccCA and CCSD(T) may be attributed to this molecular quality. Additionally, Jiang et al.[51] utilized ccCA-TM for the TAE of first row transition metal oxides (CrO_3 and TiO_2) included in the test of Li et al.[111] The comparison of ccCA-TM to the CCSD(T) results revealed good agreement between the values for TiO_2 and a deviation between the values for CrO_3. The evaluation of ccCA-TM, the study by Li et al., and experimental values revealed the CCSD(T)-based result was lower than the experimental value for TiO_2, but higher for CrO_3.[51] Therefore, for comparison to CCSD(T)-based calculations of molecules with possible multireference character results need to be evaluated individually.

3.3.2.3 Statistical Outliers

There are five molecules within the overall TM-4*d* set where the ROHF-rp-ccCA results deviate by nearly or more than six kcal mol^{-1}. The signed deviations are -9.5, 5.9, -6.4, -8.7, and -5.7 kcal mol^{-1} for YO, MoF_6, $RhCl_2$, CdH, and CdCl, respectively. For the cadmium molecules CdH and CdCl, the reported experimental values in the Yungman compendium do not include any experimental uncertainties.[125] Additionally, the T_1 and D_1 values are close to the diagnostic threshold values and rp-ccCA is expected to perform well for CdH and CdCl; therefore, further experimental studies or high level, e.g. CCSD(T)/CBS, calculations are warranted to address the discrepancy between experiment and rp-ccCA results. Additional work or multireference calculations may be needed for $RhCl_2$ and MoF_6, since their D_1 values are larger than 0.10. YO has the largest rp-ccCA deviation, -9.5 kcal mol^{-1}, in absolute value from the experimental data with an error bar of 2.5 kcal mol^{-1}. The diagnostic values (T_1 = 0.0352 and D_1 = 0.0794) for YO beyond the threshold values suggest the salient presence of multireference character might be the reason for the incongruity.

3.3.2.4 Dissociation Energies

In Table 3.6 bond dissociation energies (BDEs) are reported for $Mo(CO)_6$ and MoF_6. Previous calculations done with CCSD(T), by Ehlers and Frenking,[139] and DFT, by Ziegler et al.,[140] have yielded the first BDE of the hexacarbonyl $Mo(CO)_6$ as 40.4 and 42.5 kcal mol^{-1}, respectively. The experimental value obtained by photodissociation is 40.5 ± 2.0 kcal mol^{-1}.[141] The BDE determined by ROHF-rp-ccCA for the reaction $Mo(CO)_6 \rightarrow Mo(CO)_5+CO$ is 39.9 kcal mol^{-1}, which agrees well with the experimental data and CCSD(T) prediction. While the BDE for the hexacarbonyl is within

experimental uncertainty, the ROHF-rp-ccCA ΔH_f for $Mo(CO)_6$ deviates by 6.3 kcal mol^{-1} from experiment, while the ROHF-rp-ccCA ΔH_f for $Mo(CO)_5$ deviates by only 2.4 kcal mol^{-1}, suggesting the experimental value may need to be revisited for $Mo(CO)_6$.

The dissociation energy of 86.4 kcal mol^{-1} determined by rp-ccCA for MoF_6 agrees well with the value of 86.0 kcal mol^{-1} reported by Dixon et al.[109] using CCSD(T) with ECPs. Experimental values are currently not available for this reaction. The agreement between rp-ccCA, CCSD(T), and experimental values for the dissociation energies of the molybdenum molecules supports the reliable application of rp-ccCA for the determination of energetic properties.

Table 3.6. Dissociation energies (in kcal mol^{-1}) for molybdenum hexa-substituted reactions.

	rp-ccCA	CCSD(T)	DFT [b]	Expt.
$Mo(CO)_6 \rightarrow Mo(CO)_5+CO$	39.9	40.4 [53,a]	42.5 [54]	40.5 ± 2 [55]
$MoF_6 \rightarrow MoF_5+F$	86.4	86.0 [24,c]		

[a] MP2 optimized geometries are used. A small core ECP is used for the metal atom and the 6-31G(d) basis set for the carbon and oxygen atoms.
[b] The density functional is composed of a Stoll-type correlation functional and Becke non-local exchange functional. See reference 54 for further details.
[c] Dissociation energy calculated as sum of: extrapolated CCSD(T) energies to the complete basis set limit via mixed/Gaussian exponential formula, the zero point energy, a core–valence correction, a relativistic correction, and a spin–orbit correction.

3.4 Conclusions

By implementing pseudopotentials within a parameter-free MP2-based composite method, the thermochemistry of molecules containing heavier elements such as 4*p* elements and second row (4*d*) transition metals can be addressed. Specifically, the well-established ccCA method for main group molecules has been extended to

include relativistic pseudopotentials (rp-ccCA) for 4*d* transition metals. The performance of rp-ccCA has been examined in comparison to ccCA-TM for the G3/05-4p set and a 32.5% CPU time savings in computational cost was achieved. The rp-ccCA has also been benchmarked for the calculation of enthalpies of formation for 4*d* transition metal-containing molecules. For the TM-4*d* set, UHF- and ROHF-rp-ccCA MADs of 3.29 kcal mol^{-1} and 2.89 kcal mol^{-1} were obtained respectively, both lower than the average experimental uncertainty of 3.43 kcal mol^{-1}. The impact of spin contamination and multireference character on the molecule set was examined and overall neither was found to significantly increase the deviation of the ROHF-rp-ccCA results from experiment.

With the development of a pseudopotential composite method, the realm of *ab initio* computations can be expanded to include larger and more diverse molecules containing heavier elements for which small-core psuedopotentials and corresponding correlation consistent basis sets exist. The implementation of rp-ccCA greatly extends the applicability of ccCA and significantly contributes to the ccCA family as a pan-periodic model. rp-ccCA method, as a relativistic pseudopotential composite method for transition metals, is recommended as a reliable approach to complement and/or guide experimental studies of thermochemical properties of second-row transition metals.

CHAPTER 4

EXAMINING THE HEAVY P-BLOCK WITH A PSEUDOPOTENTIAL-BASED COMPOSITE METHOD: ATOMIC AND MOLECULAR APPLICATIONS OF RP-CCCA*

4.1 Introduction

Molecules containing 5*p* (In-I) and 6*p* (Tl-At) elements have magnetic, energetic, spectral, and thermal properties with applications as intermediates for hydrogen storage,[142] as precursors for semiconductors,[143] as catalysts for the partial hydrogenation of acetylene to ethylene,[144] and in nanotechnology applications where *p*-block clusters can be used in the synthesis of nanoparticles.[145] Theoretical studies can aid in the experimental design and development of these applications; for example, knowledge about the HOMO-LUMO can provide insight into whether or not a material will be a useful conductor. Recently first principle studies have been able to guide experimental work in the design of novel conducting oxide materials via doping with indium,[146] in the development of small molecule organic solar cells,[147] and in the design of novel catalysts with improved reactivity and enhanced product selectivity.[148] First principle energetic calculations can be used in conjunction with optical experimental studies to predict the molecular electronic structure. With theoretical energetic, spectroscopic, and thermodynamic data of the lower *p*-block molecules in combination with experiment, insight about the reactivity and stability of the 5*p*- and 6*p*-containing molecules can be gained, which can give rise to the design of ligands for

* This chapter has been published in M.L. Laury and A. K. Wilson, "Examining the Heavy p-Block with a Pseudopotential-based Composite Method: Atomic and Molecular Applications of rp-ccCA," *J. Chem. Phys*. **137**, 214111 (2012).

supramolecules[149] and semiconducting species for radiation detectors,[150] in addition to the previously mentioned applications.

The accuracy of theoretical methods, specifically ab initio methods, is dependent on the method and basis set selection. For high accuracy results, high-level methods, such as coupled cluster singles, doubles, and perturbative triples [CCSD(T)] and large, balanced basis sets are needed. Furthermore, for the lower *p*-block elements, it is necessary to include both scalar and spin-orbit relativistic effects in the calculation.[100,151,152] To calculate the relativistic effects, the Dirac equation can be utilized, resulting in a computationally expensive four-component approach.[80] However, the transformation of the Dirac Hamiltonian to a two-component approach via an approximate decoupling of the large and small components results in the Douglas-Kroll-Hess (DKH) Hamiltonian can provide a useful, less costly alternative. The second-order DKH Hamiltonian has proven to be an effective method for the inclusion of scalar relativistic effects within an all-electron calculation.[83,153] To account for the remaining relativistic effects, namely spin-orbit coupling, a variety of approaches are available, including spin-orbit pseudopotentials[85,154] and the Breit-Pauli operator.[155] Accounting for relativistic effects for the lower p-block elements has a larger computational cost, with respect to disk space, memory, and central processing unit (CPU) time, than for molecules composed of main group elements with a similar number of atoms. In order to mitigate the computational cost, composite methods and relativistic pseudopotentials can be implemented.

Small core relativistic pseudopotentials and corresponding valence basis sets have been developed by Peterson and co-workers for the 5*p* and 6*p* elements.[118,119,156]

The small core pseudopotentials have an [Ar]3d^{10} core for the 5*p* elements and a [Kr] 4d^{10}4f^{14} core for the 6*p* elements. The accuracy of the 5*p* and 6*p* valence basis sets and pseudopotentials developed by Peterson and co-workers has been established through molecular energetic calculations.[157] With the development of the 5*p* and 6*p* pseudopotentials, the application of rp-ccCA to these elements can be examined.

While computational studies of lower *p*-block molecules have been intermittent throughout the past two decades, the lower group 13-17 elements have been gaining interest in recent years due to their semiconductor-like properties and utilization in catalysis.[158] Early calculations were carried out by Balasubramanian and co-workers in order to determine electronic states, potential energy surfaces, and spectroscopic properties of various lower *p*-block containing molecules, such as TeH_2, PoH_2, and BiH.[159] CASSCF and SOCI calculations were employed for the comparison of the low-lying states of the molecules and spectroscopic properties. Preuss and co-workers examined the influence of core-core overlap and core-valence correlation on the spectroscopic properties of diatomics, including dimers, hydrides, and oxides, of In, Sn, and Sb.[160] In the work of Preuss *et al.*, CASSCF and CISD with energy-consistent pseudopotentials in which relativistic effects have been implicitly included, were utilized with pseudopotentials for the heavy elements and average deviations of 6.9 kcal mol^{-1} were observed between experimental dissociation energies and the calculated results.

In addition to the study of individual molecules, periodic trends, i.e., 6*p* versus 7*p,* have been examined including the relativistic effects and electron correlation effects on hydrides and halides containing group 13 elements. The quadratic configuration interaction (QCI) trend analysis by Schwerdtfeger, Dolg, and co-workers concluded that

the lower valencies observed in molecules with heavy elements is due to the trend of weaker bonding enthalpies as the atomic number increases and the dissociation of MX_3 (M is a *p*-block element, X is a halide) becomes more exergonic when moving down the group 13 elements.[161] The contribution of relativistic effects to various lower *p*-block atomic and molecular properties, such as bond lengths, atomization energies, ionization potentials, and dissociation energies, has been widely examined with ab initio methods and density functional theory.[156,161-163] Rather than include details from each study, the importance of scalar relativistic effects and spin-orbit coupling for the heavier elements (In-Xe and Tl-Rn) is noted elsewhere.[162,163] As previously mentioned, in order to mitigate the computational cost associated with ab initio calculations of heavy elements, core potentials may be introduced to decrease the number of correlated electrons in the calculation. Both model potentials and pseudopotentials have been employed in late *p*-block calculations and similar accuracy levels were obtained.[118,119,156,164]

Recent development of the correlation consistent basis sets to accompany small core relativistic pseudopotentials for the outer core electron correlation [(n-1)*spd*],[156] in addition to the previously developed correlation consistent basis sets for valence *nsp* correlation,[118,119] has provided the necessary components to extend the application of rp-ccCA past the second row transition metals. In this work, a series of 80 energies – which we refer to as the LP80 data set – was considered, including the electron affinities and ionization potentials of the 5*p* and 6*p* elements were determined with rp-ccCA. For the molecular applications, the dissociation energies and enthalpies of formation at 298 K of XH, XO, and X_2 (X=In-I, Tl-At) were determined. Additionally, to consider systems larger than diatomics, the total atomization energies were calculated

for the Pb_n clusters, n=2-6. Overall, the LP80 set includes 10 electron affinities, 10 ionization potentials, 30 dissociation energies (10 mono-hydrides, 10 mono-oxides, 10 dimers) and 30 enthalpies of formation (10 mono-hydrides, 10 mono-oxides, 10 dimers).

4.2 Computational Methodology

Geometry optimizations and single-point energy calculations were carried out with GAUSSIAN 09, Revision A.02.[165] The spin-orbit coupling calculations were performed using Molpro 2009.1.[115] The rp-ccCA methodology is detailed in Chapter 3.2. Smal core pseudopotentials (PP) were used for the *5p* and 6*p* elements,[118,119,156] while the corresponding (aug-)cc-pV*n*Z basis sets were used for the main group elements. The geometry optimization was obtained at the B3LYP/cc-pVTZ-PP level of theory. While B3LYP was selected in the original development of rp-ccCA, the effect of functional selection was examined. The impact on the rp-ccCA energy when other density functionals have been utilized in geometry optimizations was considered. The functionals were selected for their performance in prior studies of transition metal species (B97-1), for inclusion of a dispersion correction (B97-D), to examine a widely-used hybrid generalized gradient approximation (HGGA) functional (PBE1PBE), and compare a GGA functional to the HGGA (PBEPBE).

The molecular spin-orbit coupling corrections were computed with the aug-cc-pVDZ-PP basis set for the 5*p* and 6*p* elements and aug-cc-pVDZ for the main group elements. The multi-configuration self-consistent field (MCSCF) program multi in Molpro 2009 was employed for the spin-orbit coupling (SOC) calculations. The atomic SOC values were determined from the atomic energy levels.[166]

The mean absolute deviations (MADs), mean signed deviations (MSDs), standard deviations (σ), and root mean square deviations (RMSDs) were calculated for the rp-ccCA energetic property values in comparison to the reported experimental properties.

4.3 Results and Discussion

4.3.1 Atomic Properties

4.3.1.1 Electron Affinity (EA)

The electron affinities of the 10 atoms, indium through iodine and thallium through astatine, were computed with rp-ccCA and compared to experimental values as well as previously reported CCSD(T)/aug-cc-pV5Z-PP calculations. The EAs are reported in Table 4.1. With respect to the experimental values, the MAD of rp-ccCA is 3.76 kcal mol^{-1}. While the average experimental uncertainty is 2.37 kcal mol^{-1}, the experimental uncertainties range from 0.002 to 7 kcal mol^{-1}. Additionally, the MAD is skewed due to the inclusion of bismuth (deviation of 13.22 kcal mol^{-1}). A large deviation between calculated and experimental values for the EA of bismuth has previously been noted. The deviation observed for bismuth may be attributed to the experimental energy levels of the bismuth anion multiplet being derived from the neutral polonium atomic splitting;[167] therefore, comparison to high-level calculations is reasonable. If the bismuth EA is removed from the set, the MAD of rp-ccCA from the experimental values, excluding bismuth, is 2.58 kcal mol^{-1}. To gauge the performance of rp-ccCA in comparison to other theoretical methods, previous CCSD(T)/aug-cc-pV5Z-PP calculations[118,119,156] were used. rp-ccCA yielded an MAD of 1.16 kcal mol^{-1} in relation

to the CCSD(T) results. Bismuth was included in comparison and the theoretical methods differed by 1.4 kcal mol^{-1} for the EA of bismuth.

Table 4.1. Atomic electron affinities in comparison to experimental values and CCSD(T)/aug-cc-pV5Z-PP results. Units are in kcal mol^{-1}.

Atom	rp-ccCA	Expt. [a]	CCSD(T)/ a5ZPP [b]	Deviation from Expt.	Deviation from CC
In	9.4	7±5	9.94	-2.4	0.5
Sn	30.9	32.7±0.09	32.52	1.8	1.6
Sb	21.6	17.7±1.2	20.28	-2.9	-1.3
Te	47.4	45.45±0.01	47.29	-2.0	-0.2
I	74.0	77.791±0.002	76.41	3.8	2.5
Tl	7.0	5±5	7.38	-2.0	0.4
Pb	27.6	32.76±0.17	29.61	5.2	2.1
Bi	16.6	3.4±0.2	17.99	-13.2	1.4
Po	44.5	44±7	44.07	-0.5	-0.4
At	73.4				
			MSD	-1.36	0.73
			MAD	3.76[c]	1.16
			σ	5.31	1.22
			RMSD	1.59	0.37

[a] Reference 166.
[b] Reference 118,119.
[c] Reported MAD includes bismuth. The MAD without bismuth is 2.58 kcal mol^{-1}.

4.3.1.2 Ionization Potential (IP)

Analysis of the IPs of the atoms provides insight into the electronic structure and changes in the orbital configuration, which are useful for reactions involving the ground state or oxidated state of the atom. The IPs of the 5*p* and 6*p* elements were first experimentally reported over half a century ago.[166] Since then, the IPs have been studied computationally and revisited experimentally.[118,119,168] The IPs, as determined by rp-ccCA, are reported in Table 4.2. The importance of spin-orbit coupling is

demonstrated for the IPs; in comparison to the experimental IPs,[166] the rp-ccCA values without SOC resulted in an MAD of 9.84 kcal mol^{-1}. After inclusion of SOC for the atoms, the rp-ccCA MAD with respect to experiment dropped to 3.89 kcal mol^{-1}. Similar to the EA, the IP of the bismuth atom is the outlier of the set, with an absolute deviation (14.6 kcal mol^{-1}) twice that of any other atom. With the exclusion of the bismuth IP, the MAD drops to 2.55 kcal mol^{-1}. The rp-ccCA MAD in comparison to the previous computational work is 2.93 kcal mol^{-1}. The cationic and neutral states for each of the atoms are reported in Table II. The rp-ccCA IPs are plotted in Figure 4.1. A slight decrease in the ionization potential for Te and Po is observed, representing the favorable loss of an electron to obtain the quartet multiplicity. As expected, the lowest IPs are for the elements with one *p* electron (In, Tl), since the closed shell, +1 oxidation is favorable. Overall, rp-ccCA is not only able to determine qualitative trends, but has the great advantage of being able to yield quantitatively accurate results.

Table 4.2. Atomic ionization potentials in comparison to experimental values and MCDHF results. Units are in kcal mol^{-1}.

IP	Ground State	Cation	rp-ccCA	Expt.[a]	Absolute Deviation	MCDHF	Absolute Deviation
In	$^2P_{1/2}$	$^1S_0$	131.1	133.06	1.9		
Sn	$^3P_0$	$^2P_{1/2}$	168.1	168.87	0.7		
Sb	$^4S_{3/2}$	$^3P_0$	201.1	198.7	2.4		
Te	$^3P_2$	$^4S_{3/2}$	204.9	207.23	2.4	205.95	1.1
I	$^2P_{3/2}$	$^3P_2$	241.4	240.44	1.0	237.01	4.4
Tl	$^2P_{1/2}$	$^1S_0$	132.7	140.44	7.8		
Pb	$^3P_0$	$^2P_{1/2}$	167.9	170.55	2.7		
Bi	$^4S_{3/2}$	$^3P_0$	172.2	167.6	14.6		
Po	$^3P_2$	$^4S_{3/2}$	195.4	193.89	1.5	197.73	2.3
At	$^2P_{3/2}$	$^3P_2$	230.7			226.84	3.9
				MSD	0.66	**MSD**	-1.22
				MAD	3.89[b]	**MAD**	2.93
				σ	3.59	**σ**	3.40
				RMSD	1.09	**RMSD**	2.95

[a] Reference 166.
[b] Without bismuth, the IP MAD drops to 2.55 kcal mol^{-1}.

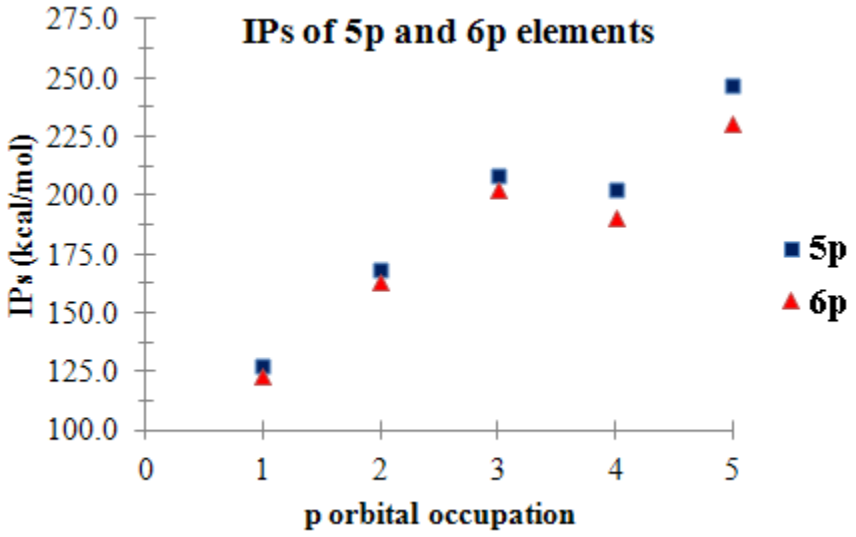

Figure 4.1. The ionization potentials of the 5*p* and 6*p* elements.

4.3.2 Diatomics

As noted in the methodology section, the selection of B3LYP for the geometry optimizations was validated by comparing B97-1, B97-D, PBEPBE, PBE1PBE, and B3LYP geometries. On average, the re-optimized geometries differed from the B3LYP geometries by ±0.002 Å. As this difference in geometry translated to differences in the energies in thousandths of a kcal mol^{-1}, which will not change the overall enthalpies of formation or dissociation energies determined by rp-ccCA, the original implementation of rp-ccCA with B3LYP geometries was employed.

4.3.2.1 Monohydrides

While various studies have determined the dissociation energies (D_0's) of the group 13-17, both 5*p* and 6*p*, monohydrides, either experimentally or via calculations,[152,162,169] a compilation of the results does not exist. Within this study, previous experimental and calculated values have been assembled for comparison (Table 4.3).

For these heavier elements, spin-orbit coupling (SOC) contributes to the molecular and atomic energies, while the magnitude of the SOC varies across the row. For example, the SOC lowers the dissociation energies of AtH and PbH by 15.6 and 16.6 kcal mol^{-1}, respectively. The SOC for IH is 0.5 kcal mol^{-1}. The inclusion of SOC in the rp-ccCA energies for the dissociation of the monohydrides results in a MAD of 2.0 kcal mol^{-1} from the compiled previously calculated data. The D_0's for InH and PoH are in exact agreement with CCSD(T) and 2-component relativistic calculations with shape-consistent relativistic pseudopotentials and valence basis sets including *f* polarization functions.[152] The statistics support the utilization of rp-ccCA, since accurate results are obtainable at a reduced computational cost. For the five available experimental values

(IH, InH, PbH, SnH, and TlH), the rp-ccCA deviations are -2.6, 0.5, 0.6, 5.3, and 1.6 kcal mol^{-1}, respectively, and the MAD with respect to experiment is 2.12 kcal mol^{-1}. Only two of the experimental values have larger uncertainties (5.0 and 3.0 kcal mol^{-1}) and the rp-ccCA MAD is within this uncertainty.

The quantity of available experimental data for comparison for the monohydride enthalpies of formation (ΔH_f's) is similar to the dissociation energies, although there are no previous theoretical results for comparison. Experimental values for only BiH, IH, InH, PbH, SnH, and TlH have been reported in the literature. The rp-ccCA results are reported in Table 4.3. In comparison to the available experimental values, rp-ccCA yielded a MAD of 1.82 kcal $mol^{-1}$and a mean signed deviation (MSD) of -0.73 kcal mol^{-1}.

Table 4.3. Group 13-17 monohydride dissociation energies and enthalpies of formation in comparison to experimental values and previously calculated results. Units are in kcal mol^{-1}.

Molecule	Ground State	D_0					$\Delta H_{f,298}$		
		rp-ccCA	Expt.[a]	Previous Calc.[b]	Deviation from expt.	Deviation from calc.	rp-ccCA	Expt.[a]	Deviation
InH	$^1\Sigma_g$	63.1	63.6	63.10	0.5	0.0	51.3	51.32	0.1
SnH	$^4\Sigma_g$	54.7	60.0±3	52.9	5.3	1.8	69.3	63.41	-5.9
SbH	$^3\Sigma_g$	59.4		62.10		2.7	56.4		
TeH	$^2\pi$	64.9		63.48		1.4	32.1		
IH	$^1\Sigma_g$	72.9	70.4	79.53	-2.6	6.6	3.2	6.35	3.2
TlH	$^1\Sigma_g$	45.7	47.4	46.00	1.6	0.3	49.4	49.16	-0.3
PbH	$^2\pi$	36.4	37.0±5	38.87	0.6	2.5	61.9	60.85	-1.1
BiH	$^2\pi$	52.9		49.68		3.2	43.4	43.01	-0.4
PoH	$^2\pi$	52.2		52.21		0.0	33.8		
AtH	$^1\Sigma_g$	52.1		53.13		1.0	21.4		
				MAD	2.12	1.95		**MAD**	1.82
				MSD	1.09	0.67		**MSD**	-0.73
				σ	2.84	1.84		**σ**	2.94
				RMSD	1.22	0.60		**RMSD**	1.10

[a] Reference 125.
[b] Reference 118,119.

4.3.2.2 Mono-oxides

Through the examination of the D_0's of mono-oxides, the thermodynamic favorability of an oxygen atom transfer, the oxidation of catalysts, properties of materials, and atmospheric catalytic ozone depletion can be deduced. Experimental D_0's are limited, but there exist a variety of computational studies (e.g. DFT, CCSD(T), QCISD) to supplement available experimental data for comparison. Table IV includes the D_0's of the 5*p* and 6*p* mono-oxides, as compared to experimental data and previously calculated values. The MAD of rp-ccCA in comparison to the compiled experimental data is 2.49 kcal mol^{-1}. Experimental uncertainties are reported for one-third of the experimental values and the average experimental uncertainty is 6.17 kcal mol^{-1}. The MSD for the set is 1.75 kcal mol^{-1}; therefore, the methodology is slightly biased toward over-estimating the D_0's of the mono-oxides. When examining the plot of the D_0's with respect to the *p* orbital occupation, the largest D_0 is observed for the *p*-block atoms with the valence configuration ns^{2}n*p*^{2}, where n = 5, 6.

For the ΔH_f's of the p-block mono-oxides, experimental data is available for Sn, Sb, Te, I, Pb, and Bi. The mono-oxide ΔH_f's are included in Table 4.4. rp-ccCA yielded a MAD of 3.13 kcal mol^{-1} and a MSD of -0.76 kcal mol^{-1}, in comparison to the experimental ΔH_f's. As observed in rp-ccCA calculations for the ΔH_f here, and in previous work, there is minimal systematic bias in the method. The largest deviation with respect to experimental ΔH_f's occurs for a different element in each set. For example, the mono-oxide of iodine has the largest deviation of -8.4 kcal mol-1, but for the mono-hydrides the deviation of iodine is 0.0 kcal mol^{-1} and the largest mono-hydride deviation is for tin (-5.9 kcal mol^{-1}).

Table 4.4. Group 13-17 mono-oxide dissociation energies and enthalpies of formation in comparison to experimental values. Units are in in kcal mol^{-1}.

Molecule	Ground State	D_0			$\Delta H_{f,298}$		
		rp-ccCA	**Expt.[a]**	**Deviation**	**rp-ccCA**	**Expt.[a]**	**Deviation**
InO	$^2\Sigma$	74.5	75.6±10	1.1	52.2		
SnO	$^1\Sigma^+$	126.2	126.1	-0.1	4.3	4.984	0.7
SbO	$^2\Pi_{1/2}$	95.7	102.8±10	7.1	26.7	24.737	-1.9
TeO	$^1\Sigma$	80.9	89.1±5	8.2	37.3	41.563	4.3
IO	$^2\Pi_{3/2}$	43.6	44±6	0.4	48.5	40.136	-8.4
TlO	$^2\Sigma$	58.3			58.3		
PbO	$^1\Sigma^+$	92.6	90.3±3	-2.3	14.3	16.455+/-1.3	2.1
BiO	$^2\Pi_{1/2}$	78.7	79.7±3	1.0	29.8	28.416	-1.3
PoO	$^1\Sigma$	67.4	66.47	-0.9	17.8		
AtO	$^2\Pi_{3/2}$	30.2	31.57	1.3	42.4		
			MSD	1.75		**MSD**	-0.76
			MAD	2.49		**MAD**	3.13
			σ	3.54		**σ**	4.37
			RMSD	2.00		**RMSD**	1.96

[a] Reference 125 except AtO and PoO (reference 170).

4.3.2.3 Dimers

The D_0's and ΔH_f's of the p-block dimers were investigated as a precursor to a study of larger clusters of the atoms. In addition, there are reported experimental values for the D_0's and ΔH_f's for all of the elements In-I and Tl-At. The average experimental uncertainty for the D_0's is 1.83 kcal mol^{-1}. The MSD and MAD, in comparison to experiment, of rp-ccCA for the D_0's of the dimers were -0.24 and 1.75 kcal mol^{-1}, respectively; therefore, rp-ccCA yields results within the limit of experimental uncertainty. The complete list of D_e's is reported in Table V. The largest D_0 is for the p^3 element in each series, Sb ($5p^3$) and Bi ($6p^3$), while the D_0's of the 6*p* dimers are less than the corresponding 5*p* dimers. The greater D_0's of the 6*p* dimers can be attributed to inner shell *f* electrons and the relativistic expansion of the outer *p* orbitals of the atoms, i.e., a larger atomic radius.

While experimental values have been reported for the ΔH_f of each *p*-block dimer, the corresponding uncertainties for each experimental value are only reported for five of the molecules. The average experimental uncertainty for the ΔH_f of the dimers is 1.92 kcal mol^{-1}. The MSD of the rp-ccCA calculations from experiment was 0.20 kcal mol^{-1} and the MAD was 2.53 kcal mol^{-1}. The dimer ΔH_f's are detailed in Table 4.5. The root mean square deviation (RMSD) was 0.93 kcal mol^{-1}, supporting the accuracy of the method.

Table 4.5. Group 13-17 dimer dissociation energies and enthalpies of formation compared to experimental data. Units are in kcal mol^{-1}.

Molecule	D_0 rp-ccCA	Experiment[a]	Deviation	$\Delta H_{f,298}$ rp-ccCA	Experiment[a]	Deviation
In_2	20.2	19.5±2.5	-0.7	98.5	98.834	0.3
Sn_2	48.4	45.8±4	-2.6	98.4	99.4	1.0
Sb_2	75.2	70.6±1.5	-4.6	52.3	57.1±0.8	4.8
Te_2	50.5	51.0±3	0.6	35.0	40.061	5.1
I_2	35.9	35.566±0.016	-0.3	17.7	14.922	0.3
Tl_2	12.8	14	1.2	76.8	72.071	-4.7
Pb_2	15.1	19.4±1.4	4.3	77.2	79.501±4.59	2.3
Bi_2	44.2	45.29±0.6	1.1	57.2	53.8±0.2	-3.4
Po_2	36.7	35.0±1.0	-1.7	34.5	34.777±1.5	0.2
At_2	25.6	26±2	0.4	20.9	20.0±2.5	-0.9
		MSD	-0.24		**MSD**	0.20
		MAD	1.75		**MAD**	2.53
		σ	2.22		**σ**	2.87
		RMSD	0.71		**RMSD**	0.93

[a] Reference 125.

4.3.3 Pb Clusters

Thermodynamic data of small clusters consisting of metal atoms, such as lead, can be used to determine catalytic properties, in addition to being used as an indicator of bulk phase properties of the metal clusters. In computational nanotechnology studies,[171] clusters composed of lower p-block elements are routinely examined due to their conducting and optical properties, which may be attributed to relativistic effects, particularly spin-orbit coupling. Spectroscopic properties, ground states, geometries, and energetic data of lead clusters composed of two to six atoms have been examined both experimentally and theoretically throughout the past few decades. The total atomization energies (TAEs), including spin-orbit coupling, for Pb_n (n=2-6) are reported in Table 4.6. Experimental and previous theoretical values are included for comparison.

Previously reported calculations with multireference configuration interaction with single and double excitations and a Davidson correction (MRSDCI+Q) were included, as they utilized a high level of theory and accounted for both scalar relativistic and spin-orbit effects.[172,173] The ground state geometries of each cluster are detailed in Figure 4.2. Agreement with the available experimental and theoretical data is observed for each lead cluster. To note, the spin-orbit coupling, on average, decreases as the size of the cluster increases. The largest SOC is observed for the lead dimer as a result of relativity causing the σ_g bonding orbital and π_g anti-bonding orbital to mix. The final structures selected for each cluster were chosen based on lowest energy criteria and previous studies.[172-176] Multiple geometries were included; for example, for Pb_3: linear ($D_{\infty h}$), planar (D_{3h}), and bent (C_{2v}) were considered. For the reported experimental values, the MAD of rp-ccCA is 2.03 kcal mol^{-1}, which is within the average experimental uncertainty of 3.13 kcal mol^{-1}. The accurate results obtained for the small lead clusters supports the utilization of rp-ccCA in future studies of group 13-17 clusters.

Table 4.6. Total atomization energy for the lead cluster Pb_n, n=2-6. Units are in kcal mol^{-1}.

Cluster size	Ground State	TAE rp-ccCA	TAE Expt.	Deviation
2	$^3\Sigma$	15.1	19.4±1.4 [a]	4.3
3	$^1\Sigma$	53.8	53.5±4 [b]	-0.3
4	$^1\Sigma$	95.7	97.5±-4 [b]	1.8
5	$^1A_1$	116.7	115.0 [c]	-1.7
6	$^1A_{1g}$	144.2	144.9 [d]	0.7
			MSD	0.96
			MAD	1.76
			σ	2.27
			RMSD	0.92

[a] Reference 125. [b] Reference 174.
[c] Reference 176. [d] Reference 173.

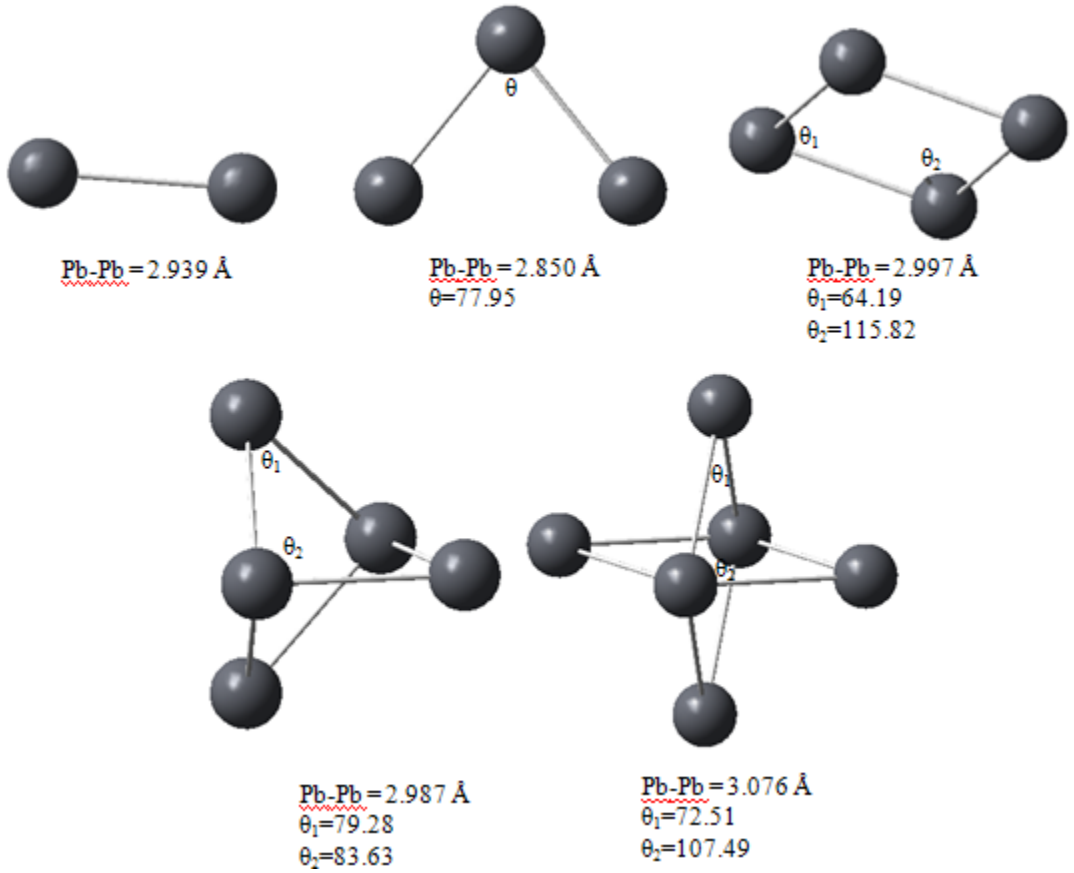

Figure 4.2. Geometries of the lead clusters Pb^n (n=2-6).

4.4 Conclusions

The relativistic pseudopotential variant of ccCA (rp-ccCA) has previously been demonstrated to yield accurate thermodynamic data for second-row transition metals. The method has been extended to lower *p*-block elements, indium through iodine (5*p*) and thallium through astatine (6*p*), as well as p-block containing molecules. The performance of rp-ccCA has been examined for energetic properties, including ionization potentials, electron affinities, and atomization energies, as well as for thermodynamic data, i.e., enthalpies of formation. In the absence of energetic and thermodynamic data from experiment for comparison, rp-ccCA results were reported in comparison to theoretical data. Scalar relativistic effects were included in the calculations via pseudopotentials, while spin-orbit coupling was included *a posteriori*. The magnitude of the spin-orbit coupling ranged from zero to the same magnitude as the property of interest. rp-ccCA results, on average, for the LP80 set were within reported experimental uncertainties, e.g. the rp-ccCA MAD was 1.75 kcal mol^{-1} whereas the average experimental uncertainty was 1.83 kcal mol^{-1} for the dissociation energies of the *p*-block dimers. For the atomic electron affinities, rp-ccCA yielded an MAD of 3.06 kcal mol^{-1} from experimental data and an MAD of 1.05 kcal mol^{-1} in comparison to CCSD(T)/aug-cc-pV5Z-PP calculations. Atomic results also included the ionization potentials, where rp-ccCA obtained an MAD of 2.49 kcal mol^{-1} from experiment. To further demonstrate the accuracy of rp-ccCA, the total atomization energy of Pb_n (n=2-6) clusters was examined and the MAD of rp-ccCA was 2.03 kcal mol^{-1}, while the reported experimental uncertainty was 3.13 kcal mol^{-1}.

By implementing rp-ccCA, energetic and thermodynamic data, on average within

3 kcal mol^{-1} of experimental values and within reported experimental uncertainties, of the lower *p*-block-containing molecules are obtainable. The quantitative performance of rp-ccCA is obtained with a significantly reduced computational cost as compared with high-level CCSD(T) calculations. Previous work detailed the utility of rp-ccCA for second row transition metals and in the current study the applicability of rp-ccCA has been extended to the lower p-block elements. rp-ccCA yields accurate results, in comparison to experimental data and previous computational studies, for the heavier elements by accounting for scalar relativistic effects within the pseudopotentials employed and for spin-orbit coupling via an a posteriori correction. The rp-ccCA results, within this work and in future applications, can be used to supplement and guide experimental work.

CHAPTER 5

HARMONIC VIBRATIONAL FREQUENCIES: SCALE FACTORS FOR PURE, HYBRID, HYBRID META, AND DOUBLE-HYBRID FUNCTIONALS IN CONJUNCTION WITH CORRELATION CONSISTENT BASIS SETS[§]

5.1 Introduction

Density functional theory (DFT) is a popular methodology due to its ability to account for electron correlation at a reduced computational cost, as compared with correlated ab initio methods.[23,177] Its uses include the determination of ground state geometries, transition structures, molecular interactions, and thermodynamic properties, including bond dissociation energies, atomization energies, enthalpies of formation, and vibrational frequencies. DFT has been used to predict thermodynamic properties of both small, simple molecules and complex molecules, including transition metals,[178] solvated species[179] and solid state materials.[180]

For the description of thermochemical properties such as enthalpies of reaction, vibrational frequencies and zero-point vibrational energies are required. Unfortunately, calculated vibrational frequencies tend to overestimate the corresponding fundamental frequencies due to basis set truncation effects, the incomplete treatment of electron correlation, and the omission of anharmonic effects.[181] As the deviation between experimental vibrational frequencies and calculated vibrational frequencies is moderately systematic, this allows for the development of multiplicative scale factors for application to the calculated frequencies to provide comparison with the experimentally observed fundamental frequencies.[1-3]

[§] The research presented has been published in M.L. Laury, S.E. Boesch, I. Haken, P. Sinha, R.A. Wheeler, and A.K. Wilson, *J. Comp. Chem*. **32**, 2339 (2011).

Since theoretical results are dependent upon the method and basis set selection, scale factors that are unique to each method and basis set combination are needed. As shown in prior studies, significant improvement in calculated vibrational frequencies as compared with experiment is achieved when scale factors are utilized for specific levels of theory.[1-3] For 38 molecules, Pople et al. observed that HF method with a 3-21G basis set overestimated experimental frequencies by 12%. A scale factor of 0.8929 was then determined for HF/3-21G.[182] Hehre et al. determined that HF/6-31G(d) overestimated experimental fundamental frequencies by 13%; similar to the results obtained by Pople et al.[182] Additionally, Hehre et al. calculated a 7% deviation between experimental frequencies and calculated frequencies for the MP2/6-31G(d) level of theory. Scale factors for Hartree-Fock (HF) and various post-HF methods, including second-order Møller-Plesset (MP2), coupled cluster with single, double, and quasi-perturbative triple excitations (CCSD(T)), and quadratic configuration interaction (QCI), previously have been developed for the methods in combination with Pople type basis sets, as well as correlation consistent basis sets.[1,2,183,184]

Previous studies have also given attention to the combination of density functionals with a variety of basis sets. For example, Scott and Radom examined exchange-correlation functionals, BLYP, B3LYP, BP86, B3P86, and B3PW91, together with the Pople type basis sets: 3-21G, 6-31G(d), 6-31+G(d), 6-31G-(d,p), 6-311G(d,p), and 6-311G(df,p).[1] Scott and Radom determined scale factors for vibrational frequencies, zero-point vibrational energy (ZPVE), and the thermal contributions to enthalpy and entropy for each method and basis set combination. The scale factors for ZPVEs were derived from a set of 25 diatomic molecules, while a set of 122 molecules

was used for the remaining scale factors. Additionally, for BLYP, B3LYP and B3PW91 used in conjunction with the Sadlej basis sets, Halls and co-workers determined scale factors for vibrational frequencies.[185] For B3LYP and the correlation consistent basis sets, scale factors were determined by Wilson and co-workers.[183] Their study also included HF and MP2 levels of theory with the correlation consistent basis sets. Irikura *et al.* assessed the uncertainty associated with scale factors for HF, MP2, QCISD, BLYP, B3LYP, B3PW91, mPW1PW91, and PBEPBE in conjunction with Pople type basis sets.[186] Irikura *et al.* concluded that the scale factors have only two significant digits, revealing the corresponding uncertainties to be larger than previously recognized. Upon evaluation of the standard uncertainties, Irikura *et al.* showed the scale factors were weakly dependent upon the selected basis set.[186] Truhlar and co-workers have recently designed functionals, including BB1K,[34] MC3BB, and MC3MPW.[34] For each of the functionals in conjunction with Pople type basis sets, the scale factors for the zero-point vibrational energies were determined. An extensive study of scale factors was recently conducted by Merrick, Moran, and Radom, where a variety of DFT formulations, specifically with respect to the amount of HF exchange, were studied in conjunction with Pople type basis sets. A few of their chosen functionals were also assessed in combination with the cc-pVDZ and aug-cc-pVDZ basis sets.[2] Merrick *et al.* included scale factors for vibrational frequencies, ZPVE, and thermal contributions to enthalpy and entropy in their study. Additionally, Halls and Schlegel reported harmonic vibrational frequency scale factors for hybrid functionals (i.e., SVWN, BLYP, B3LYP, and B3PW91) in comparison to scale factors for HF and MP2 calculations.[187] They concluded that the hybrid functionals yielded scaled results in near accord with

experimental frequencies and overall were more reliable than HF and MP2 for the prediction of vibrational frequencies.[187] Recently, Truhlar and co-workers determined scale factors for zero-point energies, harmonic frequencies, and fundamental frequencies, as well as what they have defined as universal scale factor ratios, for use with certain density functionals, semi-empirical methods, and correlated methods in conjunction with triple-zeta quality basis sets.[188] Functionals in their study with ZPE scale factors closest to unity included MPWLYP1M, BB95, MPW3LYP, BLYP, BP86, B3LYP, VSXC, and τHCTHhyb. The triple-zeta quality basis sets of interest included MG3S, 6-31G(d,p), def2-TZVPP, aug-cc-pVTZ, and maug-cc-pV(T+d)Z.[188]

The development of local, pure, hybrid, hybrid meta, and double-hybrid meta functionals continuously progresses, with a goal to design functionals that result in decreased errors in molecular property prediction and functionals that address known shortcomings in DFT, e.g. the ability to describe weak bonds[189] and van der Waals forces.[36] Following Perdew's "Jacob's Ladder"[190] of density functionals, local functionals are considered on the first rung and are determined through the local spin density approximation (LSDA). Pure functionals, e.g. BLYP, PBEPBE, are second rung functionals and follow the generalized gradient approximation (GGA). Hybrid and hybrid-meta functionals are denoted as fourth rung functionals. Hybrid functionals, such as B3P86 and B3PW91, incorporate Hartree-Fock (HF) exact exchange energy with approximate DFT exchange. Hybrid meta functionals, e.g. M05, M05, include HF exact exchange energy and kinetic energy density. Double-hybrid functionals are considered fifth rung functionals and include HF exact exchange energy, approximate DFT exchange, and MP2 correlation energy.

Foremost, scale factors should be determined for the new and widely used Minnesota, hybrid meta exchange-correlation functionals, M05,[191] M05-2X,[192] M06, and M06-2X,[193] used for the description of thermochemistry, thermochemical kinetics, and non-covalent interactions. The 2X represents the double amount of nonlocal exchange, which was specifically parameterized for non-metals. The M05-2X and M06-2X functionals are thus recommended for non-transition metal containing molecules. A few recent applications of these functionals include stacking interactions of nucleobase pairs and non-covalent interactions in biomolecules.[194] The utility of the M05, M05-2X, M06, and M06-2X functionals make them ideal hybrid meta functionals for scale factor development.

Double-hybrid functionals have received attention for their determination of thermochemical properties and barrier heights. Studies have claimed that double-hybrid functionals outperform meta-hybrid DFT with respect to equilibrium thermochemistry;[195] in fact, the thermodynamic and energetic results obtained by these functionals approach those determined by composite ab initio methods, e.g. G1 and G2.[195] An example of a double-hybrid functional is B2GP-PLYP, which is a robust functional for the determination of properties including thermochemical data and non-dynamic correlation energy, as well as the study of extremely polar molecules, e.g. SO_3.[195] No scale factors have yet been determined for this functional.

An attractive property of the correlation consistent basis sets in conjunction with ab initio methods, such as MP2 and CCSD(T), is the convergence to the CBS limit for a variety of properties (e.g. correlation energy, dissociation energy, bond lengths, total energy).[9,43-45,49,98] These characteristics have resulted in the wide use of the correlation

consistent basis sets.[35] Other properties of interest include harmonic vibrational frequencies, zero point vibrational energies, and thermal contributions. When studying vibrational properties, scale factors are necessary for accurate results. To date, a greater focus has been the development of scale factors for Pople type basis sets. However, as the correlation consistent basis sets are widely used with DFT, the corresponding scale factors are needed.

When implemented in combination with DFT, the convergence to the CBS limit (Kohn-Sham limit for DFT) seen for the correlation consistent basis sets with ab initio methods is not guaranteed for properties such as dissociation energies[196] and equilibrium geometries.[197] Convergence to the Kohn-Sham limit is dependent upon the functional selection. For example, the convergence of atomization energies was not observed for the pure functionals (BLYP, BPW91, BP86) and standard correlation consistent basis sets (cc-pV*n*Z),[196] while convergence for bond lengths and electron affinities was seen for the hybrid functional B3LYP with aug-cc-pV*n*Z (*n*=D,T,Q,5) basis sets.[198]

In this work vibrational frequencies were determined for a set of functionals in conjunction with the correlation consistent basis sets (cc-pV*n*Z and aug-cc-pV*n*Z, where *n*=D(2), T(3) ,Q(4)). The functionals include the double-hybrid B2GP-PLYP, hybrid meta M05, M05-2X, M06, and M06-2X, hybrid B3P86,[28,30,199] B3PW91,[200-202] BPW91,[26] PBE1PBE,[203] BH&HLYP,[204] and MPW1K,[204] and pure BLYP,[27,160] PBEPBE,[205] HCTH93[206,207] and BP86.[208] These broad-purpose functionals were selected based on their prevalence within computational chemistry and the lack of vibrational frequency

scale factors to accompany the functionals in conjunction with the correlation consistent basis sets.

5.2 Theoretical Procedure

Calculations were carried out with the Gaussian 09 software package.[165] Fifteen density functionals were used in combination with the correlation consistent basis sets [cc-pV*n*Z and aug-cc-pV*n*Z, where *n*=D(2),T(3),Q(4)]. The calculated vibrational frequencies were compared to the experimental fundamental frequencies for 40 main group molecules from a set previously studied by Healy and Holder.[209] Scale factors were determined for calculated vibrational frequencies, ZPVEs, and thermal contributions to enthalpy and entropy. An additional set of 24 molecules consisting of mostly main group diatomics and triatomics, by Schaefer and co-workers, was utilized to determine the scale factors for zero-point vibrational energies.[210]

5.2.1 Vibrational Frequencies

With quantum chemical predictions of low frequency vibrations, the interpretation of the fingerprint region of experimental vibrational spectra is facilitated. However, the frequencies in the lower region of the spectra are difficult to distinguish experimentally due to the high concentration of states.[187] Additionally, for thermochemical properties, such as the enthalpic and entropic thermal contributions, the lower frequencies result in larger contributions. Therefore, separate scale factors for the high and low frequencies were determined. In this study, the distinction between low and high frequencies is made at 1000 cm^{-1} based on our previous studies utilizing the same series of

molecules.[183] Determination of the scale factors followed a procedure as outlined by Scott and Radom.[1,2]

5.2.1.1 High Frequencies

The scale factors for the high frequency range were determined by the least-squares method, defined previously by Scott and Radom.[1,2] The residual, Δ, to be minimized is defined as

$$\Delta = \sum_i^{all} (\lambda \omega_i^{calc} - \nu_i^{expt})^2 \quad (5.1)$$

where ν_i^{expt} is the experimental vibrational frequency, ω_i^{calc} is the calculated frequency, and where *i* indicates the *i*th calculated harmonic vibrational frequency and the *i*th experimental fundamental frequency. The scale factor, λ, is arrived at by

$$\lambda = \frac{\sum_i^{all} (\omega_i^{calc} \nu_i^{expt})}{\sum_i^{all} (\omega_i^{calc})^2} \quad (5.2)$$

Upon obtaining the scale factor λ the minimized residual, Δ_{min}, is determined by Equation 5.1 and the root mean square (rms) error is found by

$$rms = \left(\sum_i^{n_{al}} \frac{\Delta_{min}}{n_{all}} \right)^{\frac{1}{2}} \quad (5.3)$$

where n_{all} is the total number of vibrational modes for all molecules in the set.

5.2.1.2 Low Frequencies

The low frequency scale factors were determined by an inverse method. The minimization of the residual is determined by

$$\Delta = \sum_i^{all} \left(\frac{1}{\lambda \omega_i^{calc}} - \frac{1}{\nu_i^{expt}} \right)^2 \quad (5.4)$$

between the experimental vibrational frequencies ν_i^{expt} and the calculated frequencies ω_i^{calc}, where *i* indicates the *i*th calculated harmonic vibrational frequency and the *i*th experimental fundamental frequency. The scale factor was then determined by

$$\lambda = \frac{\sum_i^{all}\left(\frac{1}{\omega_i^{calc}}\right)^2}{\sum_i^{all}\frac{1}{\omega_i^{calc}\nu_i^{expt}}} \quad (5.5)$$

and the rms was calculated as in equation 5.3.

5.2.2 Thermodynamic Properties

5.2.2.1 Enthalpic Contribution

The thermal contribution to enthalpy is rooted in the vibrational frequency, where the enthalpic contribution is expressed as

$$\Delta H_{vib}(T) = Nhc\sum_i \frac{\nu_i}{e^{\mu_i}-1} \quad (5.6)$$

where N is Avogadro's number, h is Planck's constant, c is the speed of light, and

$$\mu_i = \frac{hc\nu_i}{kT} \quad (5.7)$$

with T for temperature, k equal to Boltzmann's constant, and ν_i is the frequency in cm^{-1}. The units of the enthalpic contribution are kJ/mol. The residual to be minimized is

$$\Delta = \sum_i^{all}\left[\lambda\Delta H_{vib}^{calc}(T_i) - \Delta H_{vib}^{expt}(T_i)\right]^2 \quad (5.8)$$

5.2.2.2 Entropic Contribution

Similar to the enthalpic contribution, the thermal contribution to entropy is derived from the vibrational frequency as

$$S_{vib}(T) = R\sum_i \left[\frac{\mu_i}{e^{\mu i}-1} - \ln(1-e^{-\mu_i})\right] \quad (5.9)$$

where R is the gas constant and μ is determined as in Equation 5.8. The residual to be minimized for the entropic contribution is

$$\Delta = \sum_i^{all}\left[\lambda\Delta S_{vib}^{calc}(T_i) - \Delta S_{vib}^{expt}(T_i)\right]^2 \quad (5.10)$$

The scale factor for the entropic contribution was determined by mimicking the procedure for the enthalpic contribution.

5.2.3 Zero-point Vibrational Energies

The ZPVE is necessary for the accurate determination of thermodynamic properties such as the enthalpy of formation at 298K. The ZPVE can be derived from the computed frequency by the relation

$$ZPVE = \frac{1}{2}\sum_i h\omega_i^{calc} \quad (5.11)$$

The experimentally observed frequencies are anharmonic, while the calculated frequencies do not account for anharmonic effects. The ZPVE scale factor helps correct for the anharmonic effects. Using the scale factors, residuals were minimized as in Equation 5.1 and root mean square (rms) errors were determined for the functional/basis set combinations by Equation 5.3.

5.3 Results and Discussion

The scale factors for the high (above 1000 cm^{-1}) vibrational frequencies are reported in Table 5.1. The scale factors for the high vibrational frequencies are slightly lower than those for the low-end vibrational frequencies. A distinction between the pure DFT and the hybrid DFT is seen. The pure functionals (BLYP, PBEPBE, HCTH93,

BP86) scale factors are closer to one and are less dependent on basis set. A scale factor of 0.99 is recommended for BLYP and 0.98 for PBEPBE, HCTH93, and BP86. Overall, the root-mean-square (rms) errors for high frequencies are almost three times the size of the rms errors of the low vibrational frequencies. Through the application of the multiplicative scale factors determined here, the deviation between the harmonic vibrational frequencies and experimental fundamental frequencies is lowered.

Table 5.1. High frequency scale factors and overall root mean square (rms) in cm^{-1}.[a]

Functional	Functional Type	Scale Factors						RMS					
		cc-pVDZ	cc-pVTZ	cc-pVQZ	aug-cc-pVDZ	aug-cc-pVTZ	aug-cc-pVQZ	cc-pVDZ	cc-pVTZ	cc-pVQZ	aug-cc-pVDZ	aug-cc-pVTZ	aug-cc-pVQZ
BLYP	Pure	0.9939	0.9898	0.9914	0.9902	0.9912	0.9911	35.1	33.6	27.3	31.9	28.4	27.7
PBEPBE	Pure	0.9850	0.9864	0.9867	0.9832	0.9863	0.9865	31.2	26.1	24.4	27.8	25.1	24.8
HCTH93	Pure	0.9721	0.9750	0.9752	0.9714	0.9747	0.9752	28.5	26.3	25.9	27.2	26.0	26.3
BP86	Pure	0.9890	0.9891	0.9897	0.9874	0.9894	0.9897	32.2	24.6	24.5	30.0	25.0	24.5
B3P86	Hybrid	0.9572	0.9591	0.9595	0.9567	0.9592	0.9598	26.1	22.6	22.7	23.0	22.4	24.3
B3PW91	Hybrid	0.9599	0.9614	0.9609	0.9584	0.9611	0.9614	30.6	23.8	23.3	23.0	22.5	23.0
BPW91	Hybrid	0.9842	0.9847	0.9853	0.9826	0.9849	0.9854	30.8	24.9	25	29.5	26.9	26.7
PBE1PBE	Hybrid	0.9532	0.9565	0.9569	0.9532	0.9568	0.9569	26.0	24.2	24.1	23.8	23.9	24.3
BH&HLYP	Hybrid	0.9328	0.9344	0.9346	0.9326	0.9345	0.9347	29.3	25.9	25.7	29.4	25.3	25.6
MPW1K	Hybrid	0.9319	0.9364	0.9378	0.9345	0.9378	0.9379	29.3	32.2	29.2	30.6	39.0	31.6
M05	Hybrid meta	0.9560	0.9589	0.9577	0.9571	0.9600	0.9574	54.5	45.4	46.7	56.7	45.7	46.9
M05-2X	Hybrid meta	0.9495	0.9483	0.9493	0.9501	0.9491	0.9490	44.3	38.6	38.7	46.8	39.2	38.8
M06	Hybrid meta	0.9670	0.9674	0.9634	0.9675	0.9690	0.9635	54.2	44.9	46.1	56.1	45.1	47.2
M06-2X	Hybrid meta	0.9572	0.9567	0.9572	0.9579	0.9574	0.9574	47.9	40.4	40.4	49.2	40.7	40.6
B2GP-PLYP	Double-hybrid	0.9522	0.9528	0.9532	0.9551	0.9541	0.9535	45.5	41.8	42.4	50.9	43.2	40.8

[a] Of the molecule set, acetone was removed from the study due to the suggestion of reference 183. [b] Common practice is to report scale factors to four places past the decimal, which could overstate the accuracy of the scale factors. Application of the scale factors should include two places past the decimal to avoid introducing uncertainty.

The percent error between the harmonic vibrational frequencies and experimental fundamental frequencies are tabulated in Table 5.2 and Figures 5.2, 5.3, and 5.4 for all of the functionals, BLYP, and M06-2X, respectively. Table 5.3 documents the percent of harmonic vibrational frequencies within 3% of experimental fundamental frequencies for the augmented correlation consistent basis sets. After application of the scale factors, over 90% of the high harmonic vibrational frequencies are within 3% of the experimental fundamental frequencies for the cc-pVnZ and aug-cc-pVnZ basis sets (n=D,T,Q). Without implementation of a scale factor, around 25% of the calculated frequencies deviate more than 3% from experimental frequencies. Even though the hybrid meta functionals and double-hybrid functional present a deviation between calculated and experimental frequencies, the application of the multiplicative scale factors determined here present a means to achieve high vibrational frequencies in near agreement with experiment.

Table 5.2. Percent of scaled, calculated high frequencies within a given error range for PBE1PBE.

% error	cc-pVDZ	cc-pVTZ	cc-pVQZ	aug-cc-pVDZ	aug-cc-pVTZ	aug-cc-pVQZ
0-1	76.8	75.4	73.8	79.6	75.2	73.2
1-2	15.2	18.3	19.8	13.9	17.7	19.0
2-3	5.1	4.9	5.0	2.2	5.7	6.4
3-4	2.2	0.7	0.7	3.6	0.7	0.7
4-5	0.7	0.7	0.7	0.0	0.7	0.7
≥5	0.0	0.0	0.0	0.7	0.0	0.0

Table 5.3. Percent of scaled, calculated high frequencies within 3% error of experimental frequencies.

Functional	cc-pVDZ	cc-pVTZ	cc-pVQZ	aug-cc-pVDZ	aug-cc-pVTZ	aug-cc-pVQZ
BLYP	99.2	94.7	97.7	93.1	96.2	96.9
PBEPBE	99.2	98.5	99.3	99.2	96.2	98.5
HCTH93	98.4	99.2	99.2	98.4	99.2	99.2
BP86	98.5	99.2	99.2	96.1	99.2	99.2
B3P86	97.1	99.3	99.3	96.4	99.3	99.3
B3PW91	98.6	99.3	99.3	97.1	99.3	99.3
BPW91	99.2	99.2	99.2	96.2	99.2	99.2
PBE1PBE	97.1	98.6	98.6	95.7	98.6	98.6
BH&HLYP	93.3	99.4	99.4	90.9	99.4	99.4
MPW1K	85.5	98.2	99.4	86.6	98.8	98.2
M05	61.6	74.7	71.3	58.8	73.0	69.2
M05-2X	74.5	92.1	92.2	69.6	90.7	91.8
M06	63.5	83.9	77.4	63.7	76.4	75.5
M06-2X	68.6	91.8	91.8	69.0	91.3	91.8
B2GP-PLYP	87.5	91.6	91.0	74.3	89.1	85.5

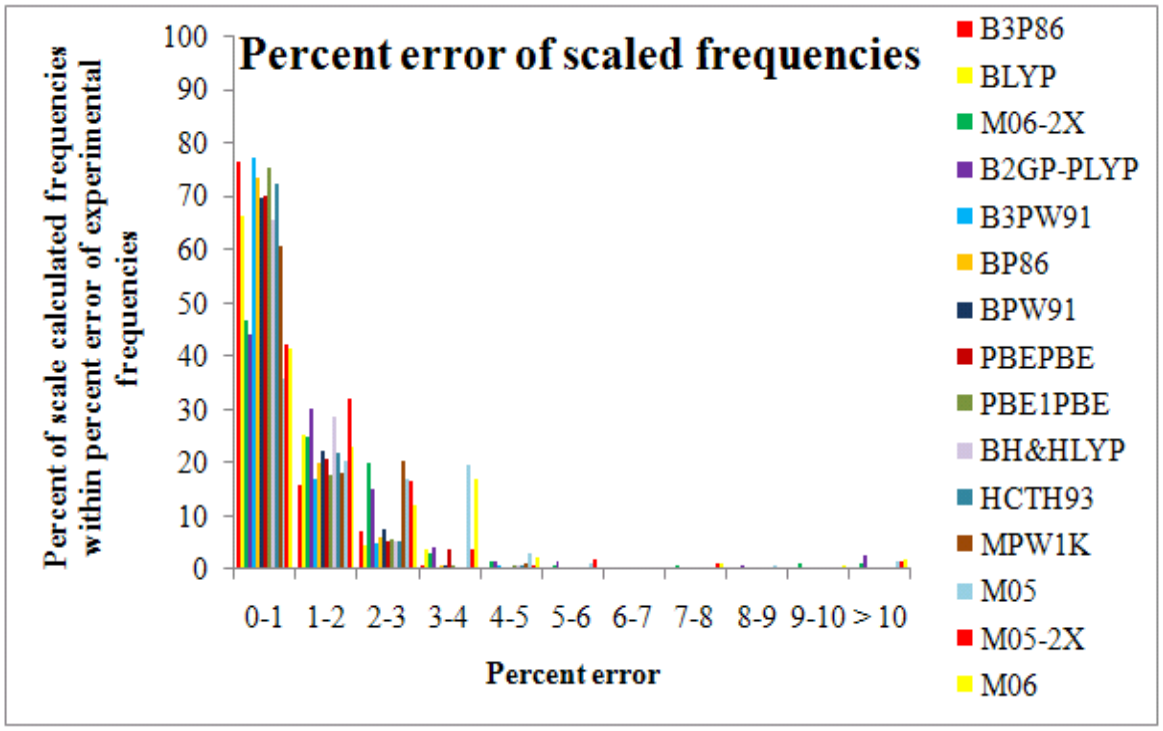

Figure 5.1. Percent error of scaled frequencies in conjunction with the aug-cc-pVTZ basis set.

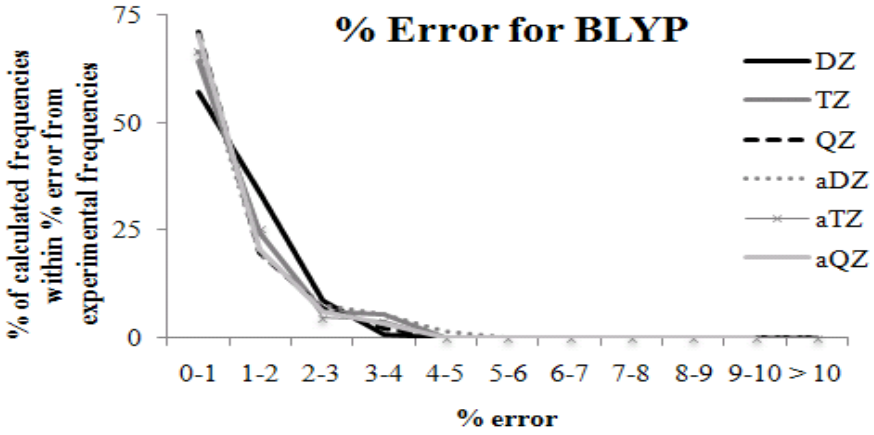

Figure 5.2. Percent of calculated frequencies within percent error of experimental values for BLYP with the cc-pVnZ and aug-cc-pVnZ (n=D,T,Q) basis sets.

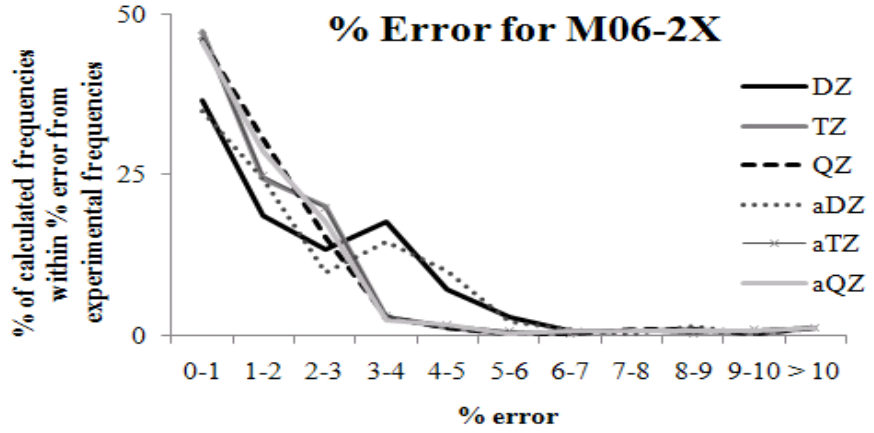

Figure 5.3. Percent of calculated frequencies within percent error of experimental values for M06-2X with the cc-pVnZ and aug-cc-pVnZ (n=D,T,Q) basis sets.

The scale factors for the low (under 1000 cm^{-1}) vibrational frequencies are reported in Table 5.4. The scale factors range from 0.9666 to 1.0500 and have a stronger dependence on the functional than the chosen basis set. The hybrid, hybrid meta, and double-hybrid functionals scale factors are less than one. The pure DFT scale factors are greater than unity; therefore, the pure functionals underestimate the low frequencies. The M06 functional in combination with the augmented double-zeta

correlation consistent basis set results in the scale factor closest to unity and, therefore, predicts the vibrational frequency closest to the experimental frequency. The scale factors for M05 and M06 are slightly higher (closer to one) than the scale factors for their corresponding 2X functionals, while the scale factors for B2GP-PLYP fall in between the 2X and non-2X functionals. The lower optimal scale factors for M05-2X and M06-2X, in comparison to M05 and M06, indicate the overestimation of the vibrational frequencies of the 2X functionals for the lower (i.e., finger-print region) frequencies. Scale factors for several of the density functionals presented have previously been reported, but in conjunction with Pople type basis sets. The underestimation of the low frequencies by the pure functionals (BLYP, BP86, HCTH93) was observed by Merrick et al.[10] when Pople type basis sets were used. The scale factors, with respect to the correlation consistent basis sets, are closer to unity than the previously determined scale factors for the Pople type basis sets and, therefore, the correlation consistent basis sets predict low vibrational frequencies in closer accord with experimental frequencies than the Pople type basis sets.

Table 5.4. Low frequency scale factors and overall rms in cm^{-1} .

Functional	Scale Factors						RMS					
	cc-pVDZ	cc-pVTZ	cc-pVQZ	aug-cc-pVDZ	aug-cc-pVTZ	aug-cc-pVQZ	cc-pVDZ	cc-pVTZ	cc-pVQZ	aug-cc-pVDZ	aug-cc-pVTZ	aug-cc-pVQZ
BLYP	1.0236	1.0292	1.0289	1.0500	1.0329	1.0298	10.30	7.60	7.10	8.50	6.90	6.70
PBEPBE	1.0141	1.0189	1.0191	1.0353	1.0230	1.0208	10.20	7.10	6.90	7.70	6.50	6.60
HCTH93	1.0010	1.0066	1.0070	1.0213	1.0098	1.0084	9.40	6.90	6.50	7.70	6.30	6.00
BP86	1.0201	1.0231	1.0234	1.0418	1.0277	1.0225	10.10	7.20	6.90	7.90	6.90	6.70
B3P86	0.9771	0.9803	0.9804	0.9934	0.9833	0.9808	8.00	6.80	6.50	6.40	6.60	6.70
B3PW91	0.9771	0.9829	0.9824	0.9940	0.9859	0.9839	8.00	6.70	6.60	6.10	6.60	6.40
BPW91	1.0204	1.0209	1.0215	1.0378	1.0249	1.0201	10.90	7.10	6.60	7.60	6.60	6.90
PBE1PBE	0.9696	0.9747	0.9743	0.9855	0.9776	0.9760	8.10	6.80	6.70	6.30	6.60	6.60
BH&HLYP	0.9397	0.9417	0.9423	0.9538	0.9444	0.9434	8.40	7.90	8.00	7.20	7.90	7.80
MPW1K	0.9450	0.9486	0.9508	0.9591	0.9521	0.9492	8.30	7.90	8.40	7.30	7.80	7.80
M05	0.9624	0.9682	0.9682	0.9840	0.9751	0.9718	15.79	14.75	13.77	14.09	15.09	13.70
M05-2X	0.9684	0.9714	0.9803	0.9837	0.9726	0.9846	14.57	14.59	18.65	12.93	14.45	19.76
M06	0.9640	0.9607	0.9662	0.9810	0.9862	0.9907	15.77	15.35	14.45	13.45	21.39	21.27
M06-2X	0.9652	0.9657	0.9654	0.9800	0.9698	0.9752	15.47	15.82	14.93	13.78	15.90	15.47
B2GP-PLYP	0.9737	0.9713	0.9705	0.9969	0.9755	0.9668	12.53	8.40	8.29	9.86	8.00	6.97

Thermodynamic scale factors and rms errors for the enthalpy contribution are reported in Table 5.5. The pure, hybrid meta, and double-hybrid functional and basis set combinations underestimated the thermal contribution to enthalpy since the scale factors are slightly greater than one. Overall, the scale factors fluctuate between 1.0058 and 1.0601. The hybrid functionals overestimated the thermal contributions to enthalpy and vary between 0.9352 and 0.9941. The lowest scale factor for each functional is at the augmented double-zeta level. The previous work with the Pople type basis sets mirrored the underestimation of the pure functionals and the overestimation of the enthalpic contribution by the hybrid functionals (B3P86, B3PW91, BH&HLYP, MPW1K).[2]

Table 5.5. Thermal contribution to enthalpy scale factors for 298.15 K and overall rms in kJ/mol.

Functional	Scale Factors						RMS					
	cc-pVDZ	cc-pVTZ	cc-pVQZ	aug-cc-pVDZ	aug-cc-pVTZ	aug-cc-pVQZ	cc-pVDZ	cc-pVTZ	cc-pVQZ	aug-cc-pVDZ	aug-cc-pVTZ	aug-cc-pVQZ
BLYP	1.0354	1.0359	1.0342	1.0564	1.0373	1.0343	0.030	0.023	0.022	0.027	0.021	0.020
PBEPBE	1.0242	1.0238	1.0233	1.0418	1.0257	1.0234	0.028	0.020	0.019	0.024	0.019	0.018
HCTH93	1.0094	1.0101	1.0101	1.0268	1.0117	1.0100	0.026	0.019	0.018	0.023	0.018	0.017
BP86	1.0299	1.0273	1.0275	1.0479	1.0303	1.0267	0.028	0.020	0.020	0.025	0.019	0.019
B3P86	0.9806	0.9781	0.9778	0.9936	0.9800	0.9796	0.021	0.019	0.019	0.016	0.019	0.019
B3PW91	0.9811	0.9801	0.9796	0.9941	0.9823	0.9801	0.022	0.019	0.019	0.020	0.019	0.018
BPW91	1.0284	1.0241	1.0243	1.0431	1.0267	1.0235	0.031	0.020	0.019	0.024	0.019	0.018
PBE1PBE	0.9724	0.9718	0.9716	0.9852	0.9735	0.9724	0.022	0.020	0.020	0.017	0.020	0.020
BH&HLYP	0.9387	0.9353	0.9353	0.9491	0.9370	0.9352	0.027	0.029	0.029	0.023	0.029	0.029
MPW1K	0.9429	0.9413	0.9442	0.9540	0.9435	0.9429	0.026	0.027	0.029	0.023	0.027	0.028
M05	1.0392	1.0401	1.0409	1.0144	1.0378	1.0397	0.160	0.150	0.160	0.110	0.150	0.160
M05-2X	1.0534	1.0601	1.0580	1.0343	1.0565	1.0561	0.200	0.210	0.210	0.160	0.200	0.200
M06	1.0310	1.0438	1.0399	1.0127	1.0288	1.0282	0.130	0.150	0.150	0.090	0.120	0.130
M06-2X	1.0503	1.0566	1.0563	1.0366	1.0511	1.0496	0.180	0.190	0.190	0.150	0.180	0.180
B2GP-PLYP	1.0343	1.0423	1.0436	1.0058	1.0370	1.0419	0.160	0.170	0.170	0.100	0.160	0.150

The scale factors and rms errors for the thermal contribution to entropy are reported in Table 5.6. Similar to the thermal contributions to enthalpy, the pure, hybrid meta, and double-hybrid functionals underestimate the thermal contribution to entropy. The scale factor of 1.0057 for the B2GP-PLYP functional and aug-cc-pVDZ is nearest to unity. For each of the functionals, variations in entropic contribution scale factors are between the cc-pVnZ basis set (n=D,T,Q) and the corresponding augmented basis set. The agreement (e.g. over or underestimation of properties) between earlier work with Pople type basis sets[2] and the current correlation consistent basis set study extends through the entropic contribution.

Table 5.6. Thermal contribution to entropy scale factors at 298.15 K and overall rms in J/K mol.

Functional	Scale Factors						RMS					
	cc-pVDZ	cc-pVTZ	cc-pVQZ	aug-cc-pVDZ	aug-cc-pVTZ	aug-cc-pVQZ	cc-pVDZ	cc-pVTZ	cc-pVQZ	aug-cc-pVDZ	aug-cc-pVTZ	aug-cc-pVQZ
BLYP	1.0298	1.0337	1.0326	1.0563	1.0361	1.0333	0.18	0.13	0.12	0.16	0.12	0.12
PBEPBE	1.0184	1.0218	1.0214	1.0401	1.0249	1.0224	0.18	0.12	0.12	0.14	0.11	0.11
HCTH93	1.0049	1.0087	1.0087	1.0253	1.0113	1.0094	0.16	0.12	0.11	0.14	0.10	0.10
BP86	1.0251	1.0260	1.0260	1.0470	1.0299	1.0251	0.18	0.12	0.12	0.15	0.12	0.12
B3P86	0.9776	0.9788	0.9787	0.9935	0.9815	0.9789	0.13	0.12	0.11	0.10	0.11	0.11
B3PW91	0.9777	0.9811	0.9806	0.9939	0.9839	0.9817	0.13	0.12	0.11	0.10	0.11	0.11
BPW91	1.0254	1.0233	1.0236	1.0425	1.0268	1.0225	0.19	0.12	0.11	0.14	0.11	0.11
PBE1PBE	0.9693	0.9726	0.9721	0.9848	0.9749	0.9735	0.14	0.12	0.12	0.10	0.12	0.12
BH&HLYP	0.9378	0.9378	0.9380	0.9507	0.9401	0.9381	0.16	0.16	0.16	0.13	0.16	0.16
MPW1K	0.9422	0.9441	0.9465	0.9554	0.9470	0.9454	0.15	0.15	0.16	0.13	0.15	0.15
M05	1.0465	1.0407	1.0419	1.0206	1.0361	1.0388	0.17	0.16	0.16	0.12	0.15	0.15
M05-2X	1.0450	1.0508	1.0439	1.0284	1.0473	1.0404	0.18	0.20	0.18	0.15	0.19	0.17
M06	1.0347	1.0438	1.0380	1.0148	1.0215	1.0207	0.05	0.05	0.06	0.06	0.10	0.11
M06-2X	1.0536	1.0583	1.0571	1.0384	1.0518	1.0459	0.19	0.19	0.19	0.16	0.18	0.17
B2GP-PLYP	1.0373	1.0432	1.0448	1.0057	1.0376	1.0467	0.16	0.17	0.17	0.10	0.16	0.16

In Table 5.7, the scale factors and rms errors for the ZPVEs are detailed. Similar to the vibrational frequencies, the pure DFT (BLYP, PBEPBE, HCTH93, BP86) scale factors are greater than one, signifying the underestimation of the ZPVE. The remaining functionals have scale factors for the ZPVE less than unity. The ZPVE scale factors for the double-hybrid functional, B2GP-PLYP, are similar to the hybrid meta functionals with twice the non-local exchange, represented by the 2X. The pure and hybrid DFT resulted in rms errors over three times greater than the rms errors of the hybrid meta and double-hybrid functionals. For HCTH93 there is a fluctuation above and below unity for the scale factor. This curiosity is mirrored in the scale factors for the Pople type basis sets;[2] though the deviation based on the change of basis for each functional is less for the correlation consistent basis sets.

Table 5.7. Scale factors for zero point vibrational energy (ZPVE) and rms in kJ/mol.

Functional	Scale Factors						RMS					
	cc-pVDZ	cc-pVTZ	cc-pVQZ	aug-cc-pVDZ	aug-cc-pVTZ	aug-cc-pVQZ	cc-pVDZ	cc-pVTZ	cc-pVQZ	aug-cc-pVDZ	aug-cc-pVTZ	aug-cc-pVQZ
BLYP	1.0165	1.0128	1.0134	1.0186	1.0136	1.0131	0.57	0.42	0.40	0.44	0.43	0.42
PBEPBE	1.0135	1.0098	1.0105	1.0134	1.0105	1.0114	0.49	0.43	0.43	0.57	0.44	0.44
HCTH93	0.9992	0.9973	0.9978	1.0018	0.9977	0.9977	0.45	0.42	0.41	0.45	0.41	0.42
BP86	1.0220	1.0173	1.0178	1.0240	1.0181	1.0176	0.56	0.43	0.41	0.44	0.44	0.43
B3P86	0.9874	0.9844	0.9847	0.9898	0.9849	0.9847	0.50	0.43	0.42	0.40	0.44	0.43
B3PW91	1.0057	1.0020	1.0029	1.0076	1.0028	1.0026	0.44	0.41	0.38	0.43	0.42	0.43
BPW91	1.0165	1.0128	1.0134	1.0186	1.0136	1.0131	0.57	0.42	0.40	0.44	0.43	0.42
PBE1PBE	0.9793	0.9768	0.9772	0.9809	0.9774	0.9775	0.54	0.50	0.50	0.52	0.51	0.52
BH&HLYP	0.9565	0.9541	0.9542	0.9589	0.9544	0.9542	0.63	0.58	0.57	0.55	0.60	0.59
MPW1K	0.9597	0.9597	0.9600	0.9633	0.9602	0.9600	0.59	0.58	0.57	0.54	0.59	0.59
M05	0.9809	0.9814	0.9801	0.9843	0.9824	0.9795	0.15	0.14	0.13	0.11	0.14	0.13
M05-2X	0.9697	0.9666	0.9678	0.9725	0.9673	0.9675	0.14	0.14	0.14	0.13	0.14	0.15
M06	0.9921	0.9881	0.9846	0.9951	0.9907	0.9849	0.18	0.17	0.15	0.14	0.18	0.16
M06-2X	0.9773	0.9735	0.9734	0.9804	0.9741	0.9733	0.16	0.14	0.14	0.14	0.14	0.15
B2GP-PLYP	0.9754	0.9732	0.9731	0.9807	0.9744	0.9735	0.10	0.12	0.11	0.12	0.12	0.10

5.4 Conclusions

Scale factors for (a) low and high harmonic vibrational frequencies, (b)thermal contributions to enthalpy and entropy, and (c) ZPVEs have been determined for seven hybrid functionals (B3P86, B3PW91, BPW91, PBE1PBE, BH&HLYP, MPW1K), four pure functionals (BLYP, PBEPBE, HCTH93, BP86), four hybrid meta functionals (M05, M05-2X, M06, M06-2X) and one double-hybrid functional (B2GP-PLYP), in conjunction with the correlation consistent basis sets (cc-pVnZ and aug-cc-pVnZ, n=D,T,Q). For the low frequency scale factors and ZPVEs, the hybrid, hybrid meta, and double-hybrid functionals scale factors are less than one, while the pure functionals underestimate the low frequencies and have scale factors greater than unity. The thermal contributions to enthalpy and entropy are overestimated by the pure, hybrid meta, and double-hybrid functionals. Overall, the properties determined are more affected by the choice of functional than the level of correlation consistent basis set and similar functionals provide similar results. Through the application of the scale factors for high vibrational frequencies, the percent of calculated frequencies within 3% of experimental values rose from 25% to approximately 90% for the augmented basis sets in conjunction with each of the pure, hybrid, hybrid meta and double-hybrid functionals. The nearly one hundred levels of theory presented here represent the largest published compilation of scale factors for a variety of density functionals in conjunction with the correlation consistent basis sets.

CHAPTER 6

VIBRATIONAL FREQUENCY SCALE FACTORS FOR DENSITY FUNCTIONAL THEORY AND THE POLARIZATION CONSISTENT BASIS SETS[**]

6.1 Introduction

Infrared (IR) and Raman spectroscopy are two widely used techniques for the characterization of chemical molecules including reaction products, inter- and intra-molecular interactions, and mixture components. The interpretation of the observed bands in a spectrum is aided by utilizing theoretically determined frequencies and intensities. However, calculated vibrational frequencies often employ the harmonic approximation, resulting in a neglect of anharmonic effects. To account for anharmonic effects, multidimensional potential energy surfaces (PES) must be computed with respect to the equilibrium geometry. The complexity, i.e., number of grid points, of the PES increases with molecular size and degrees of freedom (3N-6, where N is the number of atoms). While anharmonic frequencies have been determined via multidimensional PES[211] and anharmonic force fields,[212] the simplest and most common approach to ab initio calculations of vibrational frequencies is to determine harmonic frequencies and then utilize universal scale factors (specific to each method/basis set combination) to aid in predicting frequencies observed via experiment. The development of such scale factors for harmonic frequency calculations allows for the reliable determination of calculated vibrational frequencies. Scaled harmonic

[**] The research presented has been published in M.L. Laury, Matthew J. Carlson, and A.K. Wilson, *J. Comp. Chem*. **33**, 2380 (2012).

frequencies are within 3% error of experimental frequencies without the additional calculations for anharmonicity.[184]

The scaling factors for the harmonic frequencies correct for the neglect of anharmonic effects, in addition to the incomplete treatment of electron correlation and basis set truncation effects inherent in the methodology selection.[181] In general, theoretically determined vibrational frequencies overestimate the experimental fundamental frequencies. For example, harmonic frequencies determined by Hartree-Fock typically overestimate fundamental frequencies by 10%. The gap between calculated and experimental frequencies lessens when correlated methods [e.g. CCSD(T)] are employed.[213] The deviations between calculated vibrational frequencies and the fundamental frequencies are, on the whole, systematic. Because of the systematic nature of the deviations, uniform multiplicative scale factors are determinable for a theory.[1-3] Previous scaling work has examined what contribution to the frequency should be scaled. For example, should a separate scale factor be applied to the stretching and to the bending force constants?[214] Should the force constants included in the Hessian be scaled?[215] Or should the vibrational frequencies themselves be scaled?[1-3]

Common practice is to determine one scale factor for the harmonic vibrational frequencies obtained with a method and basis set combination. Scale factors have been developed for vibrational frequencies determined with the Pople-type basis sets, correlation consistent basis sets,[2,183,216] segmented contracted basis sets,[217] the Sadlej basis sets,[185] as well as semi-empirical methods.[218] For B3LYP, HF, and MP2 level calculations with correlation consistent basis sets (cc-pV*n*Z and aug-cc-pV*n*Z, n=D,T,Q),

Wilson and coworkers have determined scale factors for vibrational frequencies and ZPVEs.[183] Scale factors for the correlation consistent basis sets in conjunction with a broad range of density functionals, including Hybrid (H), Hybrid Meta (HM), Double Hybrid (DH), and those based on the Generalized Gradient Approximation (GGA) were detailed in Chapter 5.[216] Scale factors for vibrational frequencies computed with Sadlej basis sets were determined by Halls et al, where they concluded the hybrid functionals with the Sadlej pVTZ basis sets yielded the most reliable vibrational frequencies in the most cost-effective manner.[185] Generally scale factors are determined via a least-squares method, but there exist other approaches, such as the effective scaling frequency factor (ESFF) method. The ESFF method relies on local scaling factors obtained from local mode contributions to the normal mode.[219] Truhlar and co-workers have compiled a scale factor database, including a range of computational methods, such as wavefunction-based methods and semi-empirical methods.[188]

While previous scale factor development has focused on the Pople-type basis sets, correlation consistent basis sets, and Sadlej basis sets, scale factors defined for the polarization consistent basis sets developed by Jensen have been omitted. The next obvious step in scale factor development is to determine scale factors for widely-popular density functionals in combination with the polarization consistent basis sets.

An ideal method will obtain accurate results while being computationally efficient, with respect to memory, disk space, and central processing unit (CPU) time. To obtain results at the fully correlated level, extrapolations of energies have been employed. The correlation consistent basis sets were designed to systematically recover correlation energy with increasing basis set size.[9,43-45,49,98] The extrapolation of the resulting

correlation energy is an inverse power series as a function of the highest angular moment in the basis set.[77,220] Jensen and coworkers have shown Hartree-Fock and DFT energies converge as an exponential.[50,221] Based on this observation, Jensen and coworkers determined basis sets to systematically converge, in a smooth and efficient manner, for density functional calculations.[51] The resulting basis sets are referred to as polarization consistent. Since polarization effects occur within a molecule, as opposed to an atom, molecular calculations were employed in the development of the polarization consistent basis sets. The resulting basis sets are noted as pc-*n* (n=0-4), where n is the polarization level beyond the isolated atom.[51] For example, pc-0 for a first row element consists of an *s* and a *p* function. The pc-1 basis set adds a *d*-function, while the pc-2 basis set adds an *f*-function. The *s* and *p* functions were optimized for the atom, while the exponents of the additional "polarization" functions were optimized for a variety of bonding environments within molecules. The extrapolation of the polarization consistent basis sets for density functional calculations has been shown to yield total atomization energies in errors of less than 0.01 kJ/mol per atom.[51]

In this work, scale factors were determined for vibrational frequencies and ZPVEs calculated with the polarization consistent basis sets pc-n (n=0,1,2,3,4) in combination with a diverse set of density functionals. The functionals include six hybrid functionals (B3LYP,[26,27,30] B3P86,[28,30] B3PW91,[200-202] PBE1PBE,[203] BH&HLYP,[87] mPW1K),[204] five pure functionals (BLYP,[27,160] BPW91,[26,199,200] PBEPBE,[205] HCTH93,[206,207] and BP86),[208] four hybrid meta functionals (M05,[191] M05-2X,[192] M06,[193] and M06-2X)[193], one double-hybrid functional (B2GP-PLYP)[195,222], and one dispersion corrected functional (B97-D).[223] This scale factor work is a continuation of the work

presented in Chapter 5.[67] This chapter has included B97-D in the functional set, due to the increasing utilization of dispersion corrected functionals. With the previously assigned scale factors and the presently defined scale factors, vibrational frequencies determined with DFT should no longer be reported in error.

6.2 Computational Methodology

All calculations employed the Gaussian 09 software package.[165] The polarization consistent basis sets [pc-*n*, *n*=0,1,2,3,4] in combination with the seventeen functionals [B3LYP, B3P86, B3PW91, PBE1PBE, BH&HLYP, MPW1K, BLYP, BPW91, PBEPBE, HCTH93, BP86, M05, M05-2X, M06, and M06-2X, B2GP-PLYP, and B97-D] were used for the determination of the harmonic vibrational frequencies and zero-point vibrational energies (ZPVEs). Calculated vibrational frequencies were determined for 41 molecules as defined in a set by Healy and Holder.[209] For the ZPVEs, a set, organized by Schaefer and coworkers, of 24 molecules composed of diatomics, triatomics, and symmetric molecules was used.[210] With the calculated frequencies and ZPVEs, scale factors were determined for high and low vibrational frequencies, ZPVEs, and the thermal contributions to enthalpy and entropy. Additionally, the variation of the scale factor when using the augmented polarization consistent basis sets was examined. The scale factor equations have been detailed in Chapter 5.2.

6.3 Results and Discussion

6.3.1 High Frequencies

Scale factors and rms errors for the high vibrational (>1000cm^{-1}) frequencies for each of the functional and basis set combinations are reported in Table 6.1. The high vibrational frequencies are characteristic of stretching vibrations associated with the functional groups of a molecule. For example, the OH stretching is broad peak observed around 3300 cm^{-1} and the C=O stretching is a sharp peak around 1760 cm^{-1}. The scale factors for all of the density functionals included in the study are less than one; therefore, all of the functionals overestimate the high vibrational frequencies. The GGA functionals, including B97-D, have scale factors nearest one, e.g. 0.9954 for BLYP/pc-2 (written as method/basis set). To note for the functionals including Hartree-Fock (HF) exchange, as the amount of HF exchange increases, the scale factors deviate farther from one. The utility of the scale factors is supported by the rms errors, which are less than 4 cm^{-1}. The lowest errors for the scale frequencies were from BH&HLYP calculations with the pc-n basis sets (n=1,2,3,4). On average the pc-0 basis set resulted in rms errors one wavenumber greater than the rms errors for the basis sets with additional functions for polarization. The larger errors observed for the pc-0 basis set have been seen in previous frequency work by Anez et al., where they reported the importance of polarization functions in the basis set, specifically for carbonyl-containing molecules.[224] Generally, the polarization consistent basis sets with additional functions for polarization (n=1,2,3,4) are employed and this work further supports the necessity of polarization functions for the accurate determination of properties, such as vibrational frequencies.

Table 6.1. Scale factors and rms errors (cm^{-1}) for high vibrational (>1000 cm^{-1}) frequencies.

			λ					rms				
Functional	**Type[a]**	**%HF**	**pc-0**	**pc-1**	**pc-2**	**pc-3**	**pc-4**	**pc-0**	**pc-1**	**pc-2**	**pc-3**	**pc-4**
BP86	**GGA**		0.9891	0.9924	0.9932	0.9944	0.9945	3.9	2.5	2.5	2.4	2.4
BPW91	**GGA**		0.9849	0.9874	0.9889	0.9901	0.9901	4.0	3.6	2.5	2.6	2.6
BLYP	**GGA**		0.9929	0.9958	0.9943	0.9954	0.9955	4.1	2.7	2.6	2.6	2.5
HCTH93	**GGA**		0.9748	0.9752	0.9785	0.9798	0.9798	4.0	2.5	2.5	2.4	2.4
PBEPBE	**GGA**		0.9873	0.9890	0.9908	0.9919	0.9920	3.9	2.7	2.6	2.6	2.6
B97-D	**D, GGA**		0.9876	0.9904	0.9879	0.9923	0.9913	4.0	2.4	2.5	2.4	2.5
B3LYP	**H**	**20**	0.9625	0.9654	0.9662	0.9673	0.9674	3.6	2.2	2.2	2.2	2.2
B3P86	**H**	**20**	0.9560	0.9593	0.9616	0.9628	0.9629	3.6	2.3	2.3	2.2	2.2
B3PW91	**H**	**20**	0.9580	0.9606	0.9634	0.9646	0.9647	3.5	2.3	2.2	2.1	2.1
PBE1PBE	**H**	**25**	0.9539	0.9555	0.9592	0.9604	0.9605	3.5	2.4	2.3	2.2	2.2
mPW1K	**H**	**42.8**	0.9317	0.9332	0.9381	0.9393	0.9394	3.4	2.3	2.2	2.2	2.2
BH&HLYP	**H**	**50**	0.9289	0.9311	0.9342	0.9355	0.9355	3.4	1.9	1.9	1.9	1.8
M06	**HM**	**27**	0.9628	0.9648	0.9638	0.9630	0.9645	3.1	2.5	2.4	2.2	2.5
M05	**HM**	**28**	0.9516	0.9524	0.9545	0.9576	0.9590	3.6	2.8	2.8	2.6	2.9
M062X	**HM**	**54**	0.9510	0.9541	0.9557	0.9568	0.9566	3.4	2.3	2.2	2.1	2.1
M052X	**HM**	**56**	0.9367	0.9447	0.9470	0.9483	0.9470	4.0	2.6	2.4	2.4	2.6
B2GP-PLYP	**DH**	**65**	0.9464	0.9457	0.9498	0.9523	0.9526	4.0	2.3	2.3	2.2	2.1

[a] Functional types are denoted as GGA (Generalized Gradient Approximation), H (Hybrid), HM (Hybrid Meta), DH (Double Hybrid), D (Dispersion).

6.3.2 Low Frequencies

Table 6.2 details the scale factors and rms errors for low (<1000 cm^{-1}) frequencies for the polarization consistent basis sets and the density functionals. All of the GGA functionals underestimate the low vibrational frequencies and have scale factors greater than one. The scale factors associated with the pc-0 basis set are all greater than one; therefore, the omission of polarization leads to an underestimation of the low vibrational frequencies. Similar to the high vibrational frequencies, the rms errors of the pc-0 basis sets are twice as large as the rms errors of the pc-n (n=1,2,3,4) basis sets. For the functionals including HF exchange (hybrid and hybrid meta functionals) and the pc-n (n=1,2,3,4) basis sets, the scale factors are less than one. The overestimation of the low vibrational frequencies increases as the amount of HF exchange increases within the functional. If the uncertainty of the scale factors is considered (i.e., only two significant digits), then the scale factors for the low vibrational frequencies are more dependent on the functional than the level of polarization included in the basis set. This holds true except for the pc-0 basis set where there is no polarization. In fact, pc-0 should, as best be used as an anchor in an extrapolation procedure if absolutely required (as it essentially is a single-zeta basis set). pc-0 is not advocated for frequency calculations, but is included here for completion. A separate scale factor should be employed for pc-0 calculations versus pc-n (n=1,2,3,4) calculations with each density functional.

Table 6.2. Scale factors and rms errors (10^{-5} cm^{-1}) for low vibrational (<1000 cm^{-1}) frequencies.

	λ					rms				
Functional	**pc-0**	**pc-1**	**pc-2**	**pc-3**	**pc-4**	**pc-0**	**pc-1**	**pc-2**	**pc-3**	**pc-4**
BP86	1.071	1.021	1.024	1.025	1.025	2.0	0.8	0.7	0.7	0.7
BPW91	1.068	1.016	1.022	1.023	1.023	1.9	0.8	0.7	0.6	0.6
BLYP	1.073	1.028	1.030	1.031	1.031	1.8	0.9	0.7	0.7	0.7
HCTH93	1.054	0.9995	1.005	1.007	1.006	1.6	0.8	0.6	0.9	0.6
PBEPBE	1.062	1.013	1.018	1.021	1.020	1.9	0.8	0.7	0.6	0.6
B97-D	1.072	1.020	1.020	1.021	1.055	2.1	1.1	1.0	1.0	0.7
B3LYP	1.036	0.9808	0.9833	0.9844	0.9842	1.9	0.7	0.7	0.6	0.6
B3P86	1.036	0.9727	0.9776	0.9783	0.9780	2.2	0.7	0.7	0.6	0.6
B3PW91	1.035	0.9739	0.9795	0.9805	0.9803	2.0	0.7	0.7	0.6	0.6
PBE1PBE	1.023	0.9634	0.9698	0.9709	0.9708	1.9	0.7	0.7	0.7	0.7
mPW1K	1.001	0.9386	0.9435	0.9445	0.9445	1.9	0.8	0.8	0.8	0.8
BH&HLYP	0.9950	0.9352	0.9374	0.9374	0.9379	1.8	0.8	0.8	0.8	0.8
M06	1.021	0.9563	0.9577	0.9695	1.0418	2.0	0.9	0.9	0.8	0.7
M05	1.028	0.9563	0.9634	0.9713	1.0600	2.2	0.9	0.9	0.7	0.8
M062X	1.036	0.9603	0.9559	0.9631	0.9631	2.6	0.9	1.1	0.9	0.9
M052X	1.111	0.9725	0.9688	0.9852	1.0566	4.6	0.8	0.9	1.2	0.6
B2GP-PLYP	1.021	0.9710	0.9732	0.9712	0.9619	1.5	0.7	0.6	0.5	0.5

6.3.3 Vibrational contributions to thermodynamic properties (Entropy and Enthalpy)

The scale factors and rms errors for the vibrational contributions to enthalpy and entropy are reported in Tables 6.3 and 6.4, respectively. There is a distinct relationship between the number of polarized functions included in the basis set and the scale factor. The unpolarized basis sets, denoted pc-0, have scale factors that differ, on average, by 0.05 from the scale factors for the polarized basis sets, i.e., pc-n (n=1,2,3,4). This difference is within the significant digits of the scale factors and highlights the effect polarization has on calculated vibrational frequencies. The GGA functionals (BP86, BPW91, BLYP, HCTH93, PBEPBE, B97-D) all overestimate the frequencies, especially in conjunction with the pc-0 basis set. For the hybrid meta and the majority of the hybrid functionals, there is a divide, with respect to over- and underestimation, between the pc-0 and the remaining basis sets. For the pc-0 basis set, the hybrid meta and four of the six hybrid functionals overestimate the vibrational contributions to enthalpy and entropy. Additionally, the rms errors associated with the pc-0 basis set are, on average, three times the magnitude of the rms errors for the remaining basis sets. For the pc-n (n=1,2,3,4), the same functionals underestimate the contributions. The hybrid functionals with the largest percentages of HF exchange (mPW1K with 42.8% and BH&HLYP with 50%) underestimate the vibrational contributions for all of the polarization consistent basis sets. The scale factors for the two hybrid functionals and the basis sets with polarization (n=1,2,3,4) are near 1.10. The combination of a large percentage of HF exchange in the density functional design, and an increase in the number of polarization functions in the basis set, leads to a notable underestimation of the vibrational contributions to enthalpy and entropy. For

these methods, the scale factor is imperative for the accurate determination of the thermodynamic properties.

Table 6.3. Scale factors and rms errors (kJ/mol) for vibrational contributions to enthalpy.

	λ					rms				
Functional	**pc-0**	**pc-1**	**pc-2**	**pc-3**	**pc-4**	**pc-0**	**pc-1**	**pc-2**	**pc-3**	**pc-4**
BP86	0.9186	0.9493	0.9508	0.9509	0.9511	0.032	0.010	0.009	0.009	0.009
BPW91	0.9221	0.9563	0.9559	0.9558	0.956	0.032	0.010	0.009	0.009	0.009
BLYP	0.9094	0.9364	0.9394	0.9401	0.9404	0.033	0.013	0.012	0.011	0.011
HCTH93	0.9330	0.9806	0.9788	0.9789	0.9787	0.030	0.010	0.009	0.008	0.008
PBEPBE	0.9257	0.9588	0.9577	0.9571	0.9573	0.032	0.010	0.009	0.009	0.008
B97-D	0.9114	0.9490	0.9528	0.9536	0.9427	0.033	0.012	0.012	0.011	0.013
B3LYP	0.9687	1.014	1.017	1.017	1.017	0.037	0.012	0.013	0.013	0.013
B3P86	0.9794	1.030	1.030	1.030	1.030	0.037	0.010	0.012	0.012	0.012
B3PW91	0.9766	1.028	1.026	1.026	1.026	0.036	0.011	0.012	0.012	0.012
PBE1PBE	0.9911	1.045	1.043	1.042	1.042	0.036	0.011	0.016	0.012	0.012
mPW1K	1.033	1.100	1.097	1.096	1.096	0.040	0.015	0.018	0.017	0.017
BH&HLYP	1.038	1.106	1.107	1.108	1.107	0.042	0.018	0.020	0.019	0.019
M06	0.9945	1.042	1.050	1.044	1.007	0.037	0.013	0.015	0.016	0.026
M05	0.9983	1.047	1.046	1.042	0.9916	0.036	0.012	0.013	0.014	0.025
M062X	0.9969	1.050	1.059	1.054	1.055	0.042	0.016	0.019	0.018	0.019
M052X	1.006	1.047	1.056	1.051	1.036	0.047	0.016	0.020	0.019	0.018
B2GP-PLYP	0.9912	1.040	1.042	1.045	1.049	0.033	0.099	0.099	0.089	0.010

Table 6.4. Scale factors and rms errors (J/K*mol) for vibrational contributions to entropy.

	λ					rms				
Functional	**pc-0**	**pc-1**	**pc-2**	**pc-3**	**pc-4**	**pc-0**	**pc-1**	**pc-2**	**pc-3**	**pc-4**
BP86	0.8949	0.9468	0.9458	0.9458	0.9462	0.27	0.09	0.08	0.07	0.07
BPW91	0.8985	0.9540	0.9505	0.9504	0.9506	0.27	0.09	0.08	0.08	0.07
BLYP	0.8837	0.9320	0.9331	0.9337	0.9341	0.28	0.11	0.10	0.10	0.09
HCTH93	0.9108	0.9811	0.9765	0.9765	0.9763	0.25	0.09	0.08	0.07	0.07
PBEPBE	0.9036	0.9579	0.9539	0.9529	0.9532	0.27	0.09	0.08	0.07	0.07
B97-D	0.8848	0.9463	0.9481	0.9492	0.9090	0.28	0.11	0.10	0.10	0.14
B3LYP	0.9438	1.015	1.015	1.015	1.015	0.30	0.10	0.11	0.10	0.10
B3P86	0.9558	1.032	1.028	1.028	1.029	0.31	0.09	0.10	0.10	0.10
B3PW91	0.9531	1.029	1.025	1.025	1.025	0.29	0.09	0.10	0.10	0.10
PBE1PBE	0.9693	1.049	1.043	1.042	1.042	0.29	0.09	0.11	0.10	0.10
mPW1K	1.010	1.104	1.098	1.097	1.097	0.31	0.21	0.14	0.14	0.14
BH&HLYP	1.013	1.110	1.108	1.109	1.109	0.33	0.14	0.16	0.15	0.15
M06	0.9744	1.052	1.056	1.045	1.007	0.30	0.11	0.13	0.13	0.37
M05	0.9772	1.056	1.050	1.043	0.9916	0.29	0.11	0.11	0.11	0.23
M062X	0.9691	1.052	1.061	1.054	1.054	0.35	0.13	0.16	0.14	0.16
M052X	0.9700	1.043	1.052	1.041	1.036	0.43	0.13	0.15	0.17	0.21
B2GP-PLYP	0.9656	1.043	1.042	1.046	1.053	0.27	0.08	0.08	0.07	0.08

6.3.4 ZPVEs

The scale factors and rms errors for the ZPVEs are detailed in Table 6.5. Of interest is the distinct effect the inclusion of Hartree-Fock (HF) exchange has on the calculated ZPVE. For the GGA functionals and the polarization consistent basis sets, the scale factors for the ZPVEs are greater than one, signifying an underestimation of the ZPVEs. B97-D, a GGA functional with a dispersion correction, yields ZPVEs in near agreement with the GGA functionals included in this study; therefore, the inclusion of a dispersion correction has a negligible effect on the determination of the ZPVE. For the hybrid and hybrid meta functionals, the scale factors deviate farther from one as the amount of HF exchange is increased. This observation is supported by the known overestimation of HF for ZPVEs and a scale factor near 0.9000, depending on the basis set employed.[20] The majority of the rms errors for each of the functional and basis set combinations are less than 0.25 kJ/mol, demonstrating the accuracy of the scaled calculated frequencies. The lowest rms errors are for the hybrid functionals with between 20 and 25% of HF exchange (B3LYP, B3P86, B3PW91, PBE1PBE) and the GGA functional HCTH93. Raw, calculated frequencies for HCTH93 and the polarization consistent basis sets pc-n (n=1,2,3,4) are in near agreement with experimental frequencies. The scale factors, when considering uncertainty, are 1.0 and the rms errors are on the order of 0.25 kJ/mol. For the scale factors, the selection of the functional has the greatest impact, while the change in the amount of polarization included in the basis set results in an unappreciable change in the scale factor.

Table 6.5. Scale factors and corresponding rms errors (kJ/mol) for zero-point vibrational energies.

	λ					rms				
Functional	**pc-0**	**pc-1**	**pc-2**	**pc-3**	**pc-4**	**pc-0**	**pc-1**	**pc-2**	**pc-3**	**pc-4**
BP86	1.016	1.017	1.017	1.017	1.017	0.03	0.04	0.04	0.04	0.04
BPW91	1.012	1.012	1.012	1.013	1.013	0.02	0.03	0.03	0.03	0.03
BLYP	1.018	1.020	1.016	1.017	1.017	0.03	0.04	0.04	0.04	0.04
HCTH93	1.002	1.000	1.002	1.003	1.003	0.02	0.01	0.01	0.01	0.01
PBEPBE	1.015	1.014	1.015	1.015	1.016	0.03	0.03	0.03	0.04	0.04
B97-D	1.023	1.012	1.011	1.011	1.012	0.07	0.02	0.02	0.02	0.02
B3LYP	0.9870	0.9880	0.9869	0.9876	0.9877	0.04	0.03	0.03	0.03	0.03
B3P86	0.9801	0.9819	0.9834	0.9844	0.9845	0.02	0.02	0.02	0.02	0.02
B3PW91	0.9835	0.9832	0.9851	0.9861	0.9861	0.02	0.02	0.02	0.02	0.02
PBE1PBE	0.9793	0.9784	0.9812	0.9822	0.9823	0.03	0.02	0.02	0.02	0.02
mPW1K	0.9554	0.9540	0.9584	0.9594	0.9595	0.03	0.03	0.03	0.03	0.03
BH&HLYP	0.9511	0.9510	0.9526	0.9536	0.9537	0.02	0.03	0.03	0.02	0.02
M06	0.9860	0.9863	0.9849	0.9829	0.9853	0.04	0.03	0.03	0.04	0.03
M05	0.9770	0.9751	0.9771	0.9806	0.9848	0.02	0.02	0.02	0.02	0.02
M062X	0.9737	0.9728	0.9728	0.9734	0.9733	0.03	0.03	0.03	0.03	0.03
M052X	0.9635	0.9656	0.9661	0.9676	0.9670	0.06	0.05	0.05	0.04	0.05
B2GP-PLYP	0.9698	0.9669	0.9705	0.9726	0.9722	0.04	0.03	0.02	0.03	0.02

6.3.5 Augmented Basis Sets

In general, the inclusion of augmenting functions in the polarization consistent basis set has little effect on calculated frequencies. This result was also observed in previous work with the correlation consistent basis sets.[183,216] For each of the functionals, the augmented correlation consistent basis sets, in general, had negligible contributions to the vibrational frequencies. A brief analysis was carried out for frequencies calculated using the augmented pc-3 basis set with one functional of each definition (pure, hybrid, hybrid meta, and double hybrid). Augmenting functions had the greatest effect on frequencies calculated using B2GP-PLYP, with rms errors of 15 cm^{-1} from those calculated with the non-augmented basis set. The remaining functionals tested had rms errors on the order of 1 cm^{-1}. Similarly, augmenting functions do not have an effect on the calculated ZPVE, with the largest rms errors on the order of 0.01 kJ/mol when compared to the calculated ZPVE without augmenting functions. The effect of augmenting functions on the scale factor is negligible, suggesting that the same scale factor can be used for both augmented and non-augmented basis sets for vibrational frequencies and ZPVEs.

6.4 Conclusions

Scale factors for harmonic vibrational frequencies, vibrational contributions to enthalpy and entropy, and ZPVEs have been defined for five pure functionals (BP86, BPW91, BLYP, HCTH93, PBEPBE), six hybrid functionals (B3LYP, B3P86, B3PW91, PBE1PBE, mPW1K, BH&HLYP), four hybrid meta functionals (M05, M06, M05-2X, M06-2X), one double hybrid functional (B2GP-PLYP), and one dispersion corrected

functional (B97-D) in combination with the polarization consistent basis sets (pc-n, n=0,1,2,3,4). For the high (>1000 cm^{-1}) vibrational frequencies, the functional and basis set combinations all overestimate the frequencies and the recommended scale factors are less than unity. The effect of the percent of HF exchange included in the functional is evident for each property, e.g. increasing the percent of HF exchange results in greater overestimation of the high vibrational frequencies. The low vibrational frequencies, as well as the vibrational contributions to enthalpy and entropy, are sensitive to the inclusion of polarization functions in the basis set. For un-polarized basis sets (pc-0), the scale factors are distinctly different for each of the properties and methods. The rms errors of the pc-0 basis set for the calculated frequencies and vibrational contributions are twice as large as the rms errors for the rest of the polarization consistent basis sets (pc-n, n=1,2,3,4) and the pc-0 basis set is not recommended for molecular calculations. The scale factors for the ZPVEs are more dependent on the method than the level of polarization in the basis set. The pure (GGA) functionals all underestimate the ZPVEs and have scale factors greater than one. Additionally, the inclusion of a dispersion correction for a GGA functional does not significantly change the ZPVE. The remaining hybrid, hybrid meta, and double hybrid functionals overestimate the ZPVEs. If the uncertainty of scale factors is considered, i.e., scale factors have only two significant digits, then unique scale factors for each functional, when employed with polarization consistent basis sets, can be defined for the determination of vibrational frequencies, vibrational contributions to enthalpy and entropy, and ZPVEs.

CHAPTER 7

PERFORMANCE OF DENSITY FUNCTIONAL THEORY FOR FIRST AND SECOND ROW TRANSITION METAL THERMOCHEMISTRY[††]

7.1 Introduction

Density functional theory (DFT) is widely used to study transition metal (TM) molecules since it accounts for electron correlation at a reduced computational cost, as compared to correlated ab initio methods. DFT is routinely employed for TM-containing molecules to determine ground state geometries, transition structures, spectroscopic constants, and energetic properties, including bond dissociation energies and enthalpies of formation.[193,225] Through numerous studies of main group species, shortcomings of DFT, such as self-interaction and neglect of long-range effects have emerged.[23,226] For transition metal species, where functionals are not well (or at all) parameterized, many fewer studies indentifying successes and shortcomings of functionals have been done. In fact, only some of the shortcomings of certain density functionals for TM, namely 3*d* TM, species have been identified in the literature (see, e.g., Ref. 71,72,104,107), e.g. deviations from 3*d* TM experimental enthalpies of formation on the order of 100 kcal mol^{-1} for B3LYP, while a focus on calibrating functional performance for 4d TM species is needed.

Benchmark studies of functional performance for 4*d* metal thermochemistry have been limited at best, despite the importance of these species in areas such as

[††] The work regarding the first row transition metals has been published in W. Jiang, M.L. Laury, M. Powell, and A.K. Wilson, "Comparative Study of Single and Double Hybrid Density Functional for the Prediction of 3d Transition Metal Thermochemistry", *J. Chem. Theory Comput.* **8**, 4102 (2012).

catalysis[91] and medicine.[92] Only recently have Truhlar and co-workers examined the performance of DFT for 4*d* atom multiplicities and ionization states.[227]

While DFT is widely employed, ab initio calculations are generally preferred for more accurate prediction of energetic properties. For example, for first row transition metals, an ab initio composite method, the correlation consistent composite approach (ccCA-TM)[70,72] results in a mean absolute deviation (MAD) of 3 kcal mol^{-1} from experiment for enthalpies of formation (ΔH_f's), whereas DFT, e.g. B97-1, has been shown to have errors in excess of 6 kcal mol^{-1} from experimental ΔH_f's and widely-used functionals, such as B3LYP, have deviations of more than 10 kcal mol^{-1} from experiment.[71,228] Based upon the larger average experimental uncertainties observed for transition metal enthalpies of formation in comparison to main group species, chemical accuracy for 3*d* transition metals has been defined as ab initio calculations being within 3 kcal mol^{-1} from experimental values (as opposed to the main group definition of chemical accuracy of within 1 kcal mol^{-1} of experiment).

In considering second row transition metals, ab initio methods such as CCSD(T) are often hindered by the large number of correlating electrons requiring additional basis functions and the scaling of the method (N^7 for CCSD(T), where N is the number of basis functions). To mitigate the computational cost associated with the 4*d* elements, pseudopotentials or effective core potentials (ECP) may be employed with valence basis sets. By replacing the core electrons with an effective potential, the ECPs reduce the total number of electrons in the calculation and, in turn, the number of basis functions in a calculation.[101]

Recently the authors developed a relativistic pseudopotential-based composite method, defined as rp-ccCA, and examined the performance of the method for 4*p* and 4*d* molecules.[67] The rp-ccCA methodology[67] follows a similar schematic as defined for main group ccCA[68,69] and ccCA-TM[70,72] for first row transition metals. ccCA and its variants have proven to be robust methodologies for main group and first row transition metal energetic and thermodynamic studies.[64,65,67-70,72,95,96,121,229] The reduced computational cost afforded by the composite strategy was then further reduced by the use of energy-consistent, small core ECPs for 4*p* and 4*d* elements.[67] In the rp-ccCA work (Chapters 3 and 4) a molecule set composed of 30 ΔH_f's of 4*d* TM-containing molecules was defined, called TM-4*d*.[67] It is composed of TM halides, oxides, hydrides, carbides, dimers, and carbonyls, as well as open and closed shell molecules. Selection for inclusion in this set was based the availability of reliable experimental data. The TM-4*d* set and rp-ccCA will be utilized as measures for DFT performance in the current work.

The density functionals considered in the current study were selected based on past studies of those demonstrating more successful performances in 3*d* TM and 4*d*, their level of parameterization, and the frequency of their use in chemical application studies, e.g. the design of a novel catalyst, for both main group and transition metal research. The selected density functionals include third, fourth, and fifth rung functionals.

Due to the diverse methods of parameterization and the goal to address shortcomings of DFT, there are density functionals that have been designed for specific properties such as barrier heights (B3LYP-LOC),[233] nonbonded interactions

(PW6B95),[234] and kinetics (BMK).[235] When comparing average DFT results for main group species to those obtained for transition metals, two observations are made: 1) the best functionals for main group chemistry are not typically the best for transition metal chemistry,[236] and, 2) the average errors observed for DFT for transition metal thermochemistry are generally at least 3-5 kcal mol^{-1} greater than the DFT errors observed for main group molecules containing the same number of non-hydrogen atoms and/or the same functional groups.[71,228]

Though most functionals do not include transition metal data within their parameterization sets, there are a few density functionals that include transition metals within the parameterization of the functional (e.g. the TMAE9/05 set of 9 atomization energies of metal diatomics, MLBE21/05 of 21 metal-ligand bond energies, 3*d*TMRE18/06 of 18 reaction energies, and MAEE5 of 5 metal atom excitation energies).[193] These functionals include M06 and M06-2X, and they are included within the current study.

In a recent study by Truhlar and Luo, the multiplicities and ionization states of 4*d* TM atoms were examined with a variety of density functionals.[227] Within the study the occupancies of the 4*d* and 5*s* orbitals, as determined by DFT, were used as one of the measurements of error for functional performance. Overall it was observed that GGA functionals favored filling the 4*d* orbitals before the 5*s* orbitals, while Hartree-Fock favored filling the 5*s* orbitals before the 4*d* orbitals. The observation about the order of orbital occupation via GGA functionals is counter to what is reported experimentally. In order to fill the 4*d* and 5*s* orbitals in agreement with experiment, a percentage of HF exchange must be introduced to the GGA functional, i.e., employ HGGAs.

In this study, the performance of a variety of density functionals in conjunction with ECPs and valence basis sets is gauged for the prediction of 4*d* TM thermochemistry to determine preferred functionals for TM thermochemistry and to compare with prior studies. The TM-4*d* set of 4*d* ΔH_f's was utilized to compare the DFT results to those previously obtained with rp-ccCA.[67] Because of the well-established success of the correlation consistent sets, these basis sets were used as the valence basis sets in conjunction with the small core ECP in both this study and in the construction of rp-ccCA. Here, ground states of the 4*d* molecules and the ΔH_f's determined by DFT are examined in comparison to rp-ccCA results and experimental data.

7.2 Computational Methodology

All DFT calculations were carried out with the GAUSSIAN 09 software package.[165]

7.2.1 3*d* Transition Metals

For the first row transition metals, the ccCA-TM/11 molecule set of enthalpies of formation was employed.[72] Geometry optimizations and separate single point energy calculations were carried out for each functional. Overall, the 3d study examined the performance of 13 density functionals, though the results of the B97 family of functionals (B97-1, B97-2, wB97, wB97X, wB97XD) will be detailed in this dissertation. For each functional in the B97 family of functionals, aug-cc-pVQZ single point calculations were conducted at the aug-cc-pVTZ geometry (i.e., B97-1/aug-cc-

pVQZ//B97-1/aug-cc-pVTZ). "Fine" grids were applied to all calculations.

7.2.2 4*d* Transition Metals

For the second row transition metals, the small core, energy-consistent relativistic pseudopotentials and the corresponding valence correlation consistent basis sets of triple- and quadruple-zeta quality were employed.[114] For each molecule in the TM-4*d* set (see Table 7.1), B3LYP/cc-pVTZ-PP optimized geometries were utilized for single-point energy calculations for each functional and molecular ΔH_f's were determined. 22 functionals were considered, including GGAs (BLYP,[26,27,160] BP86,[28] TPSSKCIS,[237] PBEPBE,[24,205] M06-L[238]), hybrid (B3LYP,[30] B97-1,[207] PBE1PBE,[239] B3P86, X3LYP,[241] mPW1LYP,[242] B1LYP,[243] BMK,[235] M06 and M06-2X[193]), range-separated (ωB97 and ωB97X,[39] ωB97XD,[40] CAM-B3LYP,[232] LC-ωPBE[244]), and double hybrid functionals (B2GP-LYP,[195] mPW2-PLYP[33]). The list of functionals by type, including percentage HF exchange, percentage PT2 correlation, and the value of the range-separation parameter for the pertinent functionals, is summarized in Table 7.2. Fine grids were employed for all calculations. Fine grids are defined as 75 radial shells with 302 angular points per shell (approximately 7000 points per atom). Enthalpies of formation were calculated via the atomization energy approach, i.e., via the dissociation of the ground state molecule into its constituent ground state atoms. Experimental data was used for the atomic enthalpies of formation.[245] Zero-point energies were scaled by the appropriate scaling factor for each functional as determined in previous work by the authors.[216] The impact of functional choice upon the optimized structure and the corresponding impact on the ΔH_f's was examined for each functional. The cc-pVTZ-PP basis set was used for the geometry optimization to compare to the B3LYP/cc-pVTZ-PP

geometries from rp-ccCA and the cc-pVQZ-PP basis set was used for the determination of the ΔH_f's based on previous TM studies.

Table 7.1. The TM-4*d* molecule set.

Molecule	Ground State	Molecule	Ground State
YO	$^2\Sigma^+$	MoF_2	$^5B_2$
ZrO	$^1\Sigma^+$	MoF_6	$^1A_{1g}$
ZrO_2	$^1A_1$	$Mo(CO)_5$	$^1A_1$
ZrCl	$^2\Delta$	$Mo(CO)_6$	$^1A_1$
$ZrCl_2$	$^3\Delta$	RuO_4	$^1A_1$
$ZrCl_4$	$^1A_1$	RhC	$^2\Sigma^+$
ZrBr	$^2\Delta$	RhO	$^4\Sigma^-$
$ZrBr_4$	$^1A_1$	$RhCl_2$	$^4\Sigma_g^+$
NbO	$^4\Sigma^-$	AgH	$^1\Sigma^+$
NbO_2	$^2A_1$	Cd_2	$^1\Sigma_g^+$
MoO_2	$^3B_1$	CdH	$^2\Sigma^+$
MoO_3	$^1A_1$	CdCl	$^2\Sigma^+$
$MoOCl_4$	$^1A_{1g}$	$CdCl_2$	$^1\Sigma_g^+$
MoO_2Cl_2	$^1A_{1g}$	CdBr	$^2\Sigma^+$
MoF	$^6\Sigma^+$	$CdBr_2$	$^1\Sigma_g^+$

Table 7.2. The twenty-two functionals arranged by type and parameter values.

Functional	$\%E_x^{HF}$	$\%E_c^{PT2}$	ω	Type[1]	Functional	$\%E_x^{HF}$	$\%E_c^{PT2}$	ω	Type[1]
BLYP				GGA	B1LYP	25			HGGA
BP86				GGA	M06	27			HGGA
PBEPBE				GGA	BMK	42			HGGA
TPSSKCIS				GGA	M06-2X	54			HGGA
M06-L				GGA	ωB97XD	22.2		0.2	RSH
B3P86	20			HGGA	ωB97X	15.8		0.3	RSH
B3LYP	20			HGGA	CAM-B3LYP	20		0.33	RSH
B971	21			HGGA	ωB97			0.4	RS
X3LYP	21.8			HGGA	LC-ωPBE			0.4	RS
PBE1PBE	25			HGGA	mPW2-PLYP	55	25		DH
mPW1LYP	25			HGGA	B2GP-LYP	65	36		DH

[1] Generalized Gradient Approximation (GGA), hybrid (H), Range-separated (RS), Double (D).

7.3 Results and Discussion

7.3.1 First Row Transition Metal Thermochemistry-Overall Results

Of the 13 density functionals studied in conjunction with the correlation consistent basis sets, the hybrid B97-1 and double hybrid mPW2-PLYP functionals yielded the lowest overall mean absolute deviations (MAD) from experimental enthalpies of formation with 7.2 and 7.3 kcal mol^{-1}, respectively.

The B97-1 functional, using the cc-pVQZ basis set, yields an MAD of 7.2 kcal mol^{-1} for the overall ccCA-TM/11 set, significantly less than the MAD of 13.0 kcal mol^{-1} obtained with B3LYP (Figure 7.1). The relatively large errors of B3LYP might originate from an overestimation of metal-ligand binding energies by B3LYP, as shown by the overall B3LYP MSD of -11.1 kcal mol^{-1}, comparing to the B97-1 MSD of -2.4 kcal mol^{-1}. When utilizing ccCA-TM for the ccCA-TM/11 set, a monotonic decrease of the MAD is observed as the experimental uncertainty decreases.[228] In contrast to the ccCA-TM results, the B97-1 MADs do not show any discernible increasing/decreasing patterns across the subsets of decreasing experimental uncertainty. The B98 functional, sharing the same formulas of B97-1, was re-optimized using the G2/97[208] set of 148 main group ΔH_f's. However, B98 yields larger MADs than B97-1 for the TM systems, and the overall MAD is 8.9 kcal mol^{-1}, which is 2.7 kcal mol^{-1} greater than that of B97-1. The B97-1 and B98 MADs (7.2 and 8.9 kcal mol^{-1}, respectively) for the ccCA-TM/11 set are much higher than their MADs (3.1 and 6.9 kcal mol^{-1}, respectively) for the 19-molecule set in our earlier study.[71] The substantial increase of the B97-1 MADs from the 19-molecule set to the ccCA-TM/11 set suggests that the assessment of certain functionals may lead to fortuitous results if the molecule set is limited in size and/or

bonding features. The ωB97X functional, containing a long range correction to the exchange energy, has more empirical parameters (17 parameters) than B97-1 (10 parameters) and outperforms B97-1, for the G3/99 set of 223 main group ΔH_f's, by a notable margin (MAD of 2.09 kcal mol^{-1} vs. 4.85 kcal mol^{-1}).[40] However, the modifications in ωB97X deteriorate the overall quality of calculated ΔH_f's for TM species considered in this study, yielding an overall MAD of 10.4 kcal mol^{-1} for the ccCA-TM/11 set.

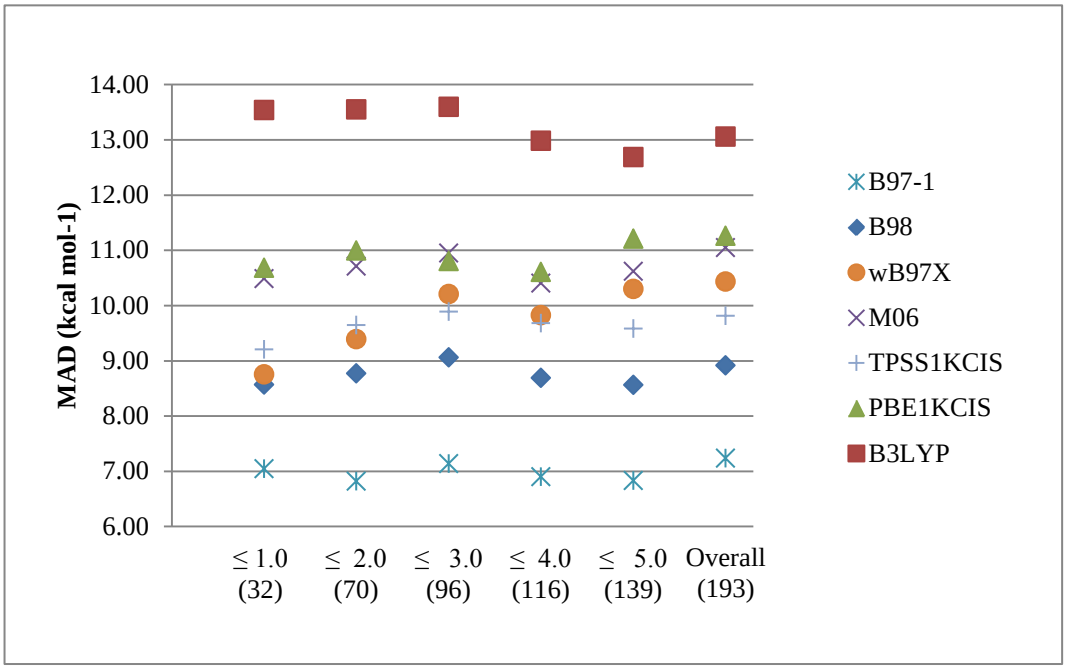

Figure 7.1. MADs of the single-hybrid functionals in the 3*d* DFT thermochemistry study organized by increasing experimental uncertainties.

Due to the promising performance of B97-1, we considered additional variants of the B97 functional, including B97-2, ωB97, ωB97X, and ωB97XD (Figure 7.2). To examine the highest level of accuracy obtainable with DFT for transition metals, augmented basis sets (aug-cc-pVnZ, n=T,Q) were utilized in the extended study of the variants of the B97 functional. While the hybrid GGA functionals B97-1 and B97-2 were

each fit to energetic data from the G2-1 training set, the B97-2 functional has the additional fitting to a Zhao, Morrison, and Parr (ZMP) exchange-correlation potential derived from ab initio Brueckner doubles or MP2 electron densities.[246] The ω of the ωB97, ωB97X, and ωB97XD has been used to correct the asymptotic behavior of a pure exchange functional by defining the regions described by the long-range Coulomb operator. Three range-separated hybrid functionals based on PBE were compared to other functionals for the predictions of equilibrium geometries and dissociation energies of TM complexes,[247] but none of the ωB97, ωB97X, and ωB97XD functionals have been considered systematically for TM thermochemistry prior to our study. The X in ωB97X and ωB97XD indicates the inclusion of Hartree–Fock exact exchange in the short-range exchange and the D represents the inclusion of a dispersion correction within the ωB97XD functional. For a few of the molecules, severe convergence problems in the calculations were encountered with all or some of the functionals. The absolute deviations of ΔH_f from experimental data by ωB97X and ωB97XD were greater than 150 kcal mol^{-1} for Cr_2. As a result, 13 molecules including Cr_2 were excluded from the ccCA/TM11 set for the B97/aug-cc-pVQZ//B97/aug-cc-pVTZ calculations (Figure 1b). Compared to the B97/cc-pVQZ calculations, the performance of B97-1 was comparable, but the MAD of ωB97X was slightly larger. The increases in MAD are 0.2 ~ 0.4 kcal mol^{-1} for B97-1 and 0.3 ~ 1.5 kcal mol^{-1} for ωB97X.

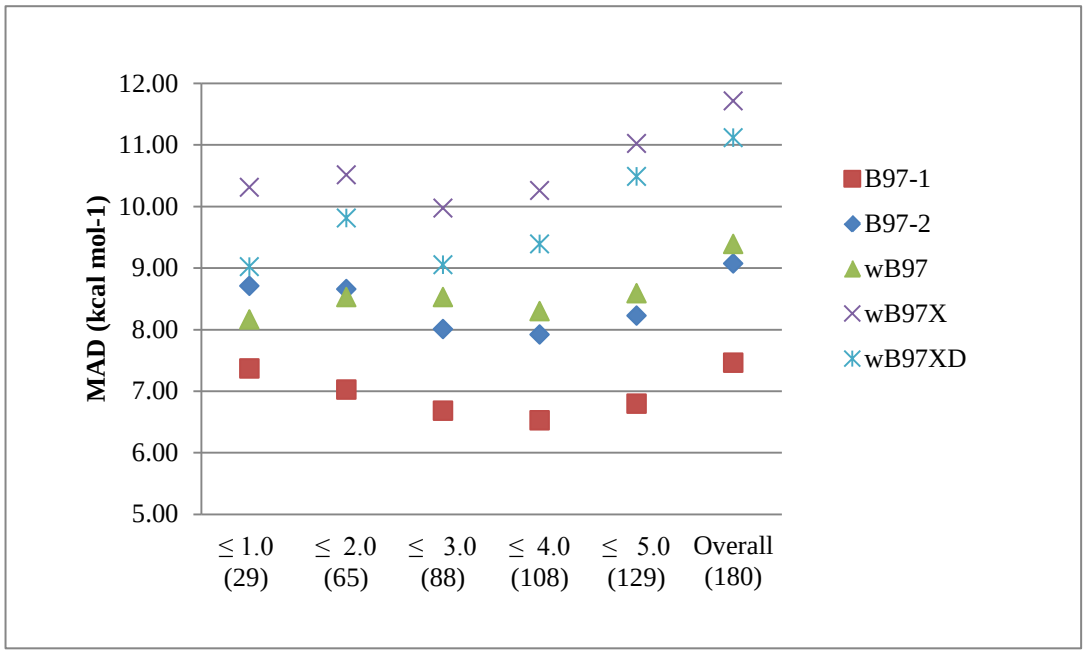

Figure 7.2. MADs of the B97 family of functionals organized by increasing experimental uncertainties.

B97-1 gives the lowest MADs among the five B97 functionals. The parameterization using the ZMP potential in the fitting of the B97-2 functional does not improve the results as compared to B97-1, possibly because the ZMP potential derivation is based upon main group species. The B97-2 MADs show the same patterns across the subsets as those of B97-1, but are 1.4 ~ 1.7 kcal mol^{-1} greater. The long-range corrected ωB97 functional results are inferior to B97-1 (overall MAD of 9.4 kcal mol^{-1} for ωB97 and 7.5 kcal mol^{-1} for B97-1), but show improvements over ωB97X (overall MAD of 11.7 kcal mol^{-1}) and ωB97XD (overall MAD of 11.1 kcal mol^{-1}). The hybrid use of Hartree-Fock exchange for the short-range interactions in ωB97X, where ω already introduces the Hartree-Fock exchange for the long-range interactions, increases the overall MAD for the TM ΔH_f's by over 2.5 kcal mol^{-1}. The introduction of a

dispersion parameter slightly improves the performance of the long-range corrected hybrid functional for the prediction of TM ΔH_f's.

7.3.2 Second Row Transition Metal Thermochemistry

7.3.2.1 Overall Results

The mean absolute deviation (MAD), mean signed deviation (MSD), root-mean-square deviation (RMSD), and standard deviation (σ) for the predicted enthalpies of formation of the TM-4*d* set relative to experiment for each functional are reported in Table 7.3. The MADs are depicted in Figure 7.3 and the MSDs are represented in Figure 7.4. The double hybrid functional, mPW2-PLYP, yields the lowest MAD of 4.25 kcal mol^{-1} for the TM-4*d* molecule set. The MAD of mPW2-PLYP is approximately two kcal mol^{-1} greater than the MAD obtained with rp-ccCA, supporting the utility of the double hybrid functional for 4d molecules outside the scope of rp-ccCA. Similarly, a low MAD was obtained by the other double hybrid functional studied, B2GP-LYP (5.19 kcal mol^{-1}). The experimental uncertainty for the TM-4*d* molecule set is 3.43 kcal mol^{-1}.

Table 7.3. Overall DFT statistics (MAD, MSD, RMSD, σ) for the TM-4*d* molecule set. Geometries obtained with B3LYP/cc-pVTZ-PP.

Functional	MSD	MAD	RMSD	σ	Functional	MSD	MAD	RMSD	σ
BLYP	12.09	16.69	25.39	19.13	**B1LYP**	-16.37	16.71	22.43	14.96
BP86	22.87	23.87	37.13	28.44	**M06**	1.74	8.36	10.63	6.26
PBEPBE	25.07	26.03	40.32	30.80	**BMK**	-1.28	12.86	15.76	9.10
TPSSKCIS	13.31	14.15	22.74	17.80	**M06-2X**	-8.76	10.84	14.09	8.62
M06-L	9.43	11.98	17.80	12.73	**ωB97XD**	0.04	6.52	8.71	5.78
B3P86	4.93	8.34	13.40	10.48	**ωB97X**	3.05	7.42	10.15	6.93
B3LYP	-5.81	8.74	10.53	5.93	**CAM-B3LYP**	-5.53	8.06	10.65	6.96
B971	5.28	8.10	12.28	9.24	**ωB97**	4.92	8.74	13.03	9.66
X3LYP	-5.63	8.32	9.92	5.40	**LC-ωPBE**	-4.60	11.47	14.84	9.42
PBE1PBE	-5.18	8.53	11.01	6.96	**mPW2-PLYP**	-2.21	4.25	5.67	3.76
mPW1LYP	-12.08	12.61	16.87	11.20	**B2GP-LYP**	-1.26	5.19	7.87	5.92

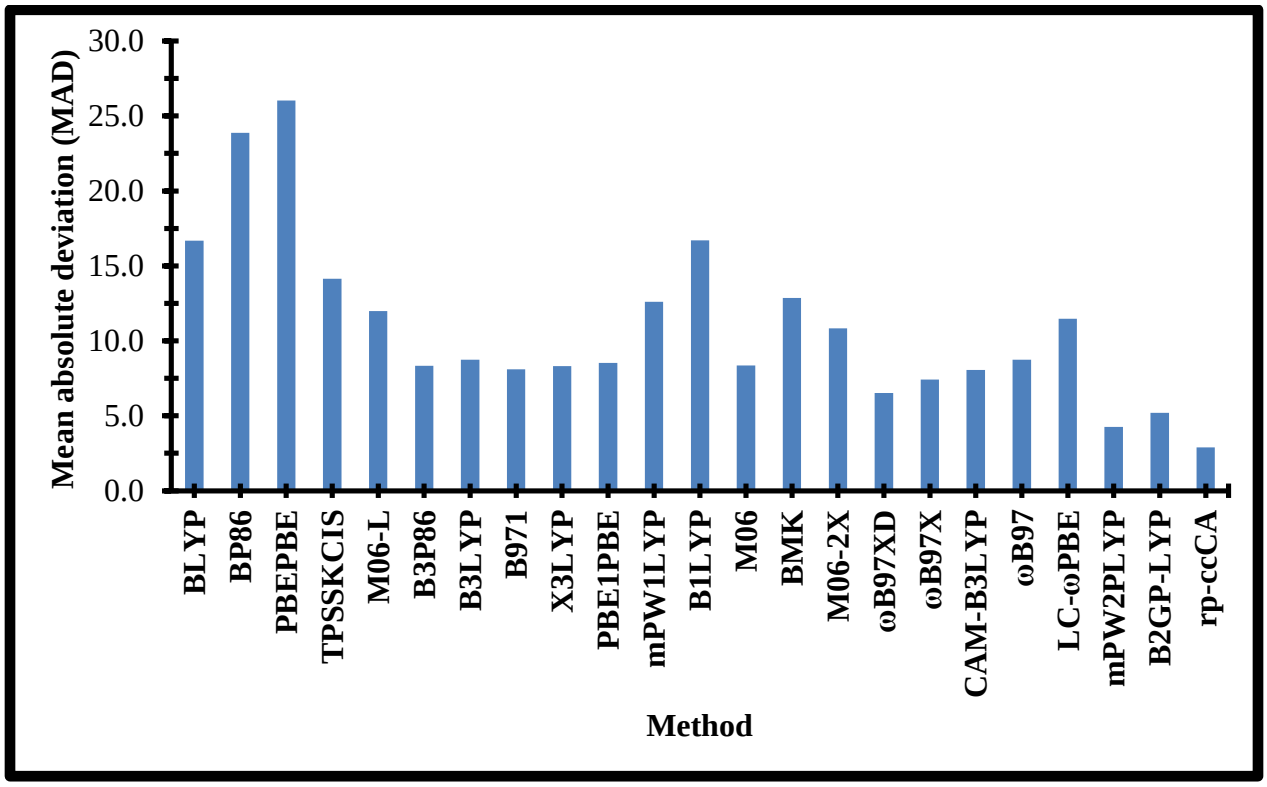

Figure 7.3. Mean absolute deviations (MADs) of the density functionals and rp-ccCA.

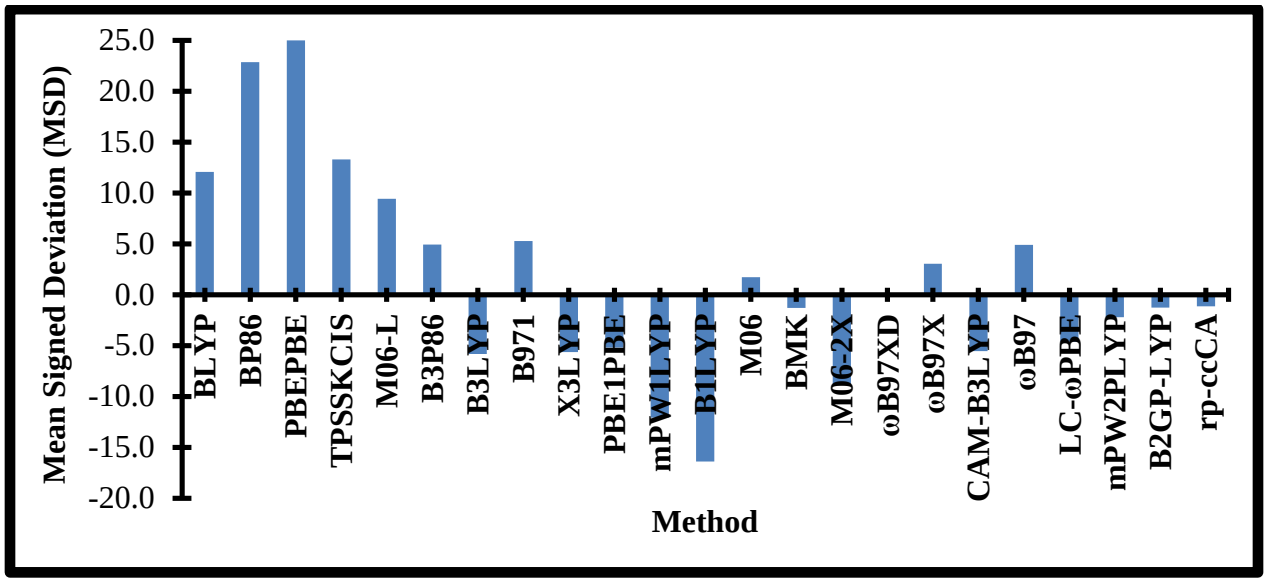

Figure 7.4. Mean signed deviations (MSDs) of the density functionals and rp-ccCA.

While the fifth rung functionals, the double hybrids, yielded the most accurate ΔH_f's, in comparison to experiment, for the TM-4*d* set, the third run functionals, GGAs, resulted in the largest MADs. BP86 and PBEPBE had MADs of 23.87 and 26.03 kcal mol^{-1}. The large MAD was rooted in the carbonyl-containing molecules, three of the molybdenum molecules and RuO_4. The determination of the enthalpy of formation of 3*d* TM carbonyl-containing molecules has previously been shown by Tekarli *et al*. to result in large deviation from experiment for DFT calculations (e.g. over 50 kcal mol^{-1} for GGAs, over 80 kcal mol^{-1} for MGGAs, and over 40 kcal mol^{-1} for HGGAs)[71] and these deviations are also observed in this work for 4*d* TM carbonyl systems. When the 3*d* TM carbonyls were studied with ccCA-TM, a high-level ab initio composite method, the deviations were significantly reduced (the majority of the ccCA-TM enthalpies of formation deviating less than 10 kcal mol^{-1} from experiment), but the average absolute deviation of the 3*d* TM carbonyls was 6.3 kcal mol^{-1}, a considerable deviation when the accuracy goal of ccCA-TM is properties within 3 kcal mol^{-1} from experiment.[72] A similar trend is observed when comparing the DFT deviations for the 4*d* TM carbonyls to the deviations obtained with rp-ccCA. The significant lowering of the deviation, when changing from DFT to ab initio methods, of the calculated enthalpy of formation from the experimental value signifies the need for high-level methods for the carbonyl-containing molecules. With a higher level of theory, a more accurate description of the π-back bonding present in the TM-carbonyl systems is obtainable and, in turn, the calculated enthalpy of formation of the TM-carbonyl systems is more accurate.

The previous DFT 4*d* atomic study by Truhlar and Luo reported that the hybrid functionals SOGGA11-X, B1LYP, B3LYP, CAM-B3LYP, BMK, and PW6B95 provide the

best comparison with experimental ionization potentials and spin states of the 4*d* atoms.[227] These observations are mirrored in the current study for 4*d* molecular ΔH_f's; the hybrid functionals, both single and double, with a percentage of HF exchange between 20% and 40% yield the lowest deviations from experimental ΔH_f's. This percentage of HF exchange for 4*d* thermochemistry is in agreement with the ideal percentage of HF exchange for 3*d* transition metal ΔH_f's as observed in a previous study by Tekarli *et al*. Furthermore, the ideal percentage of HF exchange (20-40%) for 4*d* ΔH_f's is in agreement with observations for 4*d* reaction energies involving C-O bond cleavage.{Liu, 2013 #355}

The overall experimental uncertainty for the TM-4*d* molecule set is 3.43 kcal mol^{-1}. Furthermore, the ΔH_f's determined via rp-ccCA resulted in an MAD of 2.89 kcal mol^{-1} from experimental ΔH_f's. Except for RhO and ZrO_2, ΔH_f's from DFT calculations exceed the experimental uncertainties for each molecule. It should be noted that the ΔH_f's for these two molecules had the largest experimental uncertainties of 10.0 and 11.0 kcal mol^{-1}, respectively.

7.3.2.2 Generalized Gradient Approximation (GGA) Functionals

Common outliers for the GGA functionals were $MoCO_5$, $MoCO_6$, MoF_6, and RuO_4. The BP86 and PBEPBE functionals resulted in significant deviations, near 100 kcal mol^{-1}, for these molecules. By excluding the outliers for BP86, PBEPBE, and BLYP, the MADs dropped by nearly 70% to 8.75, 10.18, and 10.60 kcal mol^{-1}, respectively. The deviation observed for the outliers of TPSSKCIS and M06-L were nearly half of the deviations seen for BP86, PBEPBE, and BLYP; therefore, the drop in

the MAD with the exclusion of the outliers was not as drastic (50%) for TPSSKCIS and M06-L, 7.12 and 6.91 kcal mol^{-1}, respectively. All of the GGA functionals overestimated the enthalpies of formation by, on average, 15 kcal mol^{-1}. Since the enthalpies of formation are determined via atomization energies, the overestimation of the enthalpies of formation is in agreement with the known overestimation of the binding energies. As mentioned previously in this chapter, the introduction of HF exchange into the GGA formula, as designed by Becke, yields the HGGA functionals, where the HF exchange has been shown to mitigate the overestimation of binding energies.

7.3.2.3 Hybrid GGA Functionals

Since there were ten hybrid functionals included in the study, the effect the percentage of Hartree-Fock exchange has on the performance of the functional for the TM-4*d* set could be examined. For the hybrid functionals there was not a trend with respect to the MADs and the percent of Hartree-Fock exchange. The inclusion of three parameters in the Becke exchange (i.e., B3) significantly reduces the overall MAD in comparison to the Becke exchange (B), while one parameter did not have any impact (B1). The MAD's of B3P86 and B3LYP were 8.3 and 8.7 kcal mol^{-1}, respectively, in contrast to 16.7 kcal mol^{-1} of BLYP and B1LYP and 23.9 kcal mol^{-1} of BP86. While non-local Hartree-Fock exchange did not improve the accuracy of the functionals with Becke-type exchange, Hartree-Fock exchange did improve the performance of the PBE functionals; the MAD of PBE1PBE was 8.5 kcal mol^{-1} and 26.0 kcal mol^{-1} for PBEPBE. The M06 functional yielded a comparable MAD (8.4 kcal mol^{-1}) to PBE1PBE. Doubling the amount of exchange for the M06 functional, i.e., M06-2X, did not improve the

performance of the functional for 4*d* enthalpies of formation (MAD of 10.8 kcal mol^{-1}). The failure of M06-2X for transition metals, specifically 4*d* transition metals, is consistent with observations from Truhlar and Luo's study of DFT for 4*d* atoms.[227] For the TM-4*d* set, the HGGAs with the percentage of Hartree-Fock exchange ranging from 20 to 27 percent have lower MADs in comparison to the HGGAs with additional HF exchange, with the exception of mPW1LYP and B1LYP; the 4*d* results, with respect to HF exchange, are in agreement with previous results for 3*d* thermochemistry. The outliers for these two HGGAs are similar to the outliers of the GGA functionals (e.g. carbonyls, RuO_4); therefore, the inclusion of the additional parameter for HF exchange, even the desired percentage in the twenties, does not necessarily improve the performance of a density functional for second row transition metal thermochemistry. To note, the inclusion of the second order perturbation correlation energy significantly reduces the errors observed, specifically for mPW1LYP (HGGA) versus mPW1PLYP (DHGGA).

7.3.2.4 Range-Separated Functionals

The range-separated functionals ωB97X, ωB97XD, and CAM-B3LYP include Hartree-Fock exchange in the long- and short-range description of exchange, while ωB97 and LC-ωPBE include Hartree-Fock exchange only in the long-range description of exchange. The remaining short-range exchange is described by DFT for each of the range-separated functionals. The inclusion of short-range HF exchange yields lower overall MADs for the range-separated functionals. There is no trend in error with respect to increasing the percentage of Hartree-Fock short-range exchange, but there is

an increase in the overall MAD with respect to the increase in the value of ω, the range-separation parameter. The ωB97XD functional, with ω value of 0.2, obtains the lowest MAD, 6.52 kcal mol^{-1}, for the range-separated functionals. Examination of the impact of the value of ω on the theoretical enthalpies of formation, as the ω value increases from 0.30 (ωB97X) to 0.33 (CAM-B3LYP) to 0.40 (ωB97, LC-ωPBE), the MADs increase (7.42, 8.06, 8.74, 11.47 kcal mol^{-1}, respectively). Comparison of the B97-based functionals yields the observation, as the sophistication of the functional definition increases (ωB97<ωB97X<ωB97XD), the deviation of the functional-determined ΔH_f's from experimental values decreases, where ωB97XD is the most accurate. While the molecules within the TM-4*d* set are not composed of long-range interactions, the inclusion of a dispersion correction within the B97 family of functionals appears to reduce deviations from experiment for the enthalpies of formation. This observation is misleading since the inclusion of a dispersion correction is also accompanied by a decrease in the value of ω and an increase in the percentage of HF exchange. The trend in the B97-based functionals is counter to the conclusion for first row transition metals; the functionals performed worse as the number of terms in the functional increased.[228] As noted for the HGGA functionals, the percent of HF exchange is ideally in the range of 20-27. The ωB97X functional includes 15.8% HF exchange, while ωB97XD includes 22.2%.

7.3.2.5 Double-Hybrid Functionals

Of the functionals included in the study, the two double-hybrid functionals had the lowest overall MADs (mPW2-PLYP, 4.25 kcal mol^{-1} and B2GP-LYP, 5.19 kcal mol^{-1}).

Similar conclusions were made for 3*d* transition metals, where the double hybrid functionals (B2-PLYP, B2GP-PLYP, and mPW2-PLYP) yielded the smallest deviations from experimental enthalpies of formation. The double functionals have 55% and 65% Hartree-Fock exchange, respectively. In comparison to the single hybrid functional M06-2X, which has a comparable amount of Hartree-Fock exchange with 54%, the inclusion of second-order perturbation theory correlation is noticeable. The M06-2X functional resulted in an MAD of 10.84 kcal mol^{-1}. The addition of 25% PT2 correlation energy, with 55% Hartree-Fock exchange, of mPW2-PLYP resulted in an MAD lowering of over 6 kcal mol^{-1}. While the different parameterizations of M06-2X and mPW2-PLYP may account for some of the discrepancy, the effect of ab initio correlation energy is evident for the second row transition metals. As noted in the original examination of the molecule set with rp-ccCA, the use of a single-reference method does not compromise the theoretically-determined enthalpies of formation. This observation is reinforced by examining the effect of double versus single hybridization for density functionals.

7.3.2.6 Geometry Comparison

The geometries for the complete TM-4*d* set were also optimized for each of the functionals in combination with the cc-pVTZ-PP basis set. The DFT/cc-pVTZ-PP geometries were compared to the geometries used within rp-ccCA (B3LYP/cc-pVTZ-PP, i.e., functional/basis set). On average the bond lengths differed by 0.016 Å. Using ZrO_2 as an example, the Zr-O bond length as determined by B3LYP, B97-1, wB97XD, and mPW2-PLYP was 1.776, 1.770, 1.759, and 1.786 Å, respectively. The O-Zr-O

bond angle as determined by the same functionals (B3LYP, B97-1, wB97XD, and mPW2-PLYP) was 108.5°, 108.4°, 109.2°, and 108.1°, respectively.

While the deviations between the B3LYP geometries and the geometries determined by the other functionals included in this study may seem trivial, the impact of the geometries optimized for each functional on the enthalpies of formation (ΔH_f's) and the overall deviations of the ΔH_f's from experiment were examined. On average, utilizing the geometry optimized by a functional for the single point energy calculation used to determine the ΔH_f did not change the MADs and MSDs from experiment. The MAD and MSD for the ΔH_f's based upon the DFT-specific optimized structure for each functional are reported in Table 7.4. The most notable changes in MADs and MSDs were for two of the GGAs (TPSSKCIS and M06-L). The utilization of the TPSSKCIS and M06-L optimized geometries resulted in a reduction of the MADs for these two functionals by 7.0 and 2.0 kcal mol^{-1}, respectively.

Table 7.4. Overall DFT statistics (MAD, MSD, RMSD, σ) for the TM-4*d* molecule set. Geometries were re-optimized with each functional.

Functional	MSD	MAD	RMSD	σ	Functional	MSD	MAD	RMSD	σ
BLYP	13.48	17.87	28.95	21.47	**B1LYP**	-15.41	15.76	22.90	15.49
BP86	14.35	15.90	28.53	22.47	**M06**	3.20	7.96	10.83	6.63
PBEPBE	11.06	24.75	43.99	32.99	**BMK**	0.88	11.53	14.69	8.26
TPSSKCIS	5.05	7.17	15.85	13.51	**M062X**	-7.52	9.57	12.56	7.43
M06-L	8.25	9.87	18.84	13.98	**wB97XD**	-8.35	10.61	16.04	11.26
B3P86	5.24	8.89	14.85	11.24	**wB97X**	1.25	9.31	15.67	11.37
B3LYP	-4.72	8.46	11.55	7.25	**CAM-B3LYP**	-4.11	7.85	11.11	7.30
B971	3.00	6.27	11.08	8.66	**wB97**	-3.67	8.79	13.52	9.64
X3LYP	-5.96	9.51	14.84	10.71	**LC-wPBE**	-2.88	11.68	15.96	10.04
PBE1PBE	-3.97	8.44	11.76	7.59	**mPW2-PLYP**	-2.40	5.14	12.14	9.87
mPW1LYP	-20.72	20.72	29.42	19.40	**B2GP-LYP**	-0.92	4.95	8.38	6.39

7.4 Conclusions

The performance of density functional theory in conjunction with ECPs for the determination of the enthalpy of formation of 4*d* TM molecules has been evaluated. Overall, the performance of 22 density functionals, including GGAs, HGGAs, HMGGAs, RS, and DHGGAs, in combination with the correlation consistent basis sets and effective core potentials, was examined for the determination of the enthalpy of formation of 30 second row transition metal-containing molecules (TM-4*d* set). Previously, rp-ccCA was used to study the molecule set and an MAD of 2.89 kcal mol^{-1} from experimental enthalpies of formation was observed. The average experimental uncertainty for the set is 3.43 kcal mol^{-1}. None of the functionals included in the current study matched the accuracy level of rp-ccCA, though the double hybrid functionals, mPW2-PLYP and B2GP-PLYP, yielded the lowest MADs (4.25 and 5.19 kcal mol^{-1}, respectively). The GGA functionals had the largest deviations from experiment and are not recommended for second row transition metal thermochemistry. The HGGAs, specifically those with 20-30% Hartree-Fock exchange, deviated from experiment by, on average, 6-10 kcal mol^{-1}, depending on the functional employed. For the range separated functionals, the inclusion of short-range HF exchange did not systematically improve the deviation of the functionals, but it was observed that increasing the value of ω, the range separation parameter, increased the MAD of the range separated functional [0.30 (ωB97X) to 0.33 (CAM-B3LYP) to 0.40 (ωB97, LC-ωPBE), the MADs increase (7.42, 8.06, 8.74, 11.47 kcal mol^{-1}, respectively)]. Overall, to obtain the best performance with DFT and the small core ECPs with the valence correlation consistent basis sets, the double hybrid functionals, namely mPW2-PLYP, in combination with the

cc-pVQZ-PP basis set and ECP should be employed for second row TM thermochemistry.

CHAPTER 8

CONCLUDING REMARKS

In this dissertation the presented research exhibits advances in the accuracy and reliability of electronic structure methods for the prediction of energetic and spectroscopic properties. Developments include the design of a variant of a composite method for heavier elements (e.g. second row transition metals), the development of scaling factors to account for common approximations employed within electronic structure methods, and the identification of density functionals suitable for transition metals. The presented research can be utilized as a launching point for future studies and a synopsis of each project with ensuing investigations are detailed.

In Chapter 3, the development and initial study of the relativistic pseudopotential correlation consistent Composite Approach (rp-ccCA) was presented. The pseudopotential variant of ccCA allowed for the accurate examination of second row transition metal thermochemistry via an ab initio method. The developed method was first studied for molecules containing *4p* elements (Ga-Kr) and the accuracy and time savings of rp-ccCA was compared to ccCA with all-electron basis sets. Overall, a 32.5% CPU time savings was observed and chemical accuracy for the main group molecules of interest (within 1 kcal/mol of experimental values) was maintained. rp-ccCA was then applied to second row transition metals where the experimental uncertainty for the enthalpies of formation of 30 molecules was 3.43 kcal/mol. rp-ccCA yielded an average absolute deviation of 2.89 kcal/mol (within the experimental uncertainty). Chapter 4 detailed the further application of rp-ccCA to lower *p*-block (5*p* and 6*p*) elements. The method was applied to both atomic (ionization potentials,

electron affinities) and molecular (dissociation energies, enthalpies of formation) properties. Agreement between the calculated and experimental values was observed. Since rp-ccCA represents the furthest extension of ccCA down the periodic table, additional development of the method in order to address third row transition metals and lanthanides and actinides is warranted. The challenges faced with second row transition metals, such as the limited amount of experimental data and the design of components of the methodology to recover all electronic effects, will need to be addressed in the design of a new variant or extension of rp-ccCA to the heavier metals, lanthanides and actinides. The current formulation of rp-ccCA will be useful in future studies of second row transition metals; for example, in transition metal-catalyzed reactions.

In Chapters 5 and 6, scale factors for density functional theory in conjunction with the correlation consistent basis sets and the polarization consistent basis sets were introduced. The scale factors for harmonic vibrational frequencies, zero-point vibrational energies, and thermal contributions to enthalpy and entropy were presented. With the application of the scale factors to the vibrational frequencies, deviations between calculated and experimental frequencies were reduced. The developed scale factors were designed for calculations employing the harmonic approximation, therefore, neglecting anharmonic effects. Scale factors typically are generated based upon a test set of organic molecules; therefore, it would be of interest to generate a test set of inorganic molecules and examine how the scale factors may differ for inorganics in comparison to organic species. In the scale factor development for organic molecules (Chapters 5 and 6), there were over 1,000 experimental frequencies from 40

molecules used to determine the scale factors. The main challenge of in the development of scale factors for inorganics would be the need for a large number of reported experimental vibrational frequencies for the inorganic molecules, including both main group (non-carbon-based molecules) and transition metals. There are experimental vibrational frequencies reported in the literature for transition metal systems, e.g. chalcogenides, but the ability to compose a test set of vibrational frequencies of a range of transition metal systems (e.g. different ligands) could be a limiting factor because in order to capture the diversity of the inorganics, the needed data set would be enormous (much larger than the prior work including 40 molecules with similar molecular-type composition). Examination of the deviations between experimental and theoretical vibrational frequencies for main-group (non-carbon-based) molecules is also of interest, though the hurdles for comparison are similar to those for transition metals.

In Chapter 7, the accuracy level of density functional theory for transition metal thermochemistry was investigated. Both first row and second row transition metals were studied. The type of functional employed (e.g. GGA versus HGGA versus DHGGA) significantly impacted the accuracy of the calculated enthalpies of formation. Furthermore, the percent of Hartree-Fock exchange in the HGGA functionals played a role in the accuracy of the methodologies. This study pinpoints the failures of DFT for transition metal systems and the development of a functional for transition metal molecules is of interest. Density functionals are parameterized based upon experimental data, but very few functionals have included transition metal data in their parameterization and, if they have included transition metals, the number of molecules

and properties is marginal. For example, the M06 functional includes transition metals in the parameterization, but there are only 53 transition metal data points (9 metal atomization energies, 21 metal-ligand bond energies, 18 reaction energies, and 5 metal atom excitation energies) in comparison to 350 main group energetic properties (e.g. barrier heights, dissociation energies, noncovalent interaction energies). Furthermore, as highlighted in the 3*d* DFT study (Chapter 7), the M06 functional yields a deviation of 11.0 kcal/mol for the ccCA-TM/11 test set, which is composed of over 200 enthalpies of formation for transition metal molecules. Through the 3*d* and 4*d* transition metal DFT studies presented in this dissertation, the B97-1 functional seems to be a strong starting point for re-parameterization for transition metals. By utilizing the ccCA-TM/11 test set, in addition to ionization potentials and electron affinities reported in the literature and/or determined via ccCA-TM and selected main group test sets (e.g. noncovalent interaction energies, bond dissociation energies, atomization energies) for completeness, the ten parameters of the B97-1 functional can be re-optimized, most likely through a least-squares fitting procedure, for transition metals. Since the parameterization of the functional would include a large number of transition metal systems and at least a half-dozen properties, the expected performance of the new functional should be improved over current density functionals.

REFERENCES

[1] L. Radom and A. P. Scott, J. Phys. Chem. **100**, 16502 (1996).

[2] J. P. Merrick, D. Moran, and L. Radom, J. Phys. Chem. A **111**, 11683 (2007).

[3] M. W. Wong, Chem. Phys. Lett. **256**, 391 (1996).

[4] E. Schrödinger, Phys. Rev. **28**, 1049 (1926); E. Schrödinger, Ann. Phys. **79**, 361 (1926); E. Schrödinger, Ann. Phys. **80**, 437 (1926); E. Schrödinger, Ann. Phys. **81**, 109 (1926).

[5] M. Born and R. Oppenheimer, Ann. Phys. **389**, 457 (1927).

[6] W. Pauli Jr, Z. Phys. **31**, 765 (1925).

[7] J. C. Slater, Phys. Rev. **34**, 1293 (1929).

[8] V. Fock, Z. Phys. **61**, 126 (1930); V. Fock, Z. Phys. **62**, 795 (1930); D. R. Hartree, Proc. Cambridge Philos. Soc. **24**, 89 (1928).

[9] T. H. Dunning Jr., J. Chem. Phys. **90**, 1007 (1989).

[10] S. Green, J. Chem. Phys. **52**, 210 (1970).

[11] J. A. Pople, R. Seeger, and R. Krishnan, Int. J. Quantum Chem. **Suppl. Y-11**, 149 (1977); K. Raghavachari, H. B. Schlegel, and J. A. Pople, J. Chem. Phys. **72**, 4654 (1980); K. Raghavachari and J. A. Pople, Int. J. Quantum Chem. **20**, 1067 (1981).

[12] J. A. Pople, R. Krishnan, H. B. Schlegel, and J. S. Binkley, Int. J. Quantum Chem. **14**, 545 (1978); I. R.J. Bartlett; G.D. Purvis, Int. J. Quantum Chem. **14**, 561 (1978).

[13] J. D. Watts, J. Gauss, and R. J. Bartlett, J. Chem. Phys. **98** (1993).

[14] J. A. Pople, M. Head-Gordon, and K. Raghavachari, J. Chem. Phys. **87**, 5968 (1987).

[15] P. O. Löwdin, J. Chem. Phys. **19**, 1396 (1951); J. A. Pople, S. Binkley, and R. Seeger, Int. J. Quantum Chem. **10**, 1 (1976).

[16] C. Møller and M. S. Plesset, Phys. Rev. **46**, 618 (1934).

[17] E. Fermi, Rend. Accad. Naz. Lincei **6**, 602 (1927); L. H. Thomas, Proc. Cambridge Philos. Soc. **23**, 542 (1927).

[18] J. C. Slater, Phys. Rev. **81**, 385 (1951).

[19] P. Hohenberg and W. Kohn, Phys. Rev. **136**, B864 (1964).

[20] W. Kohn and L. J. Sham, Phys. Rev. **140**, A1133 (1965).

[21] J. P. Perdew and K. Schmidt, AIP Conf. Proc. **1**, 511 (2001).

[22] U. v. Barth and L. Hedin, J. Phys. Chem. C: Solid State Phys. **5**, 1629 (1972); J. C. Stoddart and N. H. March, Ann. Phys. **64**, 174 (1970).

[23] F. Jensen, *Introduction to Computational Chemistry*, 2 ed. (John Wiley and Sons, Ltd., West Sussex, 2007).

[24] J. P. Perdew, K. Burke, and M. Ernzerhof, Phys. Rev. Lett. **77**, 3965 (1996).

[25] J. P. Perdew and Y. Wang, Phys. Rev. B **33**, 8800 (1986).

[26] A. D. Becke, Phys. Rev. A **38**, 3098 (1988).

[27] C. Lee, W. Yang, and R. G. Parr, Phys. Rev. B **37**, 785 (1988).

[28] J. P. Perdew, Phys. Rev. B, 8822 (1986).

[29] A. D. Becke, J. Chem. Phys. **109**, 2092 (1998); R. M. Koehl, G. K. Odom, and G. E. Scuseria, Mol. Phys. **87**, 835 (1996); T. v. Voorhis and G. E. Scuseria, Mol. Phys. **92**, 601 (1997).

[30] A. D. Becke, J. Chem. Phys. **98**, 5648 (1993).

[31] M. Born and V. A. Fock, Z. Phys. A **51**, 165 (1928).

[32] S. Grimme, J. Chem. Phys. **124**, 034108 (2006).

[33] T. Schwabe and S. Grimme, Phys. Chem. Chem. Phys. **8**, 4398 (2006).

[34] Y. Zhao, B. J. Lynch, and D. G. Truhlar, J. Phys. Chem. A **108**, 4786 (2004).

[35] Y. Zhao, B. J. Lynch, and D. G. Truhlar, Phys. Chem. Chem. Phys. **7**, 43 (2005).

[36] S. Grimme, J. Comput. Chem. **25**, 1463 (2004).

[37] H. Irikura, T. Tsuneda, T. Yanai, and K. Hirao, J. Chem. Phys. **115**, 3540 (2001).

[38] S. Kristyan and P. Pulay, Chem. Phys. Lett. **229**, 175 (1994); P. Hobza, J. Sponer, and T. Reschel, J. Comput. Chem. **11**, 1315 (1995); M. Allen and D. J. Tozer, J. Chem. Phys. **117**, 11113 (2002).

[39] J.-D. Chai and M. Head-Gordon, J. Chem. Phys. **128**, 084106 (2008).

[40] J.-D. Chai and M. Head-Gordon, Phys. Chem. Chem. Phys. **10**, 6615 (2008).

[41] J. C. Slater, Phys. Rev. **36**, 57 (1930).

[42] S. F. Boys, Proc. Royal Soc. **200**, 542 (1950).

[43] D. E. Woon and T. H. DunningJr., J. Chem. Phys. **98**, 1358 (1993).

[44] D. E. Woon and T. H. Dunning Jr., J. Chem. Phys. **100**, 2975 (1994); N. B. Balabanov and K. A. Peterson, J. Chem. Phys. **123**, 064107 (2005); T. H. Dunning Jr., K. A. Peterson, and A. K. Wilson, J. Chem. Phys. **114**, 9244 (2001).

[45] K.A. Peterson; T.H. Dunning Jr., J. Chem. Phys. **117**, 10548 (2002).

[46] T. H. Dunning Jr, J. Chem. Phys. **90**, 1007 (1989).

[47] T. H. Dunning Jr., K. A. Peterson, D. E. Woon, and A. K. Wilson, ACTC (1999).

[48] K.A. Peterson; R.A. Kendall; T.H. Dunning Jr., J. Chem. Phys. **99**, 1930 (1993).

[49] D.E. Woon; T.H. Dunning Jr., J. Chem. Phys. **103**, 4572 (1995).

[50] F. Jensen, J. Chem. Phys. **110**, 6601 (1999); F. Jensen, Theor. Chem. Acc. **104**, 484 (2000).

[51] F. Jensen, J. Chem. Phys. **115**, 9113 (2001); F. Jensen, J. Chem. Phys. **116**, 3502 (2001); F. Jensen, J. Chem. Phys. **116**, 7372 (2002); F. Jensen, J. Chem. Phys. **117**, 9234 (2002); F. Jensen, J. Chem. Phys. **118**, 2456 (2003); F. Jensen, J. Chem. Phys. **121**, 3463 (2004).

[52] S. Arrhenius, Z. Phys. Chem. **4**, 226 (1889).

[53] J. A. Pople, M. Head-Gordon, D. J. Fox, K. Raghavachari, and L. A. Curtiss, J. Chem. Phys. **90**, 5622 (1989).

[54] L. A. Curtiss, J. E. Carpenter, K. Raghavachari, and J. A. Pople, J. Chem. Phys. **96**, 9030 (1992); L. A. Curtiss, K. Raghavachari, G. W. Trucks, and J. A. Pople, J. Chem. Phys. **94**, 7221 (1991); L. A. Curtiss, K. Raghavachari, and J. A. Pople, J. Chem. Phys. **98**, 1293 (1993); L. A. Curtiss, P. C. Redfern, K. Raghavachari, V. Rassolov, and J. A. Pople, J. Chem. Phys. **110**, 4703 (1999); A. G. Baboul, L. A. Curtiss, P. C. Redfern, and K. Raghavachari, J. Chem. Phys. **110**, 7650 (1999); L. A. Curtiss and K. Raghavachari, Theor. Chem. Acc. **108**, 61 (2002); L. A. Curtiss, P. C. Redfern, and K. Raghavachari, J. Chem. Phys. **127**, 124105 (2007); L. A. Curtiss, P. C. Redfern, and K. Raghavachari, J. Chem. Phys. **126**, 084108 (2007).

[55] L. A. Curtiss, K. Raghavachari, P. C. Redfern, V. Rassolov, and J. A. Pople, J. Chem. Phys. **109**, 7764 (1998).

[56] A. D. Boese, M. Oren, O. Atasoylu, J. M. L. Martin, M. Kállay, and J. Gauss, J. Chem. Phys. **120**, 4129 (2004).

[57] J. V. Burda, M. Zeizinger, J. Sponer, and J. Leszczynski, J. Chem. Phys. **113**, 2224 (2000); S. Parthiban and J. M. L. Martin, J. Chem. Phys. **114**, 6014 (2001); J. M. L. Martin and G. d. Oliveria, J. Chem. Phys. **111**, 1843 (1999); A. Karton, E. Rabinovich, J. M. L. Martin, and B. Ruscic, J. Chem. Phys. **125**, 144108 (2006).

[58] A. Tajiti, P. G. Szalay, A.G.Császár, M. Kállay, J. Gauss, E. F. Valeev, B. A. Flowers, J. Vázquez, and J. F. Stanton, J. Chem. Phys. **121**, 11599 (2004); M. E. Harding, J. Vázquez, B. Ruscic, A. K. Wilson, J. Gauss, and J. F. Stanton, J. Chem. Phys. **128**, 114111 (2008); Y. J. Bomble, J. Vázquez, M. Kállay, C. Michauk, P. G. Szalay, A. G. Császár, J. Gauss, and J. F. Stanton, J. Chem. Phys. **125**, 064108 (2006).

[59] G. A. Petersson and M. A. Al-Laham, J. Chem. Phys. **94**, 6081 (1991); J. A. Montgomery Jr., J. W. Ochterski, and G. A. Petersson, J. Chem. Phys. **101**, 5900 (1994); J. A. Montgomery Jr., M. J. Frisch, J. W. Ochterski, and G. A. Petersson, J. Chem. Phys. **110**, 2822 (1999); G. A. Petersson, A. Bennett, T. G. Tensfeldt, M. A. Al-Laham, W. A. Shirley, and J. Mantzaris, J. Chem. Phys. **89**, 2193 (1988); M. R. Nyden and G. A. Petersson, J. Chem. Phys. **75**, 1843 (1981); P. M. Mayer, C. J. Parkinson, D. M. Smith, and L. Radom, J. Chem. Phys. **108**, 604 (1998).

[60] A. L. L. East and W. D. Allen, J. Chem. Phys. **99**, 4638 (1993); A. L. L. East, C. S. Johnson, and W. D. Allen, J. Chem. Phys. **98**, 1299 (1993); *Structure and Conformations in Non-rigid Molecules*, edited by A. L. L. East, W. D. Allen, and

A. G. Császár (Kluwer, Dordrecht); A. G. Császár, W. D. Allen, and H. F. SchaeferIII, J. Chem. Phys. **108**, 9751 (1998); M. S. Schuurman, S. R. Muir, W. D. Allen, and H. F. Schaefer III, J. Chem. Phys. **120**, 11586 (2004).

[61] P. L. Fast and D. G. Truhlar, J. Phys. Chem. A **104**, 6111 (2000); P. L. Fast, J. C. Corchado, M. L. Sanchez, and D. G. Truhlar, J. Phys. Chem. A **103**, 5129 (1999).

[62] D. Feller, K. A. Peterson, W. A. de Jong, and D. A. Dixon, J. Chem. Phys. **118**, 3510 (2003); D. Feller, K. A. Peterson, and D. A. Dixon, J. Chem. Phys. **129**, 204105 (2008); D. Feller, K. A. Peterson, and D. A. Dixon, J. Phys. Chem. A **114**, 61 (2010); D. Feller, K. A. Peterson, and D. A. Dixon, J. Phys. Chem. A **115**, 1440 (2011); D. Feller, K. A. Peterson, and J. G. Hill, J. Chem. Phys. **133**, 184102 (2010).

[63] S. A. Nedd, N. J. DeYonker, A. K. Wilson, P. Piecuch, and M. S. Gordon, J. Chem. Phys. **136**, 144109 (2012); W. Jiang and A. K. Wilson, J. Chem. Phys. **134**, 034101 (2011).

[64] A. Mahler and A. K. Wilson, J. Chem. Theory Comput. (2013); *Advances in the Theory of Atomic and Molecular Systems*, edited by N. J. DeYonker, T. R. Cundari, and A. K. Wilson (Springer Science, Netherlands, 2009); T. G. Williams, B. Ho, N. J. DeYonker, and A. K. Wilson, Chem. Phys. Lett. **504**, 88 (2011).

[65] B. P. Prascher, J. D. Lai, and A. K. Wilson, J. Chem. Phys. **131**, 044130 (2009).

[66] B. P. Prascher, R. M. Lucente-Schultz, and A. K. Wilson, Chem. Phys. **359**, 1 (2009).

[67] M. L. Laury, N. J. DeYonker, W. Jiang, and A. K. Wilson, J. Chem. Phys. **134**, 214103 (2011).

[68] N. J. DeYonker, B. R. Wilson, A. W. Pierpont, T. R. Cundari, and A. K. Wilson, Mol. Phys. **107**, 1107 (2009).

[69] N. J. DeYonker, T. R. Cundari, and A. K. Wilson, J. Chem. Phys. **124**, 114104 (2006).

[70] N. J. DeYonker, T. G. Williams, A. E. Imel, T. R. Cundari, and A. K. Wilson, J. Chem. Phys. **131**, 024106 (2009).

[71] S. M. Tekarli, M. L. Drummond, T. G. Williams, and A. K. Wilson, J. Phys. Chem. A **113**, 8607 (2009).

[72] W. Jiang, N. J. DeYonker, J. J. Determan, and A. K. Wilson, J. Phys. Chem. A **116**, 870 (2012).

[73] A. Halkier, T. Helgaker, P. Jorgensen, W. Klopper, H. Koch, J. Olsen, and A. K. Wilson, Chem. Phys. Lett. **286**, 243 (1998).

[74] D. Feller, J. Chem. Phys. **98**, 7059 (1993).

[75] A. Halkier, T. Helgaker, P. Jørgensen, W. Klopper, and J. Olsen, J. Chem. Phys. Lett. **302**, 347 (1999).

[76] K.A. Peterson; D.E. Woon; T.H. Dunning Jr., J. Chem. Phys. **100**, 7410 (1994).

[77] C. Schwartz, Phys. Rev. **126**, 1015 (1962).

[78] N. Bohr, Philos. Mag. **26**, 1 (1913).

[79] L. H. Thomas, Nature **117**, 514 (1926).

[80] P. A. M. Dirac, Proc. Royal Soc. A **117**, 778 (1928).

[81] P. A. M. Dirac, Proc. Royal Soc. A **126**, 801 (1930); P. A. M. Dirac, Proc. Royal Soc. A **801**, 360 (1930).

[82] G. Jansen and B. A. Hess, Phys. Rev. A **39**, 6016 (1989).

[83] M. Douglas and N. M. Kroll, Ann. Phys. **82**, 89 (1974).

[84] H. Hellmann, J. Chem. Phys. **3**, 61 (1935).

[85] *Relativistic Methods for Chemists*, edited by Z. Cao and M. Dolg (Springer, Berlin, 2009).

[86] R. Saue, K. Fægri, T. Helgaker, and O. Gropen, Mol. Phys. **91**, 937 (1997).

[87] C. Froese-Fischer, *The Hartree-Fock Method for Atoms*. (Wiley, New York, 1977).

[88] H. Stoll, B. Metz, and M. Dolg, J. Comp. Chem. **23**, 767 (2002).

[89] B. A. Heβ, C. M. Marian, U. Wahlgren, and O. Gropen, Chem. Phys. Lett. **251**, 365 (1996).

[90] H.-J. Werner and P. J. Knowles, J. Chem. Phys. **82**, 5053 (1985); P. J. Knowles and H.-J. Werner, Chem. Phys. Lett. **115**, 259 (1985).

[91] C. E. Housecroft, *The Heavier d-block Metals: Aspects of Inorganic and Coordination Chemistry*. (Oxford Science Publications, Oxford, 1999).

[92] A. Levina, A. McLeod, J. Seuring, and P. A. Lay, J. Inorg. Biochem. **101**, 1586 (2007).

[93] A. Veillard, *Quantum Chemistry: The Challenge of Transition Metals and Coordination Chemistry*. (D. Reidel Publishing Company, Dordrecht, Holland, 1985).

[94] D. S. Ho, N. J. DeYonker, A. K. Wilson, and T. R. Cundari, J. Phys. Chem. A **110**, 9767 (2006); N. J. DeYonker, D. S. Ho, A. K. Wilson, and T. R. Cundari, J. Phys. Chem. A **111**, 10776 (2007); N. J. DeYonker, K. A. Peterson, G. Steyl, A. K. Wilson, and T. R. Cundari, J. Phys. Chem. A **111**, 11269 (2007); N. J. DeYonker, T. R. Cundari, A. K. Wilson, C. A. Sood, and D. H. Magers, Theochem. **775**, 77 (2006); C. Liu, L. Munjanja, T. R. Cundari, and A. K. Wilson, J. Phys. Chem. A **114**, 6207 (2010).

[95] B. Mintz, T. G. Williams, L. Howard, and A. K. Wilson, J. Chem. Phys. **130**, 234104 (2009); T. G. Williams and A. K. Wilson, J. Sulfur Chem. **29**, 353 (2008).

[96] T. G. Williams, N. J. DeYonker, and A. K. Wilson, J. Chem. Phys. **128**, 044101 (2008).

[97] W. J. Lauderdale, J. F. Stanton, J. Gauss, J. D. Watts, and R. Bartlett, Chem. Phys. Lett. **187**, 21 (1991); M. Head-Gordon, J. A. Pople, and M. J. Frisch, Chem. Phys. Lett. **153**, 503 (1988); M. J. Frisch, M. Head-Gordon, and J. A. Pople, Chem. Phys. Lett. **166**, 275 (1990); A. E. Azhary, G. Rauhut, P. Pulay, and H.-J. Werner, J. Chem. Phys. **108**, 5185 (1998).

[98] A.K. Wilson; D.E. Woon; K.A. Peterson; T.H. Dunning Jr., J. Chem. Phys. **110**, 7667 (1999).

[99] C. J. Jones, *d- and f-block Chemistry*. (Wiley Interscience, New York, 2002).

[100] P. Pyykko, Chem. Rev. **88**, 563 (1988).

[101] edited by G. Frenking, I. Antes, M. Bohme, S. Dapprich, A. W. Ehlers, V. Jones, A. Neuhaus, M. Otto, and R. Stegmann (VCH, New York, 1996), Vol. 8.

[102] P. Schwerdtfeger, T. Fischer, M. Dolg, G. Igel-Mann, A. Nicklass, H. Stoll, and A. Haaland, J. Chem. Phys. **102**, 2050 (1995); T. Leininger, A. Nicklass, H. Stoll, M. Dolg, and P. Schwerdtfeger, J. Chem. Phys. **105**, 1052 (1996); P. Schwerdtfeger, J. R. Brown, J. K. Laerdahl, and H. Stoll, J. Chem. Phys. **113**, 7110 (2000); H. Stoll, Chem. Phys. Lett. **429**, 289 (2006).

[103] P. Schwerdtfeger, *Relativistic Electronic Structure Theory*. (Elsevier Science, Amsterdam, 2002).

[104] L. Cheng, M. Y. Wang, Z. J. Wu, and Z. M. Su, J. Comp. Chem. **28**, 2190 (2007).

[105] B. Kharat, S. B. Deshmukh, and A. Chaudhari, Int. J. Quantum Chem. **109**, 1103 (2009).

[106] S. Zein, M. P. Kalhor, L. F. Chibotaru, and H. Chermette, J. Chem. Phys. **131** (2009); M. Swart, J. Chem. Theory Comput. **4**, 2057 (2008); K. Yang, R. Peverati, D. G. Truhlar, and R. Valero, J. Chem. Phys. **135**, 044118 (2011).

[107] T. R. Cundari, H. A. R. Leza, T. Grimes, G. Steyl, A. Waters, and A. K. Wilson, Chem. Phys. Lett. **401**, 58 (2005).

[108] Z. J. Wu and Y. Kawazoe, Chem. Phys. Lett. **423**, 81 (2006).

[109] R. Cracium, R. T. Long, D. A. Dixon, and K. O. Christe, J. Phys. Chem. A **114**, 7571 (2010).

[110] J. Uddin, C. M. Morales, J. H. Maynard, and C. R. Landis, Organometallics **25**, 5566 (2006).

[111] S. Li, J. M. Hennigan, D. A. Dixon, and K. A. Peterson, J. Phys. Chem. A **113**, 7861 (2009).

[112] D.E. Woon; T.H. Dunning Jr., J. Chem. Phys. **98**, 1358 (1993).

[113] D. A. Dixon, W. A. de Jong, K. A. Peterson, K. Christe, and G. J. Schrobilgen, J. Am. Chem. Soc. **127**, 8627 (2005).

[114] K. A. Peterson, D. Figgen, M. Dolg, and H. Stoll, J. Chem. Phys. **126**, 124101 (2007).

[115] R. Lindh, F. R. Manby, and M. S. et al., MOLPRO (2009).

[116] M. J. Frisch; G. W. Trucks; H. B. Schlegel; G. E. Scuseria; M. A. Robb; J. R. Cheeseman; J. A. Montgomery, Gaussian 03, Revision D.02 (Gaussian, Inc., Wallingford, CT, 2004).

[117] P. J. Knowles, C. Hampel, and H.-J. Werner, J. Chem. Phys. **99**, 5219 (1993).

[118] K. A. Peterson, J. Chem. Phys. **119**, 11099 (2003).

[119] K. A. Peterson, D. Figgen, E. Goll, H. Stoll, and M. Dolg, J. Chem. Phys. **119**, 11113 (2003).

[120] D. Feller, J. Chem. Phys. **96**, 6104 (1992).

[121] N. J. DeYonker, B. Mintz, T. R. Cundari, and A. K. Wilson, J. Chem. Theory Comput. **4**, 328 (2008).

[122] P. E. M. Siegbahn, Chem. Phys. Lett. **201**, 15 (1993).

[123] *Organometallic Thermochemistry Database*, edited by P. J. Linstrom and W. G. Mallard (NIST, Gaithersburg, MD, 2005), Vol. 69.

[124] P. E. M. Siegbahn, J. Phys. Chem. **97**, 9096 (1993).

[125] V. S. Yungman, *Thermal Constants of Substances*. (Wiley, New York, 1999).

[126] P. E. M. Siegbahn, Theor. Chim. Acta **87**, 441 (1994).

[127] M. G. M. V. de Vis, E. H. P. Cordfunke, and R. J. M. Konings, Theochem. Acta. **302**, 93 (1997).

[128] Z. J. Wu, Chem. Phys. Lett. **383**, 251 (2004).

[129] I. A. Topol, N. F. Stepanov, and V. M. Kovba, Theoret. Chim. Acta. (Berl.) **56**, 297 (1980).

[130] V. Pershina and B. Fricke, J. Phys. Chem. **100**, 8748 (1996).

[131] H. Nakai, H. Morita, P. Tomasello, and N. Nakatsuji, J. Phys. Chem. A **102**, 2033 (1998).

[132] E. Hossain and C. C. Jarrold, J. Chem. Phys. **130**, 064301 (2009).

[133] S. R. Langhoff and C. W. Bauschlicher, Ann. Rev. Chem. **39**, 181 (1988).

[134] K. Balasubramanian, J. Chem. Phys. **93**, 8061 (1990).

[135] J. C. Schug and D. H. Phillips, J. Chem. Phys. **59**, 1616 (1973).

[136] C. C. Roothaan, J. Rev. Mod. Phys. **32**, 179 (1960).

[137] C. L. Janssen and I. M. B. Nielsen, Chem. Phys. Lett. **290**, 423 (1998); T. J. Lee and P. R. Taylor, Int. J. Quantum Chem. Symp. **23**, 199 (1989).

[138] T. J. Lee, Chem. Phys. Lett. **372**, 362 (2003).

[139] A. W. Ehlers and G. Frenking, J. Am. Chem. Soc. **116**, 1514 (1994).

[140] T. Ziegler, V. Tschinke, and C. Ursenbach, J. Am. Chem. Soc. **109**, 4825 (1987).

[141] K. E. Lewis, D. M. Golden, and G. P. Smith, J. Am. Chem. Soc. **106**, 3905 (1984).

[142] J.-M. Denis, H. Forintos, H. Szelke, L. Toupet, T.-N. Pham, P.-J. Madec, and A. C. Gaumont, Chem. Commun. **54** (2003); T. J. Clark, K. Lee, and I. Manners, Chem. Eur. J **12**, 8634 (2006); T. B. Marder, Angew. Chem. Int. Ed. **46**, 8116 (2007); H. W. Langmi and G. S. McGrady, Coord. Chem. Rev. **251**, 925 (2007).

[143] R. J. Jouet, A. P. Purdy, R. L. Wells, and J. F. Janik, J. Cluster Sci. **13**, 469 (2002); A. H. Cowley and R. A. Jones, Polyhedron **13**, 1149 (1994); D. A. Atwood, A. H. Cowley, R. A. Jones, and M. A. Mardones, J. Organomet. Chem. **449**, C1 (1993).

[144] M. A. Volpe, P. Rodriguez, and C. E. Girola, Catal. Lett. **61**, 27 (1999); J.-L. Malleron, J.-C. Fiaud, and J.-Y. Legros, *Handbook of Palladium-Catalyzed Organic Reactions*. (Academic Press, New York, 1997); A. Molnar, A. Sarkany, and M. Varga, J. Mol. Catal. A: Chem. **173**, 175 (2001).

[145] J. Bu, C. Nie, J. Liang, L. Sun, Z. Xie, Q. Wu, and C. Lin, Nano. **22**, 125602 (2011); M. D. Moreira, P. Venezuela, and R. H. Miwa, Nano. **21**, 285204 (2010).

[146] M. Niu, D. Cheng, L. Huo, and X. Shao, J. All. Com. **539**, 221 (2012).

[147] L. Zhang, K. Pei, H. Zhao, S. Wu, Y. Wang, and J. Gao, Chem. Phys. Lett. **543**, 199 (2012).

[148] K. M. Osten, I. Yu, I. R. Duffy, P. O. Lagaditis, J. C.-C. Yu, C. J. Wallis, and P. Mehrkhodavandi, Dalton Trans. **41**, 8123 (2012).

[149] T. Brotin, D. Cavagnat, P. Berthault, R. Montserret, and T. Buffeteau, J. PHys. Chem. B **116**, 10905 (2012).

[150] N. Amrane, M. Benkraouda, and F. Hamed, J. Cond. Matt. Phys. **1**, 63 (2011).

[151] J. Leszczynski, M. Barysz, and Y. Ishikawa, *Relativtistic Methods for Chemists*. (Springer, New York, 2010).

[152] Y.-K. Han, C. Bae, S.-K. Son, and Y. S. Lee, J. Chem. Phys. **112**, 2684 (2000).

[153] B. A. Hess, Phys. Rev. A **32**, 756 (1985); B. A. Hess, Phys. Rev. A **33**, 3742 (1986).

[154] C. Teichteil, L. Maron, and V. Vallet, *Relativistic Electronic Structure Theory: II-Applications*. (Elsevier, Amsterdam, 2004).

[155] L. L. F. S. A. Wouthuysen, Phys. Rev. **79**, 29 (1059).

[156] K. A. Peterson and K. E. Yousaf, J. Chem. Phys. **133**, 174116 (2010).

[157] N. Drebov and R. Ahlrichs, J. Chem. Phys. **134**, 124308 (2011); V. E. Jackson, D. A. Dixon, and K. O. Christe, Inorg. Chem. **51**, 2472 (2012); D. K. W. Mok, E. P. F. Lee, F. Chau, and J. M. Dyke, Phys. Chem. Chem. Phys. **13**, 9540 (2011); P. V. Nhat, V. T. Ngan, T. B. Tai, and M. T. Nguyen, J. PHys. Chem. A **115**, 3523 (2011); S. Yockel and A. K. Wilson, J. Chem. Phys. **122**, 174310 (2005).

[158] S. Mukhopadhyay, S. Gowtham, R. Pandey, and A. J. Costales, Molec. Struct.: Theochem **31**, 948 (2010); C. Yan and P. S. Lee, J. Phys. Chem. Lett. **113**, 2208 (2009); F. Oba, M. Choi, A. Togo, A. Seko, and I. J. Tanaka, Phys.: Condens. Matter **22**, 384211 (2010); A. Yella, E. Mugnaioli, M. Panthofer, H. A. Therese, U. Kolb, and W. Tremel, **Angew. Chem. Int. Ed.** (2009).

[159] K. Balasubramanian, J. Molec. Spec. **115**, 258 (1986); K. Sumathi and K. Balasubramanian, J. Chem. Phys. **92**, 6604 (1990).

[160] B. Miehlich, A. Savin, H. Stoll, and H. Preuss, Chem. Phys. Lett. **157**, 2000 (1989).

[161] P. Schwedtfeger, G. A. Heath, M. Dolg, and M. A. Bennett, J. Am. Chem. Soc. **114**, 7517 (1992).

[162] W. A. Al-Saidi, J. Chem. Phys. **129**, 064316 (2008); T. Zeng, D. G. Fedorov, and M. Klobukowski, J. Chem. Phys. **132**, 074102 (2010).

[163] L. Visscher and K. G. Dyall, J. Chem. Phys. **104**, 9040 (1996); V. Pershina, A. Borschevsky, J. Anton, and T. Jacob, J. Chem. Phys. **132**, 194314 (2010); K. A. Peterson, B. C. Shepler, D. Figgen, and H. Stoll, J. Phys. Chem. A **110**, 13877 (2006); M. Ilias, H. J. A. Jensen, V. Kello, B. O. Roos, and M. Urban, Chem. Phys. Lett. **408**, 210 (2005); C. L. Barros, P. J. P. d. Oliveria, F. E. Jorge, A. C. Neto, and M. Campos, Mol. Phys. **108**, 1965 (2010); K. Balasubramanian and C. Ravimohan, J. Molec. Spec. **126**, 220 (1987); M. Mayer, S. Kruger, and N. Rosch, J. Chem. Phys. **115**, 4411 (2001); K. Faegri and T. Saue, J. Chem. Phys. **115**, 2456 (2001); S. A. Wildman, G. A. DiLabio, and P. A. Christiansen, J. Chem. Phys. **107** (1997); B. Metz, H. Stoll, and M. Dolg, J. Chem. Phys. **113**, 2563 (2000); Y.-K. Han and K. Hirao, J. Chem. Phys. **112**, 9353 (2000).

[164] P. Matczak, Comp. Theor. Chem. **983** (2012).

[165] M. J. Frisch; G. W. Trucks; H. B. Schlegel; G. E. Scuseria; M. A. Robb; J. R. Cheeseman; J. A. Montgomery, Gaussian 09 (Gaussian, Inc., Wallingford, CT, 2009).

[166] C. E. Moore, *Atomic Energy Levels*. (National Burear of Standards, Washington, D.C., 1949-1958).

[167] D. Figgen, W. Muller, M. Schweizer, H. Stoll, and K. A. Peterson, J. Chem. Phys. **118**, 4766 (2003).

[168] M. Riaz, M. Anwar-ul-Haw, R. Ali, and M. A. Baig, Opt. Comm. **233**, 323 (2004); H. Merlitz, G. Gopakumar, R. K. Chaudhuri, B. P. Das, S. Mahapatra, and D. Mukherjee, Phys. Rev. A **63**, 022507 (2001).

[169] Y. J. Choi and Y. S. Lee, J. Chem. Phys. **119**, 2014 (2003); S. Yu, D. Fu, A. Shayesteh, I. E. Gordon, D. R. T. Appadoo, and P. Bernath, J. Molec. Spec. **229**, 257 (2005); K. Balasubramanian, N. Tanpipat, and J. E. Bloor, J. Molec. Spec. **124**, 458 (1987); C. Song, T. Gao, H. Han, M. Wan, and Y. Yu, J. Molec. Struct. (Theochem) **870**, 65 (2008); K. Balasubramanian and K. S. Pitzer, J. Molec. Spec. **103**, 105 (1984); C. W. BauschlicherJr, J. Phys. Chem. A **103**, 6429 (1999).

[170] K. P. Huber and G. Herzberg, *Molecular Spectra and Molecular Structure. IV. Constants of Diatomic Molecules*. (Van Nostrand Reinhold Company Inc., New York, 1979).

[171] M. Argeri, A. Freccarollo, F. Grassi, L.Marchese, and M. Cossi, J. Phys. Chem. C: Solid State Phys. **115**, 11382 (2011).

[172] D. Dai and K. Balasubramanian, Chem. Phys. Lett. **271**, 118 (1997).

[173] C. Zao and K. Balasubramanian, J. Chem. Phys. **116**, 10287 (2002).

[174] K. Balasubramanian and D. Majumdar, J. Chem. Phys. **115**, 8795 (2001).

[175] K. S. Pitzer and K. Balasubramanian, J. Phys. Chem. **86**, 3068 (1982); K. A. Gingerich, D. L. Cocke, and F. Miller, J. Chem. Phys. **64**, 4027 (1976); R. Kelting, R. Otterstatter, P. Weis, N. Drebov, R. Ahlrichs, and M. M. Kappes, J. Chem. Phys. **134**, 024311 (2011).

[176] D. Dai and K. Balasubramanian, J. Chem. Phys. **96**, 8345 (1992).

[177] W. Koch, *A Chemist's Guide to Density Functional Theory*. (Wiley-VCH, Weinheim, 2003); R. A. Friesner, R. B. Murphy, M. D. Beachy, M. N. Ringnalda, W. T. Pollard, B. D. Dunietz, and Y. Cao, J. Phys. Chem. A **103**, 1913 (1999).

[178] C. Sosa, J. Andzelm, B. C. Elkin, E. Wimmer, K. D. Dobbs, and D. A. Dixon, J. Phys. Chem. **96**, 6630 (1992); A. Berces and T. Ziegler, Top. Curr. Chem. **182**, 42 (1996).

[179] T. A. Wesolowski and A. Warshel, J. Phys. Chem. **97**, 8050 (1993).

[180] J. Kohanoff, *Electronic Structure Calculations for Solids and Molecules: Theory and Computational Methods*. (Cambridge University Press, Cambridge, 2006).

[181] W. J. Hehre, L. Radom, P. V. R. Schleyer, and J. A. Pople, *Ab initio Molecular Orbital Theory*. (John Wiley and Sons, New York, 1986).

[182] R. F. Hout, B. A. Levi, and W. J. Hehre, J. Comput. Chem. **2**, 234 (1982).

[183] P. Sinha, S. E. Boesch, C. Gu, R. A. Wheeler, and A. K. Wilson, J. Phys. Chem. A **108**, 9213 (2004).

[184] J. R. Thomas, B. J. DeLeeuw, G. Vacek, and H. F. Schaefer III, J. Chem. Phys. **98**, 1336 (1993).

[185] M. D. Halls, J. Velkovski, and H. B. Schlegel, Theor. Chem. Acc. **105**, 413 (2001).

[186] K. K. Irikura, R. D. JohnsonIII, and R. N. Kacker, J. Phys. Chem. A **109**, 8430 (2005).

[187] M. D. Halls and H. B. Schlegel, J. Chem. Phys. **109**, 10587 (1998).

[188] I. M. Alecu, J. Zheng, Y. Zhao, and D. G. Truhlar, J. Chem. Theory Comput. **6**, 2872 (2010).

[189] X. Wu, M. C. Vargas, S. Nayak, V. Lotrich, and G. Scoles, J. Chem. Phys. **115**, 8748 (2001).

[190] J. P. Perdew and K. Schmidt, AIP Conf. Proc. **577**, 1 (2001).

[191] Y. Zhao, N. E. Schultz, and D. G. Truhlar, J. Chem. Phys. **123**, 161103 (2005).

[192] Y. Zhao, N. E. Schultz, and D. G. Truhlar, J. Chem. Theory Comput. **2**, 364 (2006).

[193] Y. Zhao and D. G. Truhlar, Theor. Chem. Acc. **120**, 215 (2008).

[194] E. G. Hohenstein, S. T. Chill, and C. D. Sherrill, J. Chem. Theory Comput. **4**, 1996 (2008).

[195] A. Karton, A. Tarnopolsky, J. L. Lame're, G. C. Schatz, and J. M. L. Martin, J. Phys. Chem. A **112**, 12868 (2008).

[196] N. X. Wang and A. K. Wilson, J. Chem. Phys. **121**, 7632 (2004).

[197] S. Sekusak and G. Frenking, J. Mol. Struct. Theochem. **541**, 17 (2001).

[198] K. S. Raymond and R. A. Wheeler, J. Comp. Chem. **20**, 207 (1999).

[199] H. L. Schmider and A. D. Becke, J. Chem. Phys. **108**, 9624 (1998).

[200] J. P. Perdew, J. A. Chevary, S. H. Vosko, K. A. Jackson, M. R. Pederson, D. J. Singh, and C. Fiolhais, Phys. Rev. B **46**, 6671 (1992); J. P. Perdew, J. A. Chevary, S. H. Vosko, K. A. Jackson, M. R. Perderson, D. J. Singh, and C. Fiolhais, Phys. Rev. B **48**, 4978 (1993).

[201] J. P. Perdew, K. Burke, and Y. Wang, Phys. Rev. B **54**, 16533 (1996).

[202] K. Burke, J. P. Perdew, and Y. Wang, *Derivation of a generalized gradient approximation: The PW91 density functional*. (Plenum Press, New York, 1998).

[203] M. Ernzerhof, J. P. Perdew, and K. Burke, Int. J. Quantum Chem. **64**, 285 (1997); M. Ernzerhof and G. E. Scuseria, J. Chem. Phys. **110**, 5029 (1999).

[204] B. J. Lynch, P. L. Fast, M. Harris, and D. G. Truhlar, J. Phys. Chem. A **104**, 4811 (2000).

[205] J. P. Perdew, K. Burke, and M. Ernzerhof, Phys. Rev. Lett. **78**, 1396 (1997).

[206] A. D. Boese and N. C. Handy, J. Chem. Phys. **114**, 5497 (2001); A. D. Boese, N. L. Doltsinis, N. C. Handy, and M. Sprik, J. Chem. Phys. **112**, 1670 (2000).

[207] F. A. Hamprecht, A. J. Cohen, D. J. Tozer, and N. C. Handy, J. Chem. Phys. **109**, 6264 (1998).

[208] L. A. Curtiss, K. Raghavachari, P. C. Redfern, and J. A. Pople, J. Chem. Phys. **106**, 1063 (1997).

[209] E. F. Healy and A. Holder, Theochem. **281**, 141 (1993).

[210] R. S. Grev, C. L. Janssen, and H. F. Schaefer, J. Chem. Phys. **95**, 5128 (1991).

[211] P. Borowski, J. Molec. Spec. **264**, 66 (2010); M. Mladenovic, P. Botschwina, and C. Puzzarini, J. Phys. Chem. A **110**, 5520 (2006); T. Hrenar, H.-J. Werner, and G. Rauhut, J. Chem. Phys. **126**, 134108 (2007); S. N. Yurchenko, J. Breidung, and W. Thiel, Theor. Chem. Acc. **114**, 333 (2005).

[212] P. Carbonniere, T. Lucca, C. Pouchan, N. Rega, and V. Barone, J. Comp. Chem. **26**, 384 (2005); V. Barone, J. Chem. Phys. **122**, 014108 (2005); M. W. D. Hanson-Heine, M. W. George, and N. A. Besley, J. Phys. Chem. A (ASAP); A. D. Boese and J. M. L. Martin, J. Molec. Struct. **780**, 310 (2006).

[213] F. Pawlowski, A. Halkier, P. Jorgensen, K. L. Bak, T. Helgaker, and W. Klopper, J. Chem. Phys. **118**, 2539 (2003).

[214] P. Pulay and W. Meyer, Mol. Phys. **27**, 473 (1974); Y. N. Panchenko, Russ. Chem. Bull **45**, 753 (1996); G. Rauhut and P. Pulay, J. Phys. Chem. **99**, 3093 (1995); J. Baker, A. A. Jarzecki, and P. Pulay, J. Phys. Chem. A **102**, 1412

(1998); P. Pulay, G. Fogarasi, G. Pongor, J. E. Boggs, and A. Vargha, J. Am. Chem. Soc. **105**, 7037 (1983).

[215] J. Grunenberg and R. Herges, J. Comp. Chem. **18**, 2050 (1998); M. V. Madhav and S. J. Manogaran, J. Chem. Sci. **121**, 811 (2009); C. Fabri, T. Szidarovszky, G. Magyarfalvi, and G. Tarczay, J. Phys. Chem. A **115**, 4640 (2011).

[216] M. L. Laury, S. E. Boesch, I. Haken, P. Sinha, R. A. Wheeler, and A. K. Wilson, J. Comput. Chem. **32**, 2339 (2011).

[217] S. G. Andrade, L. C. S. Goncalves, and F. E. Jorge, J. Molec. Struct. **864**, 20 (2008).

[218] Z. A. Fekete, E. A. Hoffmann, T. Kortvelyesi, and B. Penke, Mol. Phys. **105**, 2597 (2007).

[219] P. J. Borowski, J. Phys. Chem. A **116** (2012); P. Borowski, A. Drzewiecka, M. Fernandez-Gomez, M. P. Fernandez-Liencres, and T. P. Ruiz, Vib. Spec. **52**, 16 (2010).

[220] R. N. Hill, J. Chem. Phys. **83**, 1173 (1985); W. Kutzelnigg, Theor. Chim. Acta **68**, 445 (1985).

[221] K. A. Christensen and F. Jensen, Chem. Phys. Lett. **317**, 400 (2000).

[222] A. Tarnopolsky, A. Karton, R. Sertchook, D. Vuzman, and J. M. L. Martin, J. Phys. Chem. A **112**, 1 (2008).

[223] S. Grimme, J. Comput. Chem. **27**, 1787 (2006).

[224] A. Sierraalta, G. Martorell, E. Ehrmann, and R. Anez, Int. J. Quantum Chem. **108**, 1036 (2008).

[225] I. Hyla-Kryspin and S. Grimme, Organometallics **23**, 5581 (2004); M. M. Quintal, A. Karton, M. A. Iron, A. D. Boese, and J. M. L. Martin, J. Phys. Chem. A **110**, 709 (2006); G. A. Gutzev, M. D. Mochena, P. Jena, C. W. BauschlicherJr, and H. PartridgeIII, J. Chem. Phys. **121**, 6785 (2004); Y. Zhao and D. G. Truhlar, Acc. Chem. Res. **41**, 157 (2008); C. Yao, W. Guan, P. Song, Z. M. Su, J. D. Feng, L. K. Yan, and Z. J. Wu, Theor. Chem. Acc. **117**, 115 (2007); P. Song, W. Guan, C. Yao, Z. M. Su, Z. J. Wu, J. D. Feng, and L. K. Yan, Theor. Chem. Acc. **117**, 407 (2007).

[226] A. J. Cohen, P. Mori-Sanchez, and W. Yang, Science **321**, 792 (2008).

[227] S. Luo and D. G. Truhlar, J. Chem. Theory Comput. **8**, 4112 (2012).

[228] W. Jiang, M. L. Laury, M. Powell, and A. K. Wilson, J. Chem. Theory Comput. **8**, 4102 (2012).

[229] S. R. Das, T. G. Williams, M. L. Drummond, and A. K. Wilson, J. Phys. Chem. A **114**, 9394 (2009).

[230] A. Ikeda, Y. Nakao, H. Sato, and S. Sakaki, J. Phys. Chem. A **111**, 7124 (2007).

[231] P. Mori-Sanchez, A. J. Cohen, and W. Yang, J. Chem. Phys. **125**, 201102 (2006); J. P. Perdew and A. Zunger, Phys. Rev. B **23**, 5048 (1981).

[232] T. Yanai, D. Tew, and N. Handy, Chem. Phys. Lett. **292**, 51 (2004).

[233] M. L. Hall, D. A. Goldfield, A. D. Bochearov, and R. A. Friesner, J. Chem. Theory Comput. **5**, 2996 (2009).

[234] Y. Zhao and D. G. Truhlar, J. Phys. Chem. A **109**, 5656 (2005).

[235] A. D. Boese and J. M. L. Martin, J. Chem. Phys. **121**, 3405 (2004).

[236] J. Paier, M. Marsman, and G. Kresse, J. Chem. Phys. **127**, 024103 (2007).

[237] J. Toulouse, A. Savin, and C. Adamo, J. Chem. Phys. **117**, 10465 (2002); J. B. Krieger, J. Q. Chen, and S. Kurth, *Density Functional Theory and its Application to Materials*. (A.I.P., New York, 2001); J. B. Krieger, J. Q. Chen, G. J. Iafrate, and A. Savin, *Electron Correlations and Materials Properties*. (Kluwer Academic, New York, 1999); J. Rey and A. Savin, Int. J. Quantum Chem. **69**, 581 (1998); J. M. Tao, J. P. Perdew, V. N. Staroverov, and G. E. Scuseria, Phys. Rev. Lett. **91**, 146401 (2003).

[238] Y. Zhao and D. G. Truhlar, J. Chem. Phys. **125**, 194101 (2006).

[239] C. Adamo and V. Barone, J. Chem. Phys. **110**, 6158 (1999).

[240] J. P. Perdew, *Electronic Structure of Solids*. (Akademie Verlag, Berlin, 1991); K. Burke, J. P. Perdew, and Y. Wang, *Electronic Density Funtional Theory: Recent Progress and New Directions*. (Plenum, 1998).

[241] X. Xu and W. A. Goddard III, Proc. Natl. Acad. Sci. USA **101**, 2673 (2004).

[242] C. Adamo and V. Barone, J. Chem. Phys. **108**, 664 (1998).

[243] A. D. Becke, J. Chem. Phys. **104**, 1040 (1996).

[244] O. A. Vydrov, G. E. Scuseria, and J. P. Perdew, Chem. Phys. **126**, 154109 (2007); O. A. Vydrov and G. E. Scuseria, J. Chem. Phys. **125**, 234109 (2006); O. A. Vydrov, J. Heyd, A. Krukau, and G. E. Scuseria, J. Chem. Phys. **125**, 074106 (2006).

[245] W. E. Dasent, *Inorganic Energetics*, 2 ed. (Cambridge University Press, New York, 1982).

[246] P. J. Wilson, T. J. Bradley, and D. J. Tozer, J. Chem. Phys. **115**, 9233 (2001).

[247] C. A. Jimenez-Hoyas, B. G. Janesko, and G. E. Scuseria, J. PHys. Chem. A **113**, 11742 (2009).